Landscape Evolution of the Hawaiian Islands

by

Logan Wren Raming

A Dissertation Presented in Partial Fulfillment
of the Requirements for the Degree
Doctor of Philosophy

Approved November 2022 by the
Graduate Supervisory Committee:

Kelin X Whipple, Chair
Ramon Arrowsmith
Duane E. DeVecchio
Arjun M. Heimsath
Mark Schmeeckle

ARIZONA STATE UNIVERSITY

December 2022

ABSTRACT

Rivers in steep mountainous landscapes control how, where, and when signals of base-level fall are transmitted to the surrounding topography. In doing so rivers play an important role in determining landscape evolution in response to external controls of tectonics and climate. However, tectonics and climate often covary and understanding how they influence landscape evolution remains a significant challenge. The Hawaiian Islands, where tectonics are minimized but climate signals are amplified, provide an opportunity to better understand how signals of climate are recorded by landscapes. Focusing on the Hawaiian Islands, I examine (1) how variability in rock mass properties and thresholds in sediment mobility determine where waterfalls form or stall along the Nāpali coast of Kauaʻi, (2) I then extend these findings to other volcanoes to test if observed physical limits in flood size, climate, and volcano gradient can determine where waterfalls form, and (3) I explore how thresholds in river incision below waterfalls limit information about the influence of climate on river incision rates. Findings from this analysis show that waterfalls form or stall where the maximum unit stream power is at or below a critical unit stream power for bedrock river incision. Climate appears to have little effect in determining where these conditions are met but where waterfalls stall or form does record information about discharge-area scaling for global maximum observed floods. Below waterfalls the maximum incision depth for rivers on the island of Kauaʻi (which formed ~ 4-5 million years ago) is approximately proportional to the inverse square root of mean annual rainfall. Though maximum river incision depths for some of the younger volcanoes do not exhibit the same dependency on mean annual rainfall rates they are comparable to the maximum incision depths observed on Kauaʻi even though

they are a quarter to one-tenth the age of Kaua‘i. Importantly, these patterns of incision can be explained by thresholds in sediment mobility as recorded by river longitudinal profiles and indicate that the Hawaiian Islands are dominated by threshold conditions where signals of climate are recorded in the topography through controls on incision depth but not incision rates.

DEDICATION

Dedicated to my family, but especially my boys: Logan and Harrison. May curiosity be a constant guide through your life. And to Maria Luisa Alcoba, you will forever be in our hearts.

ACKNOWLEDGMENTS

A PhD, though bestowed upon an individual, is far from an individual endeavor. The level of support I have received from my advisor, committee members, colleagues, friends, family, acquaintances and even strangers is what made my PhD possible. Although I cannot list all the ways this support has manifested, I would like to acknowledge key contributions.

First off and foremost, I would like to acknowledge my advisor Kelin Whipple. The challenges of a PhD are not only manifested in the problems of scientific research—but also in the day to day struggles of life. Kelin has not only supported my research, but he has provided support and care through some of the most trying moments in my life. I am also indebted to Arjun Heimsath for his friendship, support, and times spent climbing, those moments on the rock have kept my fire for climbing alive. I also want to thank, Ramon Arrowsmith, Duane DeVecchio, and Mark Schmeeckle, for taking time out of their busy schedules to meet with me, discuss my research, and improve my abilities as a scientist.

The role of family and friends in supporting me, especially in maintaining my mental health cannot be overstated. My family, especially my mom and sisters helped me find my inner strength required to weather some of the toughest moments in my life. My friends—both near and far—have also been a huge source support for me. This includes students and postdocs whose time overlapped with mine at ASU, including Joel Leonard, Alex Pye, Nari Miller, Chelsea Scott, Alana Williams, Adam Wade, Adam Forte, Ajay Limaye, and many others.

Lastly, I want to acknowledge the people and institutions that provided me with financial and logistical support. Ayron Strauch played invaluable role in helping gain access to remote streams and valleys on the Hawaiian Islands. I am indebted to the people of Hawaii—from the people at Limahuli Gardens on Kaua'i, to the employees at the Division of Forestry and Wildlife, and to those who helped in providing transportation during the COVID-19 pandemic. I am also thankful for the financial support provide by the NSF Graduate Fellowship, School of Earth and Space Exploration at ASU, and the Geological Society of America.

TABLE OF CONTENTS

CHAPTER Page

Page

APPENDIX

LIST OF FIGURES

PREFACE

Our Real Work

"It may be that when we no longer know what to do we have come to our real work, and that when we no longer know which way to go we have come to our real journey. The mind that is not baffled is not employed. The impeded stream is the one that sings."

–Wendell Berry

How often does a stream move the Earth beneath its bed? The small rounded cobbles, gravel, and sand common to most streams are transient features—like cars on the freeway—but what about the bedrock underneath? Walking the exposed bedrock floor of a dry stream bed one may see subtle answers to this question. Delicate and intricate fluting the result of the slow wearing of Earth, one grain at a time. Or maybe it's the terse block of bedrock, askew from an un-weathered footprint, quietly whispering a story of large and violent floods. In other cases, the bedrock is all but invisible, hidden beneath goliath size boulders, whose fate is set by the slow product of entropy. My research is inspired by the visual poetry of landscapes carved by rivers and streams, the landscapes they shape, and their stories on Earth. Here I share what I have learned from the rivers and streams of the Hawaiian Islands.

CHAPTER 1

INTRODUCTION

MOTIVATION

The Earth's surface is shaped by the transfer of mass and energy driven by tectonics, precipitation, and increasingly humans (e.g.Willett, 1999; Roe et al., 2003; Pelletier et al., 2015). At geological scales, important feedbacks potentially exist between climate and tectonics (e.g. Willett, 1999) with implications for understanding how the Earth regulates climate at a global scale (Molnar and England, 1990; Raymo and Ruddiman, 1992; Macdonald et al., 2019). At shorter timescales, understanding the effects of anthropogenic-driven climate change on the Earth's surface has become an important problem (Nearing et al., 2004; Huggel et al., 2012; Pelletier et al., 2015; Baynes et al., 2018a; Li et al., 2022). Central to both of these problems is the influence of climate on surface processes and understanding how climate is recorded in the landscape (Perron, 2017). Yet, in most settings, thresholds (Schumm, 1979) must play an important role in determining how these problems manifest as only conditions and events that exceed thresholds for a given system can create detectable changes at a landscape scale.

A prime example of this is demonstrated in mountainous rivers, where the presence of coarse sediment constrains the range of discharges capable of incising bedrock (e.g. Snyder et al., 2003). This effect has important implication for understanding non-linearities in erosion rates in landscapes that are actively responding to tectonic forcing (e.g. Tucker, 2004; Lague et al., 2005; DiBiase and Whipple, 2011; Deal et al., 2018). Similarly, thresholds in the transport of coarse sediment have been demonstrated to exhibit a direct control on channel steepness (Thaler and Covington,

2016; Finnegan et al., 2017; Shobe et al., 2018). Yet, the role of thresholds in bedrock river incision at landscape evolution scales remains overlooked (e.g. Menking et al., 2013; Whipple et al., 2017; Mitchell and Yanites, 2021), even though the presence of thresholds can have a significant impact on how signals of climate and base-level fall are recorded in the landscape.

The Hawaiian Islands present an excellent location to further understand how thresholds in bedrock river incision modulate signals of base-level fall and climate in landscape evolution. The Hawaiian Islands have long been used as a natural laboratory for understanding how surface processes shape the Earth's surface (e.g. Wentworth, 1927, 1928; White, 1949; Scott and Street, 1976; Howard et al., 1994; Ferrier et al., 2013). The general absence of tectonics plus the wide range of mean annual rainfall (Giambelluca et al., 2012) makes the Hawaiian Islands an especially suitable place for understanding how climate drives landscape evolution (Perron, 2017). Previous studies have focused on these conditions in attempts to link climate to incision rates through influences on weathering and flood size (e.g. Ferrier et al., 2013; Murphy et al., 2016). The Hawaiian Islands have also been used to document and test theories related to the rapid retreat of waterfalls due to coastal erosion and large submarine landslides (Seidl et al., 1994; Lamb et al., 2007; Mackey et al., 2014). Although, in all of this work the role of thresholds in bedrock river incision have hardly been explored (e.g. Lamb et al., 2007; Han et al., 2014). Yet, Hawaiian rivers and streams are known for their coarse sediment (e.g. Wentworth, 1928) and in the absence of significant tectonic forcing, thresholds in sediment motion are bound to eventually dominate as expected in most post orogenic landscapes (Baldwin et al., 2003). This dissertation returns to the classic problems of

knickzone retreat and the role of climate on bedrock river incision on the Hawaiian Islands, but with a threshold-oriented paradigm to improve understanding of how climate and knickzones can or cannot shape landscapes.

OVERVIEW

In this analysis I focus on two distinct parts of the landscape. Chapter 2 and Chapter 3 focus on conditions above knickzones, followed by the Chapter 4 which focuses on deeply incised canyons below knickzones. Chapter 2 and Chapter 3 broadly focus on the question: How do rock mass properties, discharge-area scaling, thresholds in sediment motion, and climate determine where knickzones form or stall? Previous work on knickzone have predominately focused on how and where knickzones respond—sometimes at a very rapid pace—to coastal erosion (Seidl et al., 1994; Lamb et al., 2007; Mackey et al., 2014). In these studies, variability in rock mass properties due to different lava flow types is assumed to be so widespread as to be inconsequential to the pace and pattern of knickzone retreat. Chapter 2 explores whether this is in fact true and tests the hypothesis that knickzones along western end of the Nāpali Coast, Kauaʻi is simply a manifestation of thresholds of bedrock river incision and explores how these conditions relate to the concept of a threshold drainage area.

Chapter 3 extends these findings to the other volcanoes on the Hawaiian Islands and builds on the notion that knickzones represent physical limits in bedrock river incision. This chapter consists of two major parts. The first section of this chapter simply examines patterns of drainage area above knickzones and potential controls related to volcano gradient and climate across regions that have and have not experienced

significant base-level fall. The results from this section clearly demonstrate that knickzones form or stall at threshold drainage area regardless of base-level fall. The second section of this chapter then examines the hypothesis that waterfall and knickzones represent a physical limit in bedrock river incision constrained by empirical limits on flood size.

Chapter 4 then transitions to the deeply incised canyons below knickzones to explore the questions: (1) how do thresholds in bedrock river incision manifest on the Hawaiian Islands? (2) how is climate recorded in a landscape dominated by thresholds? To answer these questions, we first turn to geological evidence to show that deeply incised canyons form rapidly, but once incised remain relatively stable over periods of millions of years. With this background, we then explore the consequence of thresholds on patterns of incision and also how other controls like sea-cliff height and volcano slope influence depth. We then test the hypothesis that climate influences incision depth through a reduction in the threshold slope set by wetter climates.

Chapter 5 presents a synthesis of the preceding chapters and outlines potential avenues for future research on the Hawaiian Islands.

Chapter 2 has been published elsewhere, please cite accordingly. Chapters 3 and 4 are in preparation for publication in peer reviewed journals.

Chapter 2:

Raming, L.W., and Whipple, K.X., 2022, When knickzones limit upstream transmission of base-level fall: An example from Kauaʻi, Hawaiʻi: Geology, doi:10.1130/G50019.1.

REFERENCES

Baldwin, J.A., Whipple, K.X., and Tucker, G.E., 2003, Implications of the shear stress river incision model for the timescale of postorogenic decay of topography: Journal of Geophysical Research: Solid Earth, v. 108, doi:10.1029/2001JB000550.

Baynes, E.R.C., van de Lageweg, W.I., McLelland, S.J., Parsons, D.R., Aberle, J., Dijkstra, J., Henry, P.-Y., Rice, S.P., Thom, M., and Moulin, F., 2018, Beyond equilibrium: Re-evaluating physical modelling of fluvial systems to represent climate changes: Earth-Science Reviews, v. 181, p. 82–97, doi:10.1016/j.earscirev.2018.04.007.

Deal, E., Braun, J., and Botter, G., 2018, Understanding the Role of Rainfall and Hydrology in Determining Fluvial Erosion Efficiency: Journal of Geophysical Research: Earth Surface, v. 123, p. 744–778, doi:10.1002/2017JF004393.

DiBiase, R.A., and Whipple, K.X., 2011, The influence of erosion thresholds and runoff variability on the relationships among topography, climate, and erosion rate: Journal of Geophysical Research: Earth Surface, v. 116, http://onlinelibrary.wiley.com/doi/10.1029/2011JF002095/full (accessed June 2016).

Ferrier, K.L., Huppert, K.L., and Perron, J.T., 2013, Climatic control of bedrock river incision: Nature, v. 496, p. 206–209, doi:https://doi.org/10.1038/nature11982.

Finnegan, N.J., Klier, R.A., Johnstone, S., Pfeiffer, A.M., and Johnson, K., 2017, Field evidence for the control of grain size and sediment supply on steady-state bedrock river channel slopes in a tectonically active setting: Earth Surface Processes and Landforms, v. 42, p. 2338–2349, doi:10.1002/esp.4187.

Giambelluca, T.W., Chen, Q., Frazier, A.G., Price, J.P., Chen, Y.-L., Chu, P.-S., Eischeid, J.K., and Delparte, D.M., 2012, Online Rainfall Atlas of Hawai‘i: Bulletin of the American Meteorological Society, v. 94, p. 313–316, doi:10.1175/BAMS-D-11-00228.1.

Han, J., Gasparini, N.M., Johnson, J.P.L., and Murphy, B.P., 2014, Modeling the influence of rainfall gradients on discharge, bedrock erodibility, and river profile evolution, with application to the Big Island, Hawai’i: Journal of Geophysical Research: Earth Surface, v. 119, p. 1418–1440, doi:10.1002/2013JF002961.

Howard, A.D., Dietrich, W.E., and Seidl, M.A., 1994, Modeling fluvial erosion on regional to continental scales: Journal of Geophysical Research: Solid Earth, p. 13971–13986, doi:10.1029/94JB00744@10.1002/(ISSN)2169-9356.TECTOP1.

Huggel, C., Clague, J.J., and Korup, O., 2012, Is climate change responsible for changing landslide activity in high mountains? Earth Surface Processes and Landforms, v. 37, p. 77–91, doi:10.1002/esp.2223.

Lague, D., Hovius, N., and Davy, P., 2005, Discharge, discharge variability, and the bedrock channel profile: Journal of Geophysical Research: Earth Surface, v. 110, p. F04006, doi:10.1029/2004JF000259.

Lamb, M.P., Howard, A.D., Dietrich, W.E., and Perron, J.T., 2007, Formation of amphitheater-headed valleys by waterfall erosion after large-scale slumping on Hawai ‘i: GSA Bulletin, v. 119, p. 805–822, doi:https://doi.org/10.1130/B25986.1.

Li, D. et al., 2022, High Mountain Asia hydropower systems threatened by climate-driven landscape instability: Nature Geoscience, v. 15, p. 520–530, doi:10.1038/s41561-022-00953-y.

Macdonald, F.A., Swanson-Hysell, N.L., Park, Y., Lisiecki, L., and Jagoutz, O., 2019, Arc-continent collisions in the tropics set Earth’s climate state: Science, v. 364, p. 181–184, doi:10.1126/science.aav5300.

Mackey, B.H., Scheingross, J.S., Lamb, M.P., and Farley, K.A., 2014, Knickpoint formation, rapid propagation, and landscape response following coastal cliff retreat at the last interglacial sea-level highstand: Kaua‘i, Hawai‘i: GSA Bulletin, v. 126, p. 925–942, doi:10.1130/B30930.1.

Menking, J.A., Han, J., Gasparini, N.M., and Johnson, J.P.L., 2013, The effects of precipitation gradients on river profile evolution on the Big Island of Hawai’i: GSA Bulletin, v. 125, p. 594–608, doi:10.1130/B30625.1.

Mitchell, N.A., and Yanites, B.J., 2021, Bedrock River Erosion through Dipping Layered Rocks: Quantifying Erodibility through Kinematic Wave Speed: Earth Surface Dynamics Discussions, p. 1–46, doi:10.5194/esurf-2021-3.

Molnar, P., and England, P., 1990, Late Cenozoic uplift of mountain ranges and global climate change: chicken or egg? Nature, v. 346, p. 29–34, doi:10.1038/346029a0.

Murphy, B.P., Johnson, J.P.L., Gasparini, N.M., and Sklar, L.S., 2016, Chemical weathering as a mechanism for the climatic control of bedrock river incision: Nature, v. 532, p. 223–227, doi:10.1038/nature17449.

Nearing, M.A., Pruski, F.F., and O’Neal, M.R., 2004, Expected climate change impacts on soil erosion rates: A review: Journal of Soil and Water Conservation, v. 59, p. 43–50.

Pelletier, J.D. et al., 2015, Forecasting the response of Earth's surface to future climatic and land use changes: A review of methods and research needs: Earth's Future, v. 3, p. 220–251, doi:10.1002/2014EF000290.

Perron, J.T., 2017, Climate and the Pace of Erosional Landscape Evolution: Annual Review of Earth and Planetary Sciences, v. 45, p. 561–591, doi:10.1146/annurev-earth-060614-105405.

Raymo, M.E., and Ruddiman, W.F., 1992, Tectonic forcing of late Cenozoic climate: Nature, v. 359, p. 117–122, doi:10.1038/359117a0.

Roe, G.H., Montgomery, D.R., and Hallet, B., 2003, Orographic precipitation and the relief of mountain ranges: Journal of Geophysical Research: Solid Earth, v. 108, p. 2315, doi:10.1029/2001JB001521.

Schumm, S.A., 1979, Geomorphic Thresholds: The Concept and Its Applications: Transactions of the Institute of British Geographers, v. 4, p. 485–515, doi:10.2307/622211.

Scott, G.A.J., and Street, J.M., 1976, The role of chemical weathering in the formation of Hawaiian Amphitheatre-headed valleys.: Zeitschrift fr Geomorphologie, Annals of geomorphology.,.

Seidl, M.A., Dietrich, W.E., and Kirchner, J.W., 1994, Longitudinal profile development into bedrock: An analysis of Hawaiian channels: Journal of Geology, v. 102, p. 457, doi:10.1086/629686.

Shobe, C.M., Tucker, G.E., and Rossi, M.W., 2018, Variable-Threshold Behavior in Rivers Arising From Hillslope-Derived Blocks: Journal of Geophysical Research: Earth Surface, v. 123, p. 1931–1957, doi:10.1029/2017JF004575.

Snyder, N.P., Whipple, K.X., Tucker, G.E., and Merritts, D.J., 2003, Importance of a stochastic distribution of floods and erosion thresholds in the bedrock river incision problem: Journal of Geophysical Research: Solid Earth, v. 108, p. 2117, doi:10.1029/2001JB001655.

Thaler, E.A., and Covington, M.D., 2016, The influence of sandstone caprock material on bedrock channel steepness within a tectonically passive setting: Buffalo National River Basin, Arkansas, USA: Journal of Geophysical Research: Earth Surface, v. 121, p. 1635–1650, doi:10.1002/2015JF003771.

Tucker, G.E., 2004, Drainage basin sensitivity to tectonic and climatic forcing: implications of a stochastic model for the role of entrainment and erosion thresholds: Earth Surface Processes and Landforms, v. 29, p. 185–205, doi:10.1002/esp.1020.

Wentworth, C.K., 1927, Estimates of Marine and Fluvial Erosion in Hawaii: The Journal of Geology, v. 35, p. 117–133.

Wentworth, C.K., 1928, Principles of Stream Erosion in Hawaii: The Journal of Geology, v. 36, p. 385–410.

Whipple, K.X., Forte, A.M., DiBiase, R.A., Gasparini, N.M., and Ouimet, W.B., 2017, Timescales of landscape response to divide migration and drainage capture: Implications for the role of divide mobility in landscape evolution: Journal of Geophysical Research: Earth Surface, v. 122, p. 248–273, doi:https://doi.org/10.1002/2016JF003973.

White, S.E., 1949, Processes of erosion on steep slopes of oahu, Hawaii: American Journal of Science, v. 247, p. 168–186, doi:10.2475/ajs.247.3.168.

Willett, S.D., 1999, Orogeny and orography: The effects of erosion on the structure of mountain belts: Journal of Geophysical Research: Solid Earth, v. 104, p. 28957–28981, doi:10.1029/1999JB900248.

CHAPTER 2
WHEN KNICKZONES LIMIT UPSTREAM TRANSMISSION OF BASE-LEVEL FALL: AN EXAMPLE FROM KAUA‘I, HAWAI‘I

ABSTRACT

A threshold drainage area limits fluvial transmission of base-level fall and may be expressed in the form of a waterfall or a series of waterfalls, defined here as a knickzone. Knickzones on the west coast of Kaua'i, Hawai’i, exhibit evidence of a threshold drainage area. 18 of the 25 knickzones in our study area are located at the coast or a tributary junction, have a drainage area less than 1.5 km^2, and have been stationary for at least 1.5 Myr. The other 7 knickzones are located more than 1 km upstream from the coast or nearest tributary junction and range in drainage area from 1 to 5.5 km^2. Both sets of knickzones limit incision relative to canyons without knickzones. Field observations show strong ‘a‘ā flows and dikes always crop out at the lip of knickzones, suggesting these resistant rocks and coarse sediment generated from them act to inhibit knickzone migration. A model incorporating flood records and channel conditions above knickzones show thresholds of coarse sediment entrainment are never exceeded below 1 km^2. Our results demonstrate knickzones on the west coast of Kaua’i are enduring features explained by resistant lava flows and physical limits in bedrock incision.

INTRODUCTION

Knickzones, defined here as a waterfall or a series of waterfalls, are often interpreted as recording rapid incision and upstream transmission of base-level fall (e.g. Hayakawa and Matsukura, 2003; Baynes et al., 2015; Schwanghart and Scherler, 2020).

However, knickzones can exhibit contrasting behavior where they are formed or anchored by variations in erodibility (e.g. Ortega et al., 2013; May et al., 2017). Crosby and Whipple, (2006) and Lamb et al. (2007) proposed knickzones may stall or form in place at a threshold drainage area where fluvial processes become ineffective, implying knickzones located at or below a threshold drainage area could be mis-interpreted as recording drainage area dependent retreat rates. Though studies have considered the operation of both fast and slow knickzones in landscapes (e.g. DiBiase et al., 2015) and the role of river incision thresholds in knickzone retreat (Lamb and Dietrich, 2009; Scheingross and Lamb, 2017, 2021) the possibility river incision thresholds manifest as a threshold drainage area for knickzones remains largely unexplored.

To test for a link between river incision thresholds and a threshold drainage area we focus on the west coast of Kaua'i, Hawai'i, a region that has been a focal point for studies on knickzones and their roles in landscape evolution (Seidl et al., 1994; Stock and Montgomery, 1999; Chatanantavet and Parker, 2005; Mackey et al., 2014). These studies, however, have dismissed the possibility that knickzones in this setting are anchored by resistant lava flows and bedrock incision thresholds. Yet approximately 70% of all mapped knickzones (Fig. 2.1) have not retreated from their point of formation and remain elevated above the coast or tributary junctions resulting in fluvial hanging valleys (Crosby et al., 2007). The majority of coastal erosion occurred prior to 2Ma (Seidl et al., 1994; Mackey et al., 2014), indicating these hanging valleys have been stable for a significant time and demonstrates that knickzone evolution in this landscape is dominated by threshold conditions. The question we explore here is: Can these threshold conditions

manifest as a threshold drainage area explained by fluvial incision thresholds and spatial variability in rock mass properties?

FIELD SETTINGS

Our study is located on the western end of Kaua'i, bordering the Nāpali coast and Mana Plain (Fig. 2.1). This region is formed by west to north-west dipping, ~1-5 m thick interbedded ʻaʻā and pāhoehoe lava flows of Nāpali formation (4.43 ∓ 0.45 Ma; Macdonald et al., 1960; McDougall, 1979). ʻAʻā flows are identified by their massive and dense core and rubbly exterior (i.e. clinker) with individual flows up to 15 m thick. Pāhoehoe flows are typically thinner and more fragmented (Fig. 2.2 and Fig. 2.3; Macdonald et al., 1960).

In response to lithospheric loading from shield building, Kaua'i experienced initially rapid then slow and declining subsidence rates until ~2Ma (Hearty et al., 2005; Huppert et al., 2015). Most coastal erosion occurred during this time, as slow subsidence and high-stand sea level drive base-level fall through wave erosion on bedrock sea-cliffs (Mackey et al., 2014). For the two northern most catchments in our study base-level fall may have occurred even earlier (~ 4Ma, Seidl et al., 1994) due to land sliding shortly after shield building (Moore et al., 1989). Proximal shield building of Maui Nui generated flexural uplift from ~1.5 Ma to 0.5 Ma (Hearty et al., 2005) which buffered sea-cliffs and lengthened streams, resulting in a hiatus of base-level fall (Mackey et al., 2014). Sea-cliff erosion was likely renewed during the last interglacial (120-130 ka) and for one valley in our study area may have generated 4 km of knickzone retreat (Fig. 2.1,

Mackey et al., 2014). Influence of climate on river response to this base-level history is limited as catchment-mean rainfall rates differ only slightly (0.8-1.3m/yr, Frazier et al., 2016) and orographic rainfall patterns have been stable since ~4 Ma (Ferrier et al., 2013b). Additionally, drainage area loss is minor to non-existent (see Data Repository).

EVIDENCE OF THRESHOLD CONDITIONS

Methods

We automated knickzone identification as outlined in the Data Repository. For each knickzone we measured drainage area above the knickzone and the distance from the base of the knickzone to the nearest outlet or tributary junction. From this distance we classified a knickzone as either a hanging valley (with a distance < 500 m) or as an upstream knickzone as they have either formed or retreated upstream from the outlet or tributary junction. Sea-cliff height provides an estimate for the total amount of base-level fall. We measure sea-cliff height as the difference between the current topography and estimates of the initial shield volcano at the outlet of each valley (see Appendix: Chapter 2 Supplementary). We visited 5 out of the 7 upstream knickzones in the field to document rock mass properties, channel characteristics, and to identify whether knickzones are associated with resistant lava flows. To test for differences in rock mass properties, we measured joint spacing and estimated rock strength using a Schmidt Hammer (see Appendix: Chapter 2 Supplementary).

Results

Drainage areas above hanging valleys are all below 1.5 km^2, whereas drainage area above upstream knickzones range from 1 to 5.5 km^2. For upstream knickzones, knickzone height spans an order of magnitude (~40-400m) and is well correlated with sea-cliff height (R^2 = 0.91, Fig. 2.1C). In three valleys there are no knickzones; instead deeply versus shallowly incised portions of the valleys are separated by a change in channel steepness, shown by a change in slope in χ-elevation space, and are identified as convex slope-break knickpoints (Fig. 2.1; e.g. Whipple et al., 2021). Drainage areas above slope-break knickpoints range from 1-2.7 km^2. Stream profiles show that valleys with knickzones are less incised than adjacent and otherwise similar valleys with slope-break knickpoints (Fig. 2.1B). For all of the knickzones we visited (Fig. 2.1A) ʻaʻā flows and dikes crop out at the lip of the uppermost waterfall. Rock strength and joint spacing measurements indicate ʻaʻā flows and dikes are stronger and less jointed than pāhoehoe flows and clinker (Fig. 2.3). Field observations and topography show these more resistant rocks also manifest as cliff bands in adjacent hillslopes and that there is significant variability in the extent and distribution of cliff-forming layers, with a reduction in thick cliff-forming ʻaʻā flows for valleys without knickzones (Fig. 2.3).

MODEL OF THRESHOLD EXCEEDANCE

Rapid knickzone retreat occurs where thresholds of coarse sediment entrainment and or toppling are exceeded (Lamb et al., 2007; Cook et al., 2013; Baynes et al., 2015). Conditions for toppling require that blocks of bedrock are fully detached with minimal inter-joint friction (Lamb and Dietrich, 2009). For ʻaʻā flows and dikes, our field

observations (see Appendix: Chapter 2 Supplementary) indicate these conditions are unlikely met as joints are irregular and blocks do not appear fully detached. Other processes like debris flows may be important for knickzone retreat (Mackey et al., 2014). However, debris flows are common in the steep canyons downstream of knickzones but are limited in the subdued landscapes above knickzones (Mackey et al., 2014). Consequently, we hypothesize that knickzones stabilize or form where the channel is unable to incise through resistant rock, conditions that develop once fluvial thresholds required for mobilizing coarse sediment are no longer exceeded.

Methods

The non-dimensional boundary shear stress (τ^*) required to mobilize coarse sediment can be expressed as

$$\tau^* = \frac{\rho_w g h S}{g(\rho_s - \rho_w) D}, \qquad (1)$$

where g is the acceleration due to gravity, h is flow depth, ρ_w and ρ_s are the density of water and sediment respectively, S is channel gradient, and D is a representative grain size diameter. Sediment entrainment occurs once $\tau^* \geq \tau_c^*$, where τ_c^* is the non-dimensional critical shear stress. To model these conditions, we use the range of channel gradients observed above knickzones (S = 0.05 to 0.1). Field observations (see Appendix: Chapter 2 Supplementary) indicate reaches above knickzones are typically armored by coarse sediment. Because grain size is inherently linked to the properties of joint spacing in the parent bedrock (Neely and DiBiase, 2020), we vary D between 0.7 – 1.1 m, a range of grain sizes that is bounded by the 50th to 84th percentile of joint spacing for ‘a‘ā flows and dikes

(Fig. 2.2) and is consistent with field observations (see Appendix: Chapter 2 Supplementary). For given values of *S* and *D* we use the variable power equation (VPE) of Ferguson (2007) to solve for *h* and τ^* for a range of unit discharge (q). For the same range of conditions, we estimate τ_c^* following Prancevic and Lamb (2015) where $\tau_c^* = 0.19{C_f}^{0.34}$ and C_f is the friction coefficient estimated from the VPE (see Appendix: Chapter 2 Supplementary).

We then identify a critical unit discharge q_c where $\tau^* = \tau_c^*$. We calculate the probability of threshold exceedance as the number of events where $q \geq q_c$ divided by the total number of events possible, where q is adjusted for both at-a-station width and drainage area and is a stochastic variable from a synthetic flood record of $5x10^6$ events. The synthetic flood record is from a Weibull distribution (Rossi et al., 2016) fit to the record of peak discharges from a local stream gauge (see Appendix: Chapter 2 Supplementary). There is significant uncertainty in extrapolating flood records for multiple reasons including a finite sample size and non-stationary effects of climate. For these canyons, however, historic records provide the best information we have on flood conditions. Furthermore, the climate was likely drier during glacial periods (Hotchkiss et al., 2000), suggesting modern climate provides a conservative estimate of threshold exceedance probabilities.

Results

For the range of conditions tested, thresholds are not exceeded below a drainage area of 1 km^2 (Fig. 2.4). Thresholds are rarely exceeded for large grains sizes (D = 1.1, S = 0.08) or more gentle channel gradients (S = 0.05, D = 0.9) with recurrence intervals of

threshold exceedance greater than $1x10^5$ years. For the different conditions tested, the majority of upstream knickzones (drainage area from 2 – 4 km^2) show recurrence intervals for threshold exceedance from 1000 to $5x10^6$ years (Fig. 2.4). Only in the most favorable conditions (S = 0.1, D= 0.9; D = 0.7, S= 0.08) and at large drainage areas (>5km^2) are threshold conditions exceeded more frequently, with estimated recurrence intervals between 100 to 1000 years (Fig. 2.4).

DISCUSSION AND CONCLUSIONS

Resistant rock is sufficient for the development of a knickzone (Ortega et al., 2013) and the inability to move coarse sediment limits fluvial incision of resistant bedrock. A threshold drainage area is an expression of both of these conditions. Valleys without knickzones represent cases where there is a relative lack of resistant rock (Fig. 2.3). This does not suggest knickzones never formed in these valleys, rather conditions are insufficient for their preservation. However, slope-break knickpoints in these valleys have drainage areas that align with low probabilities of threshold exceedance (Fig. 2.4) indicating even in the absence of particularly resistant lava flows, there is likely enough coarse sediment to inhibit bedrock incision. Whether these slope-break knickpoints translate upstream with increased base-level fall remains an open question. Though even typical ‘a‘ā flows may present significant resistance to incision at lower drainage areas, suggesting additional base-level fall may result in in-situ formation of a knickzone at a threshold drainage area.

The preceding hypothesis can explain the lower limit of drainage area for upstream knickzones (1-2 km^2, Fig 2.4.) and explain why hanging valleys are abundant at drainage

areas below 1km^2. Conversely, the range of drainage area from 2-5.5 km^2 for upstream knickzones may be attributed to the presence of thick and or resistant lava flows and dikes as observed in the field and in imagery (Fig. 2.3A). At larger drainage areas, thresholds of coarse sediment are more frequently exceeded (Fig. 2.4) and streams may have the capacity to cut through resistant rock, possibly resulting in rapid upstream transmission of base-level fall until encountering the next resistant section of lava flows and/or reaching threshold conditions. We hypothesize that valleys with abundant resistant rock may reach threshold conditions at larger drainage areas (Fig. 2.4) because (1) the largest blocks of bedrock must be fractured in order to be mobilized and (2) abrasion-driven incision rates are inversely proportional to the square of rock strength (Sklar and Dietrich, 2001; Beer and Lamb, 2021) indicating less incision will have occurred once thresholds conditions of sediment entrainment are reached.

Knickzone retreat, however, still remains viable at larger drainage areas. It is possible that increased channel gradients below knickzone are not offset by an equal increase in grain size, resulting in favorable conditions for threshold exceedance below knickzones. Additionally, debris flow activity below knickzones remains significant (Mackey et al. 2014). Thus, our findings do not preclude the recent formation and rapid retreat of the ~40m high knickzone marked by a red arrow in Figure 1 (Mackey et al., 2014) so long as that retreat has now stalled, consistent with its near-threshold drainage area (red arrow, Fig. 4) and the observation that it is now located on a band of resistant lava (Fig. 2.1). These conditions indicate future events of base-level fall will likely accumulate at this knickzone and not be transmitted farther upstream unless the resistant lava band is breached by mass wasting. Intriguingly, larger knickzones to the north (Fig. 2.1) may have similarly

accumulated base-level fall (mostly prior to 2 Ma) through pulses of rapid knickzone retreat, though, it is possible they attained their full height through other viable mechanisms of bedrock incision. Either way, our analysis shows that knickzone formation and retreat here and in similar settings elsewhere can occur early and rapidly, followed by long periods of stability.

FIGURES

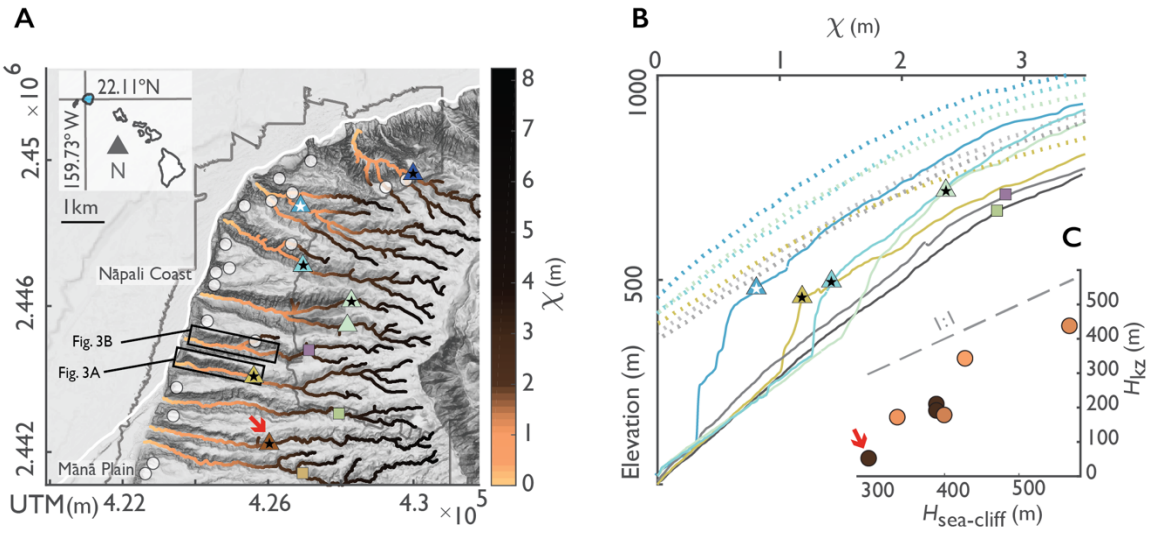

Figure 2.1. Topography of the west coast of Kaua'i. A: Slope-shade map where triangles show upstream knickzones located more than 1 km from the coast or tributary junction. White circles are fluvial hanging valleys, stalled at the coast or tributary junction. Colored squares are slope-break knickpoints. Stars represent knickzones with verified 'a'ā flows or dikes. The white star was verified through photography, black stars are field sites. Streams are colored by χ (Yang et al., 2015), a metric that linearizes stream profiles and can indicate potential drainage area dependent retreat if knickzones cluster near a single χ-value (e.g. Schwanghart and Scherler, 2020). The gray outline represents extent of lidar (OpenTopography). The white line represents current sea-level. B: Select trunk stream profiles in χ-elevation space with colors and symbols matching with A. Dotted lines represent the initial volcano surface for each profile. C: Sea-cliff height ($H_{sea\text{-}cliff}$) plotted against knickzone height (H_{kz}) and colored by χ at the knickzone. Red arrows in A and C shows knickzone studied by Mackey et al. (2014).

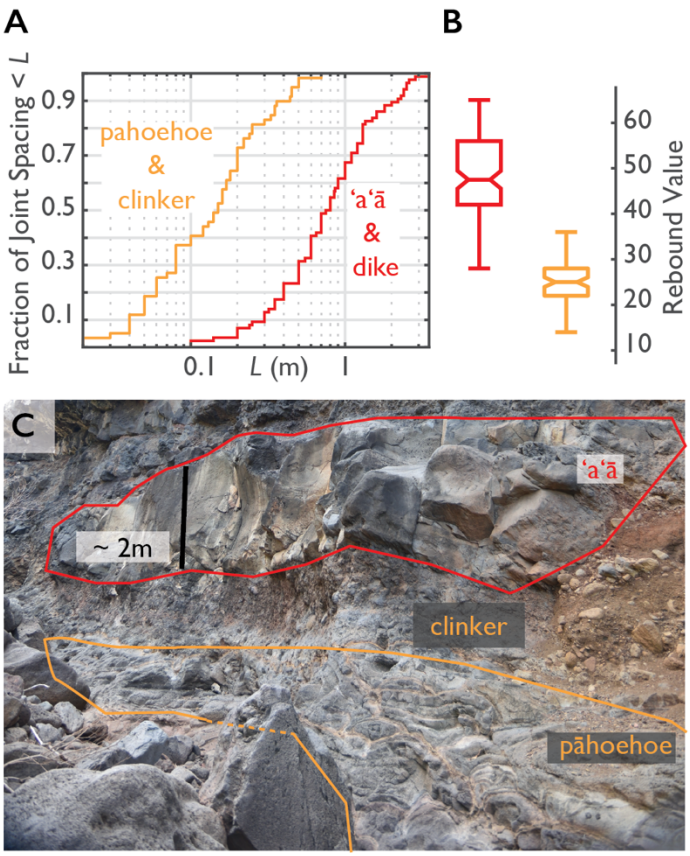

Figure 2.2. Rock mass properties of lava flow types. A: Empirical cumulative distribution of joint spacing (L) of ʻaʻā flows and dikes (red, n = 86), and pāhoehoe flows and clinker (orange, n = 60). B: Box-plot of Schmidt Hammer rebound values for ʻaʻā flows and dikes (red, n = 133), and pāhoehoe flows and clinker (orange, n = 80). C: Outcrop with example of different flow types.

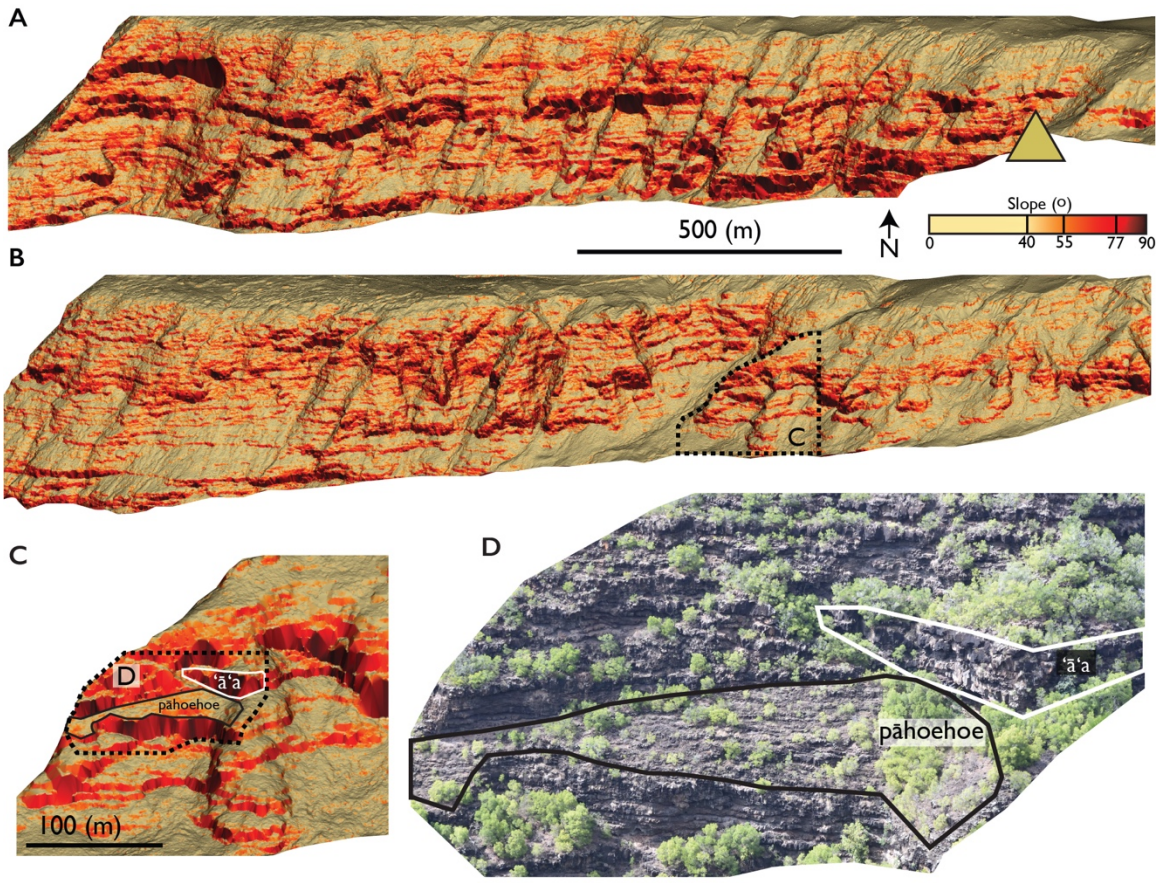

Figure 2.3. Variability of lava flow type expressed in topography and imagery. A: Lidar slope shade of a canyon with an upstream knickzone, yellow triangle shows upper limit of the knickzone. B: Lidar slope shade of canyon without an upstream knickzone. Locations of A and B are shown in Fig. 2.1A. C & D: Details of lidar slope shade illustrating differences in pāhoehoe and ‘a‘ā flows at 100 m scale.

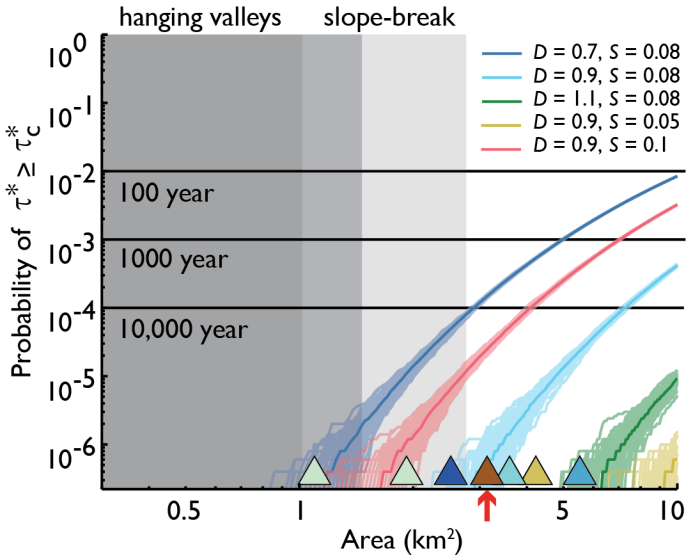

Figure 2.4. Probability of exceeding thresholds for coarse sediment entrainment ($\tau^* \geq \tau_c^*$) expressed through drainage area. Triangles on x-axis indicate drainage area for knickzones color-coded as in Fig. 2.1. Transparent lines represent individual model runs (i.e. one iteration of $5x10^6$ flood events) and solid lines represent the median of all model runs for given of set conditions. Line color indicates different variations in slope (S) and grainsize (D) as shown in the legend. Dark grey rectangle shows range of drainage areas for hanging valleys, light grey rectangle shows drainage areas for slope-break knickpoints, and medium grey rectangle indicates overlap between both regions. Numbers indicate select recurrence intervals. Red arrow indicates knickzone studied by Mackey et al. (2014).

REFERENCES

Baynes, E.R.C., Attal, M., Niedermann, S., Kirstein, L.A., Dugmore, A.J., and Naylor, M., 2015, Erosion during extreme flood events dominates Holocene canyon evolution in northeast Iceland: Proceedings of the National Academy of Sciences, v. 112, p. 2355–2360, doi:10.1073/pnas.1415443112.

Beer, A.R., and Lamb, M.P., 2021, Abrasion regimes in fluvial bedrock incision: Geology, doi:10.1130/G48466.1.

Chatanantavet, P., and Parker, G., 2005, Modeling the bedrock river evolution of western Kaua'i, Hawai'i, by a physically-based incision model based on abrasion, *in* Tunnelling. A Decade of Progress. GeoDelft 1995-2005, p. 99–110.

Cook, K.L., Turowski, J.M., and Hovius, N., 2013, A demonstration of the importance of bedload transport for fluvial bedrock erosion and knickpoint propagation: Earth Surface Processes and Landforms, v. 38, p. 683–695, doi:https://doi.org/10.1002/esp.3313.

Crosby, B.T., and Whipple, K.X., 2006, Knickpoint initiation and distribution within fluvial networks: 236 waterfalls in the Waipaoa River, North Island, New Zealand: Geomorphology, v. 82, p. 16–38, doi:10.1016/j.geomorph.2005.08.023.

Crosby, B.T., Whipple, K.X., Gasparini, N.M., and Wobus, C.W., 2007, Formation of fluvial hanging valleys: Theory and simulation: Journal of Geophysical Research: Earth Surface, v. 112, doi:https://doi.org/10.1029/2006JF000566.

DiBiase, R.A., Whipple, K.X., Lamb, M.P., and Heimsath, A.M., 2015, The role of waterfalls and knickzones in controlling the style and pace of landscape adjustment in the western San Gabriel Mountains, California: GSA Bulletin, v. 127, p. 539–559, doi:10.1130/B31113.1.

Ferguson, R., 2007, Flow resistance equations for gravel-and boulder-bed streams: Water resources research, v. 43, doi:10.1029/2006WR005422.

Ferrier, K.L., Perron, J.T., Mukhopadhyay, S., Rosener, M., Stock, J.D., Huppert, K.L., and Slosberg, M., 2013, Covariation of climate and long-term erosion rates across a steep rainfall gradient on the Hawaiian island of Kaua‘i: GSA Bulletin, v. 125, p. 1146–1163, doi:10.1130/B30726.1.

Frazier, A.G., Giambelluca, T.W., Diaz, H.F., and Needham, H.L., 2016, Comparison of geostatistical approaches to spatially interpolate month-year rainfall for the Hawaiian Islands: International Journal of Climatology, v. 36, p. 1459–1470, doi:10.1002/joc.4437.

Hayakawa, Y., and Matsukura, Y., 2003, Recession rates of waterfalls in Boso Peninsula, Japan, and a predictive equation: Earth Surface Processes and Landforms, v. 28, p. 675–684, doi:10.1002/esp.519.

Hearty, P.J., Karner, D.B., Renne, P.R., Olson, S.L., and Fletcher, S., 2005, 40Ar/39Ar age of a young rejuvenation basalt flow: Implications for the duration of volcanism and the timing of carbonate platform development during the quaternary on Kaua’i, Hawaiian Islands: New Zealand Journal of Geology and Geophysics, v. 48, p. 199–211, doi:10.1080/00288306.2005.9515110.

Hotchkiss, S., Vitousek, P.M., Chadwick, O.A., and Price, J., 2000, Climate Cycles, Geomorphological Change, and the Interpretation of Soil and Ecosystem Development: Ecosystems, v. 3, p. 522–533, doi:10.1007/s100210000046.

Huppert, K.L., Royden, L.H., and Perron, J.T., 2015, Dominant influence of volcanic loading on vertical motions of the Hawaiian Islands: Earth and Planetary Science Letters, v. 418, p. 149–171, doi:10.1016/j.epsl.2015.02.027.

Lamb, M.P., and Dietrich, W.E., 2009, The persistence of waterfalls in fractured rock: GSA Bulletin, v. 121, p. 1123–1134, doi:10.1130/B26482.1.

Lamb, M.P., Howard, A.D., Dietrich, W.E., and Perron, J.T., 2007, Formation of amphitheater-headed valleys by waterfall erosion after large-scale slumping on Hawai ‘i: GSA Bulletin, v. 119, p. 805–822, doi:https://doi.org/10.1130/B25986.1.

Macdonald, G.A., Davis, D.A., and Cox, D.C., 1960, Geology and ground-water resources of the island of Kauai, Hawaii: Bulletin Other Government Series 13, http://pubs.er.usgs.gov/publication/70160871 (accessed December 2019).

Mackey, B.H., Scheingross, J.S., Lamb, M.P., and Farley, K.A., 2014, Knickpoint formation, rapid propagation, and landscape response following coastal cliff retreat at the last interglacial sea-level highstand: Kaua‘i, Hawai‘i: GSA Bulletin, v. 126, p. 925–942, doi:10.1130/B30930.1.

May, C., Roering, J., Snow, K., Griswold, K., and Gresswell, R., 2017, The waterfall paradox: How knickpoints disconnect hillslope and channel processes, isolating salmonid populations in ideal habitats: Geomorphology, v. 277, p. 228–236, doi:10.1016/j.geomorph.2016.03.029.

McDougall, I., 1979, Age of shield-building volcanism of Kauai and linear migration of volcanism in the Hawaiian island chain: Earth and Planetary Science Letters, v. 46, p. 31–42, doi:10.1016/0012-821X(79)90063-3.

Moore, J.G., Clague, D.A., Holcomb, R.T., Lipman, P.W., Normark, W.R., and Torresan, M.E., 1989, Prodigious submarine landslides on the Hawaiian Ridge: Journal of Geophysical Research: Solid Earth, v. 94, p. 17465–17484, doi:10.1029/JB094iB12p17465.

Neely, A.B., and DiBiase, R.A., 2020, Drainage Area, Bedrock Fracture Spacing, and Weathering Controls on Landscape-Scale Patterns in Surface Sediment Grain Size: Journal of Geophysical Research: Earth Surface, v. 125, p. e2020JF005560, doi:https://doi.org/10.1029/2020JF005560.

Ortega, J.A., Wohl, E., and Livers, B., 2013, Waterfalls on the eastern side of Rocky Mountain National Park, Colorado, USA: Geomorphology, v. 198, p. 37–44, doi:10.1016/j.geomorph.2013.05.010.

Prancevic, J.P., and Lamb, M.P., 2015, Unraveling bed slope from relative roughness in initial sediment motion: Journal of Geophysical Research: Earth Surface, v. 120, p. 474–489, doi:10.1002/2014JF003323.

Rossi, M.W., Whipple, K.X., and Vivoni, E.R., 2016, Precipitation and evapotranspiration controls on daily runoff variability in the contiguous United States and Puerto Rico: Journal of Geophysical Research: Earth Surface, v. 121, p. 128–145, doi:10.1002/2015JF003446.

Scheingross, J.S., and Lamb, M.P., 2017, A Mechanistic Model of Waterfall Plunge Pool Erosion into Bedrock: Journal of Geophysical Research: Earth Surface, v. 122, p. 2079–2104, doi:10.1002/2017JF004195.

Scheingross, J.S., and Lamb, M.P., 2021, Mass balance controls on sediment scour and bedrock erosion in waterfall plunge pools: Geology, doi:10.1130/G48881.1.

Schwanghart, W., and Scherler, D., 2020, Divide mobility controls knickpoint migration on the Roan Plateau (Colorado, USA): Geology, doi:10.1130/G47054.1.

Seidl, M.A., Dietrich, W.E., and Kirchner, J.W., 1994, Longitudinal profile development into bedrock: An analysis of Hawaiian channels: Journal of Geology, v. 102, p. 457, doi:10.1086/629686.

Sklar, L.S., and Dietrich, W.E., 2001, Sediment and rock strength controls on river incision into bedrock: Geology, v. 29, p. 1087–1090, doi:10.1130/0091-7613(2001)029<1087:SARSCO>2.0.CO;2.

Stock, J.D., and Montgomery, D.R., 1999, Geologic constraints on bedrock river incision using the stream power law: Journal of Geophysical Research: Solid Earth, v. 104, p. 4983–4993, doi:10.1029/98JB02139.

Whipple, K.X., DiBiase, R.A., Crosby, B., and Johnson, J.P.L., 2022, 6.40 - Bedrock Rivers, *in* Shroder, J. (Jack) F. ed., Treatise on Geomorphology (Second Edition), Oxford, Academic Press, p. 865–903, doi:10.1016/B978-0-12-818234-5.00101-2.

Yang, R., Willett, S.D., and Goren, L., 2015, In situ low-relief landscape formation as a result of river network disruption: Nature, v. 520, p. 526–529, doi:10.1038/nature14354.

CHAPTER 3

LIMITS TO KNICKZONE RETREAT AND BEDROCK RIVER INCISION

ABSTRACT

Knickzones, defined here as a waterfall or an oversteepened reach encompassing a series of waterfalls, are intriguing landforms that are commonly thought to record landscape disequilibrium and are often associated with rapid incision and knickzone retreat following base-level fall. However, knickzones can also be persistent and stable features that record threshold conditions limited by a channel's ability to incise through resistant rock. Determining controls on these endmember behaviors offers significant insight into the role of knickzones and rivers in shaping landscapes. Knickzones on the Hawaiian Islands exhibit evidence of both behaviors. Topographic analysis shows that the transition between fluvial hanging valleys, where a stream remains elevated above the stream junction or coastline, and knickzones that have retreated or formed upstream of their outlet (i.e. upstream knickzones) can be defined by a range of catchment sizes from ~0.5 to 6 km^2. This transition is present on all of the volcanoes in our analysis whether or not significant base-level fall (i.e. coastal erosion or landslides) has occurred and there is no clear influence of volcano age on drainage area above knickzones. To explain these observations, we hypothesize that knickzones on the Hawaiian Islands represent a physical limit on a stream's ability to detach and transport jointed bedrock or large boulders. Specifically, we posit that knickzones at threshold conditions represent a location in the landscape where even the largest effective floods are unable to alter the gradient of the channel to further drive bedrock incision. That is knickzones should form or stabilize where $\omega_m \leq \omega_c$, where ω_m is the unit stream power associated with the

maximum possible flood size and ω_c is a critical unit stream power. To test this hypothesis, we developed a power-law relationship of a maximum observed flood envelop with drainage area from both global and Hawaiian flood records to set an upper boundary on ω_m. Using this estimate of a maximum possible flood, including a change in the power-law exponent at ~ 2km^2 , we calculated ω_m for all upstream knickzones and found that the drainage area above knickzones is well described by theoretical predictions of $\omega_m \leq \omega_c$ where $\omega_c \approx 23$ kW/m^2. The influence of climate on knickzones is limited with only a weak dependence of drainage area above knickzone on mean annual rainfall. Similarly, only knickzones on Kaua‘i exhibit a statistically significant inverse correlation of ω_m with mean annual rainfall. Importantly our findings indicate a limit to knickzone retreat and bedrock river incision with a clear dependence on channel gradient upstream of knickzones.

INTRODUCTION

Bedrock rivers at steady-state have smoothly concave longitudinal profiles, with channel steepness adjusted to prevailing lithologic, climatic, and tectonic conditions (Whipple et al., 2021). Waterfalls are intriguing features in landscapes as they represent a clear departure from the steady-state profile. The presence of a waterfall or a series of waterfalls, defined here as a knickzone, is often interpreted as evidence for a transient response to abrupt base-level fall (e.g. Hayakawa and Matsukura, 2003; Mackey et al., 2014; Seidl et al., 1994). However, knickzones can exhibit a wide range of contrasting behavior (DiBiase et al., 2015) and may also be stable and anchored by resistant rock and thresholds in bedrock incision (Crosby and Whipple, 2006; Kirby and Whipple, 2012;

Ortega et al., 2013, Raming and Whipple, 2022). Determining when and where transient and stable knickzones form remains an outstanding problem with important implications for understanding how bedrock rivers shape landscapes.

The ability to distinguish between transient and stable knickzones is often obscured by limited evidence that can support multiple hypotheses. Only when there is direct observational evidence of knickzone retreat (Cook et al., 2013; Anton et al., 2015) is transient behavior clearly demonstrated. In lieu of direct observational evidence, knickzone retreat rates can be estimated from former knickzone positions (Baynes et al., 2015), however, this evidence is not free from uncertainty. In most cases, evidence of knickzone retreat is altogether absent and the only available data are the current locations of knickzones and estimates of timing and location of base-level fall. To plausibly explain for the distances knickzones have retreated, most studies employ numerical models that explain knickzone position as a function of drainage area (e.g. Berlin and Anderson, 2007; Bishop et al., 2005; Brocard et al., 2016; Crosby and Whipple, 2006; Hayakawa and Matsukura, 2003; Schwanghart and Scherler, 2020; Shelef et al., 2018). However, drainage area is strongly correlated with stream length (Hack, 1957; Morisawa, 1962) and actively retreating knickzones can be indistinguishable from knickzones that stall or form at a threshold drainage area (Crosby and Whipple, 2006).

Indeed, physical explanations for knickzone retreat and formation are numerous and provide a simple explanation for the development and stabilization of knickzones. Knickzones can approach or form at a threshold state due to conditions at or above the knickzone and are dependent on rock mass properties and the mechanisms of knickzone retreat (Gardner, 1983). In jointed bedrock a threshold shear stress must be exceeded to

initiate toppling or plucking at the lip of the waterfall (Lamb and Dietrich, 2009; Dubinski and Wohl, 2013; Lamb et al., 2015). In homogenous unjointed bedrock, plunge pool mechanics can drive knickzone retreat and are dependent on thresholds in sediment supply and thresholds for initiating sediment motion (Scheingross and Lamb, 2017, 2021). Similarly, threshold conditions leading to the development of fluvial hanging valleys, where a stream remains elevated above the stream junction or coastline, possibly arise where the processes of saltation and abrasion (Sklar and Dietrich, 2004) develop a negative feedback through over-steepening of the river channel (Wobus et al., 2006; Crosby et al., 2007; Goode and Burbank, 2009). Even when fluvial processes are not the dominant mechanisms of retreat (Weissel and Seidl, 1997), flows must still exceed the threshold of coarse sediment entrainment below the knickzone to maintain knickzone form and allow knickzone retreat (Howard and McLane III, 1988; Lapotre and Lamb, 2018; Ryan and Whipple, 2020).

Clearly, mechanisms that can explain knickzone retreat and formation depend on the physical thresholds related to a stream's ability to detach and transport bedrock material. Though these mechanisms differ in detail they all depend on flood discharge and most mechanisms depend on channel gradient above the knickzone. Consequently, at the spatial and temporal scale of landscape evolution, threshold conditions for knickzone formation and/or cessation of knickzone retreat may be simply represented by a critical unit stream power (e.g. Magilligan, 1992). To explore this possibility, we focus on the knickzones of the Hawaiian Islands. Hawaii is well suited to the study of knickzone behavior (Seidl et al., 1994; Lamb et al., 2007; Mackey et al., 2014; Raming and Whipple, 2022) because knickzones are found across a wide range of conditions from

steep to shallow volcano slopes (Rowland and Garbeil, 2000), from dry to wet climates (mean annual rainfall from <1 m/yr. to +9m/yr.; Frazier et al., 2016), and in areas that have experienced a wide range of base-level conditions. Using the Hawaiian Islands as a natural experiment we pose the hypothesis that: if a threshold drainage area is a consequence of physical limits in bedrock incision and knickzone retreat, then knickzones should form at or below the conditions where a maximum unit stream power (ω_m) is less than or equal to a critical unit stream power (ω_c). To test this hypothesis, we first establish that knickzone locations appear to be well explained by a threshold drainage area and consequently flood size. In order to maintain a constant stream power channels steepen upstream to accommodate a reduction in floods size associated with a decrease in drainage area. However, if a knickzones is stabilized over long periods of time this suggests that not even the largest floods are capable of modifying the channel gradient above the knickzone. To explore if this is possible we introduce the concept of a maximum unit stream power informed by estimates of the World's maximum observed flood envelope and from local stream gauges on the Hawaiian Islands. Results from this analysis show that the majority of knickzones, whether they are fluvial hanging valleys or exhibit evidence of upstream retreat, can be described by the threshold conditions $\omega_m \leq \omega_c$ with a mean value of 22.8 kW/m^2 for ω_c and importantly can explain where knickzones stall or form in the landscape.

FIELD SETTINGS

Shield Volcanoes on The Hawaiian Islands

The Hawaiian Islands are the youngest portion of the Hawaiian-Emperor

seamount chain (Macdonald et al., 1983) resulting from the migration of the pacific plate over the Hawaii hotspot (Jackson et al., 1972). The Hawaiian islands range in age from ~6 Ma to ongoing shield building off the western end of Hawai'i (Fig. 3.1; Sherrod et al., 2021). Individual shield volcanoes are built through a sequence of pāhoehoe, ʻaʻā, and transitional lava flows varying in thickness and spatial extent (Katz and Cashman, 2003). Volcano gradients range from less than 8%, due to ponded lava, to 17-21% along rift zones axes, and slopes as steep as 70% can be found along constructional flanks (Rowland and Garbeil, 2000). Approximately 80-95 percent of a volcano's volume is emplaced during the shield building stage (Clague and Sherrod, 2014) resulting in significant isostatic subsidence (exceeding 3 mm/yr, Huppert et al., 2015). This period is followed by the post-shield stage, which is characterized by a graduated change in the chemical composition of lava flows (Clague and Sherrod, 2014) with smaller eruptions of ʻaʻā flows occurring from local vents and cinder cones (e.g. Sinton et al., 2017). At this point in the evolution of a volcanic island, subsidence has significantly decreased and is followed by a period of marginal uplift sustained by the flexural uplift from nearby shield building. Migrating past the flexural bulge, the final stage of a volcanic island is characterized by slow thermally driven subsidence (Huppert et al., 2015).

Variability in rock mass properties between lava flows and lava flow types is significant. Lava flows on the Hawaiian Islands are generally classified by the endmember lava flows: ʻaʻā and pāhoehoe (Wentworth and Macdonald, 1953). Pāhoehoe flows are less viscous, tend to produce thinner layers (less than a meter to only a couple of meters) and are characterized by a ropey bulbous texture (Wentworth and Macdonald, 1953). Conversely, ʻaʻā flows tend to be more viscous and produce thicker layers ranging

from centimeters to 10s-of-meters thick (Wentworth and Macdonald, 1953; Macdonald et al., 1960; Sinton et al., 2017). The interior of ʻaʻā flows are characterized by a massive and dense core with a rubbly and clastic exterior typically denoted as clinker (Harris et al., 2016). The spatial distribution of these flow types tend to vary with topography and proximity to vents and rift zones (Holcomb, 1987). Typically, ʻaʻā flows are associated with steeper regions of a volcano, areas affected by post-shield stage events, and in regions distal to the main caldera (Katz and Cashman, 2003). Likewise, pāhoehoe flows are found in less steep regions and are associated with the shield building stage (Katz and Cashman, 2003). Importantly, the different flow types (including the difference between clinker and the interior of ʻaʻā flows) exhibit a wide range of rock mass properties that influence the overall rock quality (e.g. Okubo, 2004), their susceptibility to weathering and mass failure (Porder et al., 2007; Voigtlander et al., 2018), and bedrock river incision (Raming and Whipple, 2022).

Climate varies considerably across the islands and though the magnitude of mean annual rainfall has likely changed through time (Hotchkiss et al., 2000) orographic rainfall patterns driven by the trade winds have remained stable (Gavenda, 1994; Ferrier et al., 2013b). Prominent rainfall gradients on Kaua'i and Kohala have been used to test and identify the influence of climate on weathering in bedrock channels (Murphy et al., 2016) and on setting the time averaged rates of bedrock incision (Ferrier et al., 2013a). Beyond bedrock channels, weathering has been shown to be an important form of denudation on the Hawaiian Islands (Li, 1988). Weathering increases with volcano age and a stepwise increase in weathering intensity is present above a climatic threshold where mean annual rainfall exceeds potential evapotranspiration (Chadwick et al., 2003)

but appears to be insensitive to further increases in precipitation (Porder et al., 2007; Voigtlander et al., 2018).

Volcanoes with No Significant Base-level Fall

East Molokaʻi, West Maui, and Lānaʻi, are all a part of the Maui-Nui Complex and prior to rapid subsidence where all connected sub-aerially (Fig. 3.2; Price and Elliott-Fisk, 2004). The southern flank of East Molokaʼi, West Maui, and the east side of Lānaʻi have not experienced flank collapse and are mostly protected from coastal erosion. Subaerial shield building for East Molokaʻi began around 1.75 Ma followed by a transition to the post-shield stage at around 1.49 Ma which was active until 1.35 Ma (Sherrod et al., 2021). Shield building on West Maui is thought to begin as early as 2 Ma with a transition to the post-shield stage from 1.3 to 1.1 Ma (Sherrod et al., 2021). The age of Lānaʻi is less constrained, but a weighted average of radiometric ages suggest Lānaʻi is similar in age to West Maui at ~1.3 Ma (Sherrod et al., 2021).

Volcanoes with Significant Base-level Fall

Shield building on the Kohala peninsula of Hawaiʻi (Fig. 3.3) may have begun as early as 1 Ma, however, exposed lava flows are all younger than 0.78 Ma (Sherrod et al., 2021). The shield building stage is represented by Pololū volcanics ranging in age from 0.45 to 0.32Ma. Hāwī volcanics are associated with the post-shield stage with the majority of flows dating from 0.26 to 0.14 Ma and the youngest flows dating to 0.12Ma (Sherrod et al., 2021). Anomalously high sea-cliffs are present along the north east coast of the Kohala peninsula and likely represent the head scarp of the Pololū slump—a large

landslide that extended 20km wide and travelled over a distance of 130km (Fig. 3.1, Moore et al., 1989). The volcanic terrace of Kohala which defines the boundary between the subaerial and submarine stage of shield building resides 1km below sea level (Moore and Clague, 1992) and is cut by the Pololū slump whereas the younger Mauna Kea Volcanic terrace at 450 m below sea-level overlays the Pololū slump (Lamb et al., 2007). Lamb et al (2007) used this evidence as well as current subsidence rates to estimate the age of the volcanic terraces and constrain timing of the Pololū slump, with the most probable timing of the slump bracketed between 0.39 to 0.17 Ma.

The northern flank of East Molokaʻi has a similar (Fig. 3.2 A), but older history of flank collapse. Concurrent with the transition to the post shield stage (~1.5 Ma) a significant portion of the northern half of East Molokaʻi collapsed, resulting in the Wailau landslide which was ~ 50km wide and sent debris more than 200km from the present shore line (Moore et al., 1989). Some ambiguity remains as to the nature of sea-cliffs bounding the Wailau landslide and whether they represent the original head scarp of the landslide (Satake et al., 2002) or alternatively record post landslide deformation (Clague and Moore, 2002). Addressing this question is outside the scope of this study but we assume that any significant events of base-level fall are associated with the timing of the Wailau landslide (ca. 1.5 Ma).

Kauaʻi is the oldest island in this study with construction of the main subaerial shield largely complete by 4 Ma (McDougall, 1979). We constrain our analysis to the western half of Kauaʻi which is dominated by the older shield and late shield flows (Fig. 3.4). Specifically we focus on the Nāpali coast, consisting of the Nāpali member (5.5-4 Ma) and the larger canyons draining the Olokele (~ 4Ma) and Makaweli (4-3.5Ma)

members of the Waimea canyon basalts (Fig. 3.3; Sherrod et al., 2021). The extent and nature of base-level fall is less constrained on Kauaʻi than other islands but large landslides (Fig 3.1.) are thought to have occurred shortly after shield building along the Nāpali coast (Moore et al., 1989). The Nāpali coast has also experienced significant base-level fall due to coastal erosion with the majority of erosion occurring prior to 2Ma (Seidl et al., 1994; Hearty et al., 2005; Mackey et al., 2014). The southern flank of Kauaʻi also experienced significant landslide event(s) but a thick accumulation of sediment on the landslide runout suggest it is likely one of the oldest landslides on the islands (Moore et al., 1989). In our analysis we only focus on two rivers, the Waimea and Makaweli, that drain to the southern coast of Kauaʻi (Fig. 3.4). These rivers cut through the lava flows of the Makaweli member which due to their younger age likely occurred after the landslide, an interpretation that is reinforced by the observation that Makaweli flows appear to be graded to current sea-level (Macdonald et al., 1960). Consequently, we assume that knickzones on the Waimea and Makaweli rivers and their tributaries are not a result of significant base-level fall.

EVIDENCE FOR A THESHOLD DRAINAGE AREA

Empirical Identification of a Threshold Drainage Area

A natural and identifiable consequence of a threshold drainage area (A_c) can be described in the context of Hack's Law (Crosby and Whipple, 2006). Hack's Law is an empirical relation of stream length to drainage area, where the length of a stream (L) from the divide to a point downstream can be expressed as a power function of drainage area, $L = kA^h$ (Hack, 1957) where k and h are empirical coefficients. Furthermore, Hack's

law applies to any point within a catchment (Rigon et al., 1996) such that the distance (D) of a knickzone measured from the nearest tributary junction or outlet to the base of the knickzone can be expressed as,

$$D = kA^h - kA_c^h \qquad A > A_c, (1a)$$

$$D = 0 \qquad A \leq A_c, (1b)$$

where A is the total drainage area measured from the outlet or tributary junction and A_c is the threshold drainage area. Equation 1 presents two testable conditions for the presence of a threshold drainage area: Equation 1a shows that by using Hack's law, the distance a knickzone is from an outlet or junction should be equal to the difference between the predicted lengths using the catchment and threshold drainage area. Equation 1b predicts the development of fluvial hanging valleys for catchments at or below the threshold drainage area. Importantly, both conditions lead to clear testable hypotheses that can be directly assessed from the topography.

Topographic Analysis and Identification of Knickzones

To identify knickzones and the distance a knickzone is from an outlet or tributary junction we used an automated algorithm built on functions from TopoToolbox and MATLAB (Schwanghart and Scherler, 2014). For Kohala, East Moloka‘i, West Maui, and the majority of Kaua‘i we used a 10 m USGS digital elevation model (DEM). Along the western end of the Nāpali coast of Kaua‘i and Lāna‘i we used a resampled 5 m lidar-derived DEM (OpenTopography and Hawaii Statewide GIS Program: https://geoportal.hawaii.gov/pages/elevation-service). Stream networks were determined

with a minimum drainage area of 0.1 km^2 to capture the full extent of the channel network. From smoothed stream profiles (we used default parameter for the constrained regularized smoothing algorithm in TopoToolbox; Schwanghart and Scherler, 2017) we automatically identified knickzones using the knickpointfinder algorithm from TopoToolbox (Schwanghart and Scherler, 2020) with a tolerance value of 85. The tolerance value controls the sensitivity of the algorithm to changes in the concavity of the longitudinal stream profile, with higher tolerance values exhibiting less sensitivity. The upper limit of a knickzone was identified by the farthest upstream waterfall on a given stream. For knickzones on the Nāpali coast and East Molokaʻi a tolerance value of 85 excludes some knickzones. In these instances, we lowered the tolerance value to 25. To verify our approach, we manually reviewed each knickzone using the DEM and Google Earth. In a few cases, the upper limit of the knickzone appeared too far upstream or downstream, consequently we modified these knickzones by manually selecting the upper limit of the knickzone. Additionally, in some locations knickzones were not appropriately identified with a channel and were removed from the analysis. For 9 out of 89 knickzones in the Pololū region, the upper identified knickzone is more consistent with a slope-break knickpoint (Whipple et al., 2022) or there is clear break between an upper and lower knickzone. We classified these knickzones separately as complex knickzones (Fig. 3.3), as they may either record initial incision prior to the base-level fall associated with the Pololū slump or a propagation of incision upstream from the main knickzone.

The lower limit of a knickzone was automatically identified using the Pruned Exact Linear Time algorithm for identifying change points (Killick et al., 2012). The

algorithm identifies a change point in data if the sum of the cost functions used to fit the data plus a threshold value is less than the cost function for fitting the whole data set. The exact cost functions used depends on the metric of interest. Here we focused on changes in the mean of the channel gradient using a threshold of 0.1. Using this method, we identified the lower limit of the knickzone by the first change point that coincides with a mean channel gradient equal to or greater than 40%. We chose this value because sediment cover is inherently unstable above 40% (Prancevic et al., 2014; Palucis et al., 2018) and prone to in-channel debris flows, indicating bedrock should be perpetually exposed at gradients > 40%. Manual inspection confirms a consistent and accurate determination of the base of knickzones. Height and length of knickzones exhibit a clear positive correlation. To avoid introducing this correlation into our analysis, we measured D to the base of the knickzone. If the knickzone is located on the trunk stream, the retreat distance (D) was estimated from the outlet at or near the coast. Whereas knickzones located on tributaries D was measured as the distance from the base of the knickzone to the confluence with the next largest stream. In some instances, D falsely incorporated the valley width of the trunk stream, in which case we manually measured retreat distance from where the stream enters the main valley to the base of the knickzone. To test the predictions from Eqn. (1) we also determined Hack's law parameters k and h for each trunk stream. We fit a linear regression to the $\log_{10} A$ vs $\log_{10} L$ and used the averaged Hack's parameters from all regions (k = 1.7, h = 0.54).

Drainage area loss can have an important influence on knickzone retreat and development (e.g. Schwanghart and Scherler, 2020). Unfortunately, we cannot account for the magnitude or even the timing of drainage area loss for the majority of potentially

affected valleys. We did identify knickzones associated with upstream drainage area loss as indicated by wind gaps and abnormal catchment boundaries. In general, drainage area loss appears to be relatively small compared to the size of most catchments, however, evidence from West Maui suggests that drainage area loss in some regions may be comparable in magnitude to drainage area above knickzones. In locations with extensive faulting or strong contrasts in rock mass properties (i.e. valleys proximal to the caldera) it may be that the majority of drainage area loss occurred prior to the main phase of knickzone retreat and or bedrock incision, in which case the prior drainage area loss would have little bearing on our analysis. Conversely, drainage area loss that occurs after the majority of incision or retreat has occurred will introduce potential bias towards a perceived smaller drainage area at the knickzone. In spite of these challenges, in our analysis we choose to highlight valleys and knickzones that have likely experienced drainage area loss with different symbols on all plots as they do not affect our interpretations.

We also examine potential controls on the drainage area above knickzones (A_{kz}). We obtained catchment averaged estimates of mean annual rainfall (P) and potential evapotranspiration (PET) above knickzone using gridded data from the Rainfall Atlas of Hawaii (Giambelluca et al., 2012, 2014; Frazier et al., 2016). To capture the influence of volcano gradient on knickzones we reconstructed the surface of each volcano. To do this for each volcano we fit convex hulls to elevation contours spaced 50 m apart starting from 600 to 200m below sea level to the highest point on the volcano. For bathymetric data we used a 50 m resolution DEM obtained from the School of Ocean and Earth Science and Technology, University of Hawaii at Manoa

(http://www.soest.hawaii.edu/hmrg/multibeam/index.php). We used a thin plate spline to interpolate between the points extracted from the convex hulls. To estimate the gradient of the volcano above the knickzone (S_v) we then measured the gradient of the channel from a best fit linear regression of the extracted reconstructed elevation against current stream length for above the knickzone.

Results: Identification of a Threshold Drainage Area

We identified 316 knickzone across all of the regions analyzed. Of these knickzones about 2/3 (194) are hanging valleys with D = 0. However, there is some ambiguity between whether knickzones have retreated or formed upstream or if they are truly hanging valleys. In part this is due to natural variability in the planform geometry of canyons walls as some knickzones are clearly associated with a recessed portion of a canyon wall though it remains unclear if the recession reflects active knickzone retreat or just variability in rock mass properties or other possible controls. To deal with this variability we selected a cutoff value on D to identify fluvial hanging valleys. Visual inspection from plots of A vs D (Fig. 3.5) suggests a value of D = 500m is a reasonable criterion for distinguishing between knickzones that have either retreated or formed some distance upstream from a tributary junction or coastline from those that have not retreated at all (effectively D = 0). Consequently, we classified each knickzone as either a fluvial hanging valley if D <= 500m or as an upstream knickzone if D> 500m. With this cutoff in D the number of identified fluvial hanging valleys increased by 17% with 60% of additional hanging valleys below a value of D = 300 m. The transition in drainage area from fluvial hanging valleys to upstream knickzones is identified by an upper and lower

boundary (yellow box in Fig. 3.5), where the upper boundary is set by the largest drainage area of the observed fluvial hanging valleys and the lower boundary is set by the drainage area for the smallest upstream knickzone. We also compared A_{kz} from upstream knickzones to the transition between fluvial hanging valleys and upstream knickzones as shown by the histograms in Figure 3.5.

For regions without significant base-level fall, the transition from hanging valleys to upstream knickzone occurs between ~0.5 to 4.5 km^2 with drainage areas greater than 2 km^2 restricted to fluvial hanging valleys on Kaua‘i. Similarly, the majority of A_{kz} for upstream knickzones are below 1 km^2 and align with the transition from hanging valleys to upstream knickzones (Fig. 3.5A). The transition from hanging valleys to upstream knickzone in regions with significant base-level fall show a shift towards higher drainage areas (from 1 to 6.2 km^2) with A_{kz} for upstream knickzones mirroring an increase in drainage area (Fig. 3.5B).

We compare these data to theoretical predictions of D as a function of A using Equation (1a) and a range of threshold drainage areas (1, 2.5, 5 km^2). Consistent with the above results, upstream knickzones in regions without significant base-level fall tend to agree better with smaller predicted values of A_c, with the majority of knickzones well described by a value of $A_c < 1$ km^2 (Fig. 3.5A). In regions with significant base-level fall, upstream knickzones are better described by $A_c >= 2.5$ km^2 (Fig. 3.5B).

A comparison of A_{kz} across regions with and without significant base-level fall in conjunction with other potential controls such as volcano gradient and mean annual rainfall is shown in Figure 3.6. The median A_{kz} for upstream knickzones (shown by horizontal line in middle of boxplot) is similar in all regions affected by significant base-

level fall and independent of volcano age (Fig. 3.6A). Regions unaffected by base-level fall, however, show more variability in A_{kz} for upstream knickzones, with systematically smaller drainage areas for West Maui and the south flank of East Moloka'i. Notably there is no evidence that A_{kz} decreases with volcano age or time since base-level fall. Outliers, defined as a value that is more than 1.5 times the interquartile range, are more abundant for hanging valleys than upstream knickzones (Fig. 3.6B). Excluding outliers, drainage area distributions of hanging valleys are similarly independent of age and somewhat larger in areas affected by significant base-level fall (Fig. 3.6B). Hanging valleys in the Poloū region do show a systematic shift towards higher drainage areas, with all of the identified complex knickzones in the Pololū regions found above the 75th percentile.

Comparing volcano gradient measured above knickzones (S_v, Fig. 3.6C) shows that both West Maui and the south flank of East Moloka'i (where observed A_{kz} is notably reduced) are significantly steeper than other regions with a median gradient around 15%. Conversely, knickzones that are unaffected by significant base-level fall in Lāna'i and Kaua'i are notably less steep. The median volcano gradient for regions affected by significant base-level fall are roughly consistent around a gradient of 5-10% with the Pololū regions exhibiting relatively higher values. Mean annual rainfall (P) varies significantly within and between regions (Fig. 3.6D). Lāna'i is systematically drier than the other regions (< 1 m/yr), whereas the Pololū region is generally wetter, with most knickzones tightly clustered around a median value of 3.2 m/yr. Both Kaua'i and West Maui include a number of knickzones with mean annual rainfall rates in excess of 5 m/yr, but as a whole these regions cover a wide range in climate. We also tested for correlation between P, S_v, and A_{kz} across all regions using Kendall's rank correlation coefficient (τ)

which is a non-parametric statistical method for testing for correlation between ranked variables with sign of τ indicating a negative or positive correlation(Kendall, 1938). Values of τ between 0.1 and -0.1 indicate a weak or negligible correlation, and values above or below 0.3 or -0.3 are considered a moderate to fair correlation (Akoglu, 2018). Using the full set of knickzones we found virtually no correlation between A_{kz} and P (τ = 0.01) and between S_v and P (τ = 0.09), but we did find a negative correlation between A_{kz} and S_v (τ = -0.24). Excluding hanging valleys, we found better agreement between P and A_{kz} (τ = -.13, Fig. 3.7B) and S_v and A_{kz} (τ = -0.36, Fig. 3.7A).

LIMITS ON STREAM POWER AND CONDITIONS FOR THE FORMATION OF A THRESHOLD DRAINAGE AREA

From the above results there is no evidence of a systematic decrease in A_{kz} with island age and regions that have experienced significant base-level fall show on average larger values of A_{kz} than regions that have not experienced significant base-level fall. These findings suggest that rapid knickzone retreat in response to base-level fall is limited and that regardless of their origin, knickzones can stabilize through time. Though processes of slow knickzone retreat may still occur (e.g. DiBiase et al., 2015; Weissel and Seidl, 1997), our findings suggest that rapid bedrock river incision and knickzone retreat (e.g. Anton et al., 2015; Baynes et al., 2015; Cook et al., 2013; Lamb and Fonstad, 2010) are no longer operable in the majority of this landscape. Furthermore, evidence for a threshold drainage area is unambiguous, demonstrated by (1) the clear transition from hanging valleys to upstream knickzones, (2) the overlap of A_{kz} for upstream knickzones with this transition, and (3) the development of knickzones in regions without base-level

fall. Yet the outstanding questions remain: if knickzones are at a threshold drainage area, then why is the transition from fluvial hanging valleys to upstream knickzones defined by such a large range in drainage area (~0.5 to 6 km^2)? And why does A_{kz} cover an even larger range (~0.1 to 10 km^2)? An answer to these questions can be framed in terms of stream power. Though there is a wide range of A_{kz}, the above results indicate that there is potential tradeoff between slope and drainage area such that where knickzones form may be described by a constant critical stream power. Furthermore, because the majority of these knickzones have likely persisted for significant periods of time (upwards of millions of years) this suggests that even the largest floods, and subsequently the maximum possible stream power, cannot exceed this critical stream power. In the remainder of this section we explore whether this range of A_{kz} can be explained by the hypothesis that knickzones form or stall where the maximum unit stream power is less than or equal to the critical unit stream power.

Hypothesis: Threshold drainage area set by maximum and critical unit stream power

Cessation of knickzone retreat associated with thresholds in bedrock river incision and coarse sediment transport can be explained by a number of mechanisms (e.g. Lamb et al., 2007; Lamb and Dietrich, 2009; Scheingross and Lamb, 2021). Here we make a simplifying assumption that regardless of the mechanism, an effective threshold condition can be expressed in terms of a critical unit stream power (ω_c). Unit stream power (ω) is a proxy for expended energy in a uniform and steady flow (Annandale, 1995) and is defined as,

$$\omega = \gamma q S_c, (2)$$

where q is discharge per channel width, γ is the specific weight of water, and S_c is channel gradient. One major challenge in employing Equation (2) is that q is a stochastic variable. To address this challenge, we assume that there is a physical limit on flood size for a given drainage area. Under these conditions we hypothesize that knickzones form or stabilize where the maximum unit stream power (ω_m) set by the maximum flood size for a given channel gradient is less than or equal to ω_c. Alternatively, ω_m may represent an extreme flood event where the frequency of occurrence is vanishingly small.

Following this argument, we define the maximum unit stream power as:

$$\omega_m = \frac{\gamma Q_m S_c}{W_m}, (3)$$

where Q_m is the maximum discharge possible and W_m is the associated channel width. Unfortunately, we lack information on trends of channel width with drainage area above knickzones within this study area. Consequently, we rely on the general statistical relationship of width-area for bedrock rivers (Whipple et al., 2022), where $W \approx k_w A^b$, and k_w is 6 and b is 0.32 and we assume $W \approx W_m$. Similarly, Q_m can be expressed as $Q_m \approx k_q A^{cm}$ constrained by maximum observed flood records.

Using the above empirical relationships, knickzones at a threshold drainage can be described by the inequality,

$$\omega_c \geq \omega_m, (4),$$

which can be re-arranged to obtain a prediction for a threshold drainage area above knickzones, where

$$A_c \leq \left[\kappa \frac{\omega_c}{S_c} \right]^{\varphi}, (5)$$

and $\kappa = \gamma k_w / k_q$ and $\varphi = 1/(c_m - b)$. Equation (5) presents the predictions that a larger value of ω_c leads to a larger threshold drainage area and conversely steeper channel gradients above the knickzone result in a smaller threshold drainage area. Though ω_c , κ, and φ, are loosely constrained, A_{kz} and S_c can be directly measured from topography and we can evaluate whether the locations of knickzones on the Hawaiian Islands are consistent with these predictions.

Methods: Identifying Controls on The Maximum Unit Stream Power

Measurement of Channel Gradient

We identified a representative channel gradient above knickzones (S_c) by linear regression of channel elevation against distance over a reference length equal to 1.5 times the square root of the drainage area above the knickzone. We evaluated a number of other methods to measure channel gradient above knickzones, including algorithms that automatically identify representative channel gradients and employing a χ transform (Perron and Royden, 2013) to measure channel steepness. However, many of the stream profiles above knickzones exhibit considerable noise and deviate from typical concave profiles. To address these challenges, we found that a consistent method is to measure channel gradient over a length scale proportional to the square root of drainage area as proposed by Veneziano and Niemann (2000). To identify an appropriate scaling factor, where available, we compared measurements of S_c between lidar derived topography and a 10m DEM. We used a range of scaling factors from 0.75 to 1.5. Smaller scaling factors (<= 1) show a bias towards higher values of S_c when compared to the lidar-derived DEM. At gradients less than 15% this bias is minor with only slightly higher values predicted by

the 10m DEM, however, above a gradient of ~ 15% measured gradients from the 10m DEM are significantly higher (5% to 10%). Using a scaling factor of 1.5 reduces the differences between the gradient measured from the lidar and the 10m DEM, with a median difference of ~2%, and above gradients of 15% the difference is closer to 4%. A scaling factor of 1.5 is comparable to values reported for the coefficients used in Hack's law (e.g. Sassolas-Serrayet et al., 2018). Consequently, the channel gradients reported here are best interpreted as the average channel or valley gradient above the knickzone. Additionally, S_c is comparable to S_v, and produces similar results (Fig. 3.7A) suggesting that in spite of potential biases and uncertainties in S_c the overall results are robust.

Identifying a Maximum Flood Envelope Curve

The largest observable floods for Earth have been reported for drainage areas at ~1 km^2 and larger (Li et al., 2013). Records for maximum observable floods at small drainage areas are rare, however, for the coterminous United States, Costa (1987) documented and compiled a list of maximum observable floods for drainage areas down to 65 hectares. We used both records from Li et al. (2013) and Costa (1987) to develop a maximum flood envelope curve for drainage areas from 65 hectares to $4.6x10^6$ km^2. Previous work on the World's maximum observable floods (Herschy, 2002) report a change in the maximum discharge-area exponent, c_m, at 90 km^2, while Li et al. (2013) show a change at ~300 km^2 and Costa (1987) shows a change at 1000 km^2. Changes in c_m at smaller drainage areas are rarely documented, however, Costa's (1987) envelope curve shows a clear break at 2.2 km^2. Besides Costa (1987), the only other study that we found with evidence of a clear change in discharge area scaling at small drainage areas is from

Goodrich et al. (1997) where they show a change in the discharge-area exponent at ~ 1.8 km^2 for the 2-year and 100-year floods (estimated from the intersection of their reported best fit linear regression).

To effectively capture changes in c_m we used a Bayesian change point regression model (Lindeløv, 2020). We used the default priors for all parameters except for change points of c_m, where we used weakly informed priors with log-normal distributions centered at $2km^2$ and 460 km^2 with a standard deviation of one. We also compared the performance of our statistical model to a single change point model and to a two-change point model with only default priors. To test the veracity of our flood envelope and applicability to the Hawaiian islands we also extracted the maximum observed floods from stream gages used in regional flood frequency analyses (Oki et al., 2010).

Results: Conditions for The Formation of a Threshold Drainage Area

Estimates of a maximum flood envelope curve

Results from the Bayesian change point regression (Fig. 3.8) predict a change in c_m at ~$2km^2$ and ~391 km^2 with the highest posterior density interval, (HPDI, from 5% to 95%) from 1 to 3 km^2 and 254-629 km^2 respectively. Below 2 km^2 c_m is estimated at 1.15 with a HPDI of 1.10 to 1.2. Between $2km^2$ and 391 km^2 the best estimate for c_m is 0.69 with HPDI of 0.648 to 0.735. Above 391 km^2 c_m = 0.316 with HPDI of 0.294 to 0.338. The predicted intercept of the model is at 108 with HDPI of 93 to 126. Whether we used weakly informed or uniformed priors has little bearing on the reported values. We compared the predictive performance of a two change point model versus a one change point model using Leave One Out Cross Validation (Vehtari et al., 2017). The one-

change point model shows a significant decrease in the expected log point wise density (-45.8) and a difference of 8 for the standard error. These results suggest that the two-change point model considerably outperforms the single change point model.

Comparison of the maximum observed floods on Hawaii show agreement with our estimated global maximum flood envelope as all of the values are on or below the predicted limit on flood size (Fig. 3.8). The 1963 flood on the Wailua River on Kauaʻi and the 1965 flood on the Hālawa River on East Molokaʻi have been previously recognized as global maximum observed floods (Rodier and Roche, 1984; Herschy, 2002). In addition to these global extreme flood events, we also identified two maximum observed floods on Oʻahu that are located on the envelope curve for drainage areas below 2 km^2 (Fig. 3.8). These floods were both located on tributaries to the Waiheʻe stream on Oʻahu but one occurred in 1965 and the other in 1981. The remaining maximum observed floods on Hawaii show significant scatter with a tendency for wetter climates to produce larger observed maximum floods. However, when reviewing global maximum observed floods available evidence (Rodier and Roche, 1984), perhaps surprisingly suggests that mean-annual precipitation has little influence on maximum observed flood size (shown by colored circles in Fig. 3.8). This may be true on the Hawaiian Islands, at least on Kaua'i, as historical records show cyclones can make landfall on the dry leeward side of the island (Knapp et al., 2010).

Maximum Unit Stream Power and Predicted Versus Observed Trends in S_c vs A_{kz}

We estimated ω_m for upstream knickzones using the empirical relationship for Q_m identified in the previous section. Importantly, in order to avoid over exaggerating the

effects of drainage area below 2 km^2 we found it necessary to incorporate a change in the exponent c_m from ~ 1 to ~ 0.7 at 2 km^2. Our results show that ω_m can be approximated by a lognormal distribution with the mean of 22.8 kW/m^2 and a standard deviation of 13 kW/m^2 (Fig. 3.9). To test theoretical predictions of a threshold drainage area to trends in S_c vs A_{kz} we visually compared estimates of A_c (Eqn. 5) using a range of values for ω_c, informed by both our estimates of ω_m and by an independent reference where we determined ω_c using a constant dimensionless critical stream power of 0.1 (Parker et al., 2011) and a boulder diameter of 1.5 m. The boulder diameter of 1.5 m is based on field observations of the maximum mobile boulders in extreme floods on the islands of Maui which is described further in the discussion section. Trends of S_c vs A_{kz} for upstream knickzones can be well described by theoretical predictions of A_c using a range of values for ω_c (Fig 3.10). For hanging valleys, we found that ω_c equal to the mean value of ω_m for upstream knickzones (22.8 kW/m2) approximately satisfies the conditions that $\omega_m \leq \omega_c$ (Fig. 3.10 C). Notably, in the Pololū region, there are 12 hanging valleys and 2 upstream knickzones that greatly exceed the predicted estimate of A_c delineated by one standard deviation above the mean value of ω_m (solid black line in Fig. 10 B and D). These knickzones have the highest values of ω_m in this analysis and most of them correspond with previously identified complex knickzones.

We also evaluated whether a change in c_m or a constant c_m is more consistent with our data. A constant c_m (b = 0.32, c_m = 0.74; Li et al., 2013) predicts $\varphi \approx -2.3$ for all drainage areas. However, incorporating a change in c_m from 1.15 to 0.69 predicts that $\varphi \approx -2.7$ and $\varphi \approx -1.2$ above and below 2 km^2 respectively. Linear regression of the $\log_{10} S_c$ and $\log_{10} A_{kz}$ for upstream knickzones below 2km^2 shows a best fit slope (an

estimate of φ) of -.912 +- 0.278 ($R^2 = 0.46$), consistent with the expected value of -1.2 from the maximum flood envelope. We did not attempt to find the best fit for $\log_{10} S_c$ and $\log_{10} A_{kz}$ above $2km^2$ because our data is limited above this drainage area and the difference in predicted values of φ are relatively small.

Comparison of ω_m across all regions and base-level (Fig. 3.11) shows greater consistency from region to region and results from a Kruskal Wallis test on upstream knickzones (excluding Lānaʻi which has too small of a sample size and complex knickzones from the Pololū region) yield a p-value of 0.1912, indicating little to no evidence against the null hypothesis that the median values of ω_m for each region are described by the same underlying distribution. Although, knickzones with significant base-level fall on Kauaʻi do show an upward shift towards higher values of ω_m, which is attributed to the dryer knickzones along the western end of the Nāpali coast. Consequently, we also explored the possibility of an influence of mean annual rainfall (P) on estimates of ω_m. When grouped together there is no clear correlation between P and ω_m for upstream knickzones (Fig. 3.12A), nor for fluvial hanging valleys. However, when examining upstream knickzones on Kauaʻi and West Maui, regions with the most extensive range in P, we found opposing trends in the $\log_{10} P$ against $\log_{10} \omega_m$. For knickzones on Kauaʻi, there is a negative correlation of $\log_{10} P$ with $\log_{10} \omega_m$ (Fig. 12B), with a coefficient of -0.49 and an $R^2 = 0.21$. Conversely, West Maui shows a positive correlation of $\log_{10} \omega_m$ with $\log_{10} P$ (Fig. 3.12C), with a coefficient of 0.41 and an R^2 value of 0.20.

DISSCUSION

The range of threshold drainage area required to explain where a knickzone will stall or form is significant (Fig. 3.5) but can be explained by the important influence of channel gradient and its effect on maximum unit stream power. These factors show the differences in A_{kz} across the regions are reduced when framed in context of a maximum unit stream power (Fig. 3.11) and though evidence of ω_c is indirect, the conditions $\omega_m \leq \omega_c$ clearly explains the formation and preservation of fluvial hanging valleys when $\omega_c \cong 23$ kW/m^2 (Fig. 3.10B). For similar values of ω_c , upstream knickzones follow the predicted trend that $A_{kz} \propto S_c^{-\varphi}$, however, not all upstream knickzones must be at ω_c. This is demonstrated by the fact that a significant portion of upstream knickzones exceed $\omega_c \cong 23$ kW/m^2 (Fig. 3.10A), indicating that they may be approaching, but not necessarily at threshold conditions.

The conditions that $\omega_m \leq \omega_c$ for the development of a threshold drainage area appears relatively robust and exhibits predictive capacity. This is demonstrated by our analysis of the Pololū region, where there are a number of knickzones with values of ω_m that greatly exceed our estimates of ω_c and were previously identified as complex knickzones. These values of ω_m are clearly distinct (Fig. 3.10 B and D) and are explained by the parsimonious argument that active knickzones should be found in the youngest regions. Identifying the possibility of active knickzones in the Pololū region highlights the effective framework of using ω_m and ω_c to detect and delineate active from stable knickzones.

Critical stream power (ω_c) as identified in this study is broadly defined as the location in a stream where even the largest floods are unable to drive significant bedrock

incision. Undoubtedly, controls on sediment mobility and sediment flux exhibit an important control on ω_c, but other important controls such as rock mass properties (Raming and Whipple, 2022) may also be expressed in ω_c. At the level of landscape evolution this definition of ω_c is useful because it can be directly estimated from simple parameters and identified by hanging valleys. However, identifying ω_c using knickzones requires that there is significant evidence that the knickzones are indeed anchored at a threshold drainage area. In the case of Hawaii, this is unambiguous because (1) we observe knickzones that formed in the absence of significant base-level fall, (2) hanging valleys are prevalent even in regions without coastal erosion precluding the hypothesis that sea-cliff retreat rate exceeds knickzone retreat rate (Lamb et al., 2007; Limber and Barnard, 2018), and (3) A_{kz} appears insensitive to volcano age or timing of base-level fall. Furthermore, though autogenic or differential incision (e.g. Groh and Scheingross, 2021; Seidl et al., 1997) may explain why knickzones form in the absence of base-level fall, a threshold area provides a simple explanation for where they form. This argument is founded on (1) the clear dependence of knickzone location on drainage area, (2) the height of knickzones identified in this study are significantly larger than the height of reported autogenic knickzones (Groh and Scheingross, 2021), and (3) autogenic knickzones are usually attributed to feedbacks in fluid and sediment dynamics (Izumi et al., 2017), however, on the Hawaiian islands variability in lava flows is sufficient to explain where knickzones form or stall (Raming and Whipple, 2022).

Controls on ω_c

Here we have considered ω_c in the broadest terms possible. Yet it's important to understand the underlying controls on ω_c to further develop testable hypotheses at a reach and field scale and to understand the conditions where ω_c may not be reflective of fluvial processes (e.g. mass wasting). From our observations we know incision can still occur above knickzones, suggesting other processes such as debris flows, weathering, and intrinsic controls such rock mass properties including its influence on latent grain size (Neely and DiBiase, 2020; Verdian et al., 2020) can also play an important role in determining ω_c. In the following sub-sections, we discuss in detail controls on ω_c, the potential influences of rock-strength and climate on ω_c, and conditions where $\omega_m \geq \omega_c$.

Mechanisms

In regions where lava flows are reasonable jointed, ω_c may be explained by the expended energy required to drive toppling or plucking (Lamb and Dietrich, 2009; Dubinski and Wohl, 2013). However, these conditions reflect local processes and if they are present are indirectly captured by our analysis since we used averaged estimates of channel gradient which cannot fully resolve the presence of a drawdown zone let alone conditions at the lip of a waterfall (e.g Haviv et al., 2006). Channel gradient and volcano slope are well correlated ($\tau = 0.52$) such that processes of toppling and plucking, which are dependent on the dip of the bedrock, could be captured by our approach of measuring channel gradient. In this case we might expect ω_c to decrease with channel gradient, however, such an effect if present is not readily detectable. Additionally, field observation at the lips of knickzones along the Nāpali coast suggest that there is little

evidence of toppling at least without significant abrasion as joints appear to be rarely through going (Raming and Whipple, 2022).

Perhaps the simplest explanation is that ω_c is set by the power required to mobilize and transport coarse sediment necessary for driving bedrock incision and or knickzone retreat, whether by abrasion, plucking, or plunge-pool scour (e.g. Chatanantavet and Parker, 2009; Scheingross and Lamb, 2017). Under this assumption, we can determine the range of grainsizes that set a critical stream power comparable to our estimates of ω_m. Assuming a constant non-dimensional critical stream power of 0.1 (Parker et al., 2011; Prancevic and Lamb, 2015) our results of ω_m predict grain size diameters ranging from 1-4 meters respectively. Field observation suggest that values between 1-2 meters may be physically realistic. In 2018 a series of large storms generated extreme floods on the island of Maui. Discharges from these storms estimated in the valleys of Honokohau and Waihe‘e (Fig. 2) suggest flood sizes (345 m^3s^{-1} and 525 m^3s^{-1} respectively) approximately 1.5 times larger than the 100-year flood or approximately 50 to 70% of the estimated maximum observed flood size for the given drainage areas. In June of 2019, in both Honokohau and Waihe‘e, below the major knickzones in these valleys we identified the largest mobile boulders across a number of reaches. Evidence of boulder mobility included the presence of fresh woody debris pinned beneath boulders, precariously balanced and imbricated boulders, and lateral and mid channel bars consisting of recently deposited boulders. Selecting the 84th percentile from the set of largest mobile boulders yields a value of ~1.5m in diameter equal to a critical stream power of 13.6 kW/m^2 a value that roughly aligns with the mode of the distribution of ω_m (Fig. 3.9).

It is unclear, however, if conditions below knickzones are similar to those above knickzones. Observations from the field (Mackey et al., 2014, Raming and Whipple, 2022) and Google Earth do indicate that coarse sediment is abundant at least above some knickzones. Immobile coarse sediment can prevent bedrock incision (Shobe et al., 2018), thereby limiting an influx of sediment to incise bedrock and drive knickzone retreat. In most cases, however, there are detectable amounts of incision above knickzones such that initial pulses of erosion may have activated hillslopes (Roda-Boluda et al., 2018; Neely and DiBiase, 2020; Verdian et al., 2020) providing substantial sediment for tools and cover. On the other hand, these channels are likely dominated by weathering (e.g. Murphy et al., 2016) with any available coarse sediment derived from corestones (Wentworth, 1928; Voigtlander et al., 2018). Regardless, if a stream encounters rock resistant enough to form or stall a knickzone, signals of base-level wall will no longer be transmitted to the hillslopes above the knickzone which in turn will attenuate the supply of coarse sediment. This mechanism presents a potential positive feedback which only further hinders bedrock river incision (Brocard et al., 2016). Consequently, the distribution of resistant rock likely exerts a first order control on where knickzones stabilize and can indirectly influence ω_c.

Rock-Mass Properties

Previous studies of knickzone behavior on the Hawaiian islands have assumed that the variability in rock mass properties is so wide spread as to be inconsequential to the formation or stalling of knickzones (e.g.Seidl et al., 1994). Yet, field observations along the western end of the Nāpali coast (Fig. 3.4) show that knickzones are associated

with stronger and more resistant ʻaʻā lava flows (Raming and Whipple, 2022) reinforcing prior interpretations that knickzone formation is inherently dependent on the presence of resistant lava flows (Macdonald et al., 1983).

Because of this potential dependence on resistant lava flows, we expect that A_{kz} and ω_c should vary across the volcanoes studied according to their constructional history and the abundance of resistant lava flows and intrusive bodies. Indeed, all else equal the presence of particularly resistant rock should yield higher values of ω_c and thus larger threshold drainage areas (Raming and Whipple, 2022). Conversely, regions with weaker rock should yield smaller threshold drainage area and smaller values of ω_c. An apparent reduction in ω_c may also occur where mass wasting and other processes drive knickzone retreat (e.g. Shelef et al., 2018; Weissel and Seidl, 1997) and thus reduce A_{kz}.

Resistant ʻaʻā lava flows are more common in post-shield stage lava flows. Out of all the volcanos in our analysis, the post-shield stage lava flows on West Maui and East Molokaʻi are the most dominant (Clague and Sherrod, 2014). The post-shield stage on East Molokaʻi consists of ʻaʻā lava flows ranging upward of 20 to 30 meters thick with an accumulated thickness of 520 meters preserved on the summit and flanks of East Molokaʻi (Sinton et al., 2017). Whereas for West Maui the aggregate thickness of the post-shield flows typically are less than 80 meters, but in places may exceed 180 meters, and only cover a limited aerial extent mostly constrained to the north slope of the volcano (Sherrod et al., 2007). West Maui is also characterized by a relatively high prevalence of intrusive bodies found within the shield-stage strata including dikes, plugs, sills, and stock (Stearns and Macdonald, 1942). As noted in the section on Field Settings, ʻaʻā

flows are associated with steeper topography therefor the presence of resistant ‘a‘ā flows may be offset to some degree by the capacity to generate higher stream power.

Notably, however, the upstream knickzone on the Hālawa river on East Moloka'i is clearly associated with post shield flows, but at relative gentle gradient of 7.6% and has the 5th largest value of ω_m (48 kW/m2) for all upstream knickzones excluding the Pololū region. This estimate of ω_m is likely biased towards higher values as channel width as measured from Google Earth is 1.5 to 2 times larger than predicted by the empirical relationship of drainage area and bedrock channel width (Whipple et al., 2022). One possible explanation for the increase in channel width may be attributed to variability in rock mass properties. For example, where a river encounters the core of a resistant ‘a‘ā flow, the channel may preferentially widen in the weaker overlaid clinker that is often associated with ‘a‘ā flows. This effect may be especially pronounced where weathering along the channel margins amplifies lateral erosion rates (Small et al., 2015) and may also interfere with a channels ability to adjust it channel width and consequently shear stress at the lip of the knickzone (Baynes et al., 2018b).

On Kaua'i the post-shield stage is limited (Clague and Sherrod, 2014) to the Olokele and Makaweli members of the Waimea basalt. The Olokele member in particular is dominated by near horizontal flows that on average are 10m thick and can reach 30m thick (Macdonald et al., 1960). The Nāpali member, though part of the shield stage, equally consists of pāhoehoe and ‘a‘ā flows with locally thick bands of ‘a‘ā ranging from 1 to 3 m (Macdonald et al., 1960). Some of the higher value of ω_m in Kaua‘i maybe attributed to these thick resistant flows of the Olokele and Makaweli members or locally thick flows in the Nāpali member (Supplementary Fig. 3). However, climate may also

play an important role for the higher values reported in the Nāpali member as discussed in the following section. In contrast to the volcanoes with an abundance of resistant ‘a‘ā flows, Lāna‘i has the distinction of being one of the only volcanoes without a post-shield stage (Sherrod et al., 2021) and consists almost entirely of pāhoehoe flows (Stearns et al., 1940). In this case, the lower observed values of ω_m (Fig. 3.11) relative to regions with abundant ‘a‘ā flows may reflect a decrease in rock strength for pāhoehoe flows.

Climate

It may be reasonable to expect climate to exert an important control on where knickzones form and or stall, especially on the Hawaiian islands where the influence of climate on landscape evolution has been clearly demonstrated (e.g Ferrier et al., 2013a; Murphy et al., 2016). However, average climate conditions may not have much influence on knickzones that form under the conditions $\omega_m \leq \omega_c$ and thus reflect only the most extreme flood events. On Reunion island, a sub-tropical volcanic island with similar conditions to Hawaii, erosion is linked with cyclone-induced variability in rainfall, not mean annual rainfall (Gayer et al., 2019). Similarly, it may be the case that knickzones on the Hawaiian Islands are largely insensitive to climate because extreme flood behavior may not be correlated with mean climate conditions. Although trends in maximum observed floods on the Hawaiian Islands do appear to be sensitive to mean annual rainfall (Fig. 3.8) and in general wetter climates produce large floods for a given probability (Rossi et al., 2016), it remains uncertain if wetter climate produce larger maximum observed floods. The tendency for wetter areas in Hawaii to have larger maximum observed floods, may instead reflect a bias towards longer and better records in wetter

areas and the likelihood that wetter areas experience extreme floods more often. Notwithstanding this point, it is possible that wetter climates facilitate an apparent reduction in ω_c as mass failure in canyon walls and knickzones (White, 1949; Scott and Street, 1976; Jones et al., 1984) is accelerated and actively reduces drainage area. Additionally, in the case of upstream knickzones, we cannot fully rule out the possibility that they are still active. To the degree that this is true $\omega_m \leq \omega_c$ may not hold and there may be climate dependency on ω_m. However, for all regions there is only a weak dependence of A_{kz} on P (Fig. 3.7B) and no dependence of ω_m on P (Fig. 3.11A).

Only on Kaua'i and West Maui, where there is the largest range of mean annual rainfall above knickzones, are there detectable trends of ω_m with P (Fig. 11B and C). However, these trends are contradictory and only further confuses understanding of how climate might influence knickzone locations. Though the Nāpali member of the Waimea Basalt does have thick resistant bands of ‘a‘ā flows, these lava flows are not notably larger or thicker than the flows in the wetter regions of Kaua‘i that are associated with Olokele and Makaweli members of the Waimea Basalt. It maybe that a trend of ω_m with P is notable on Kaua‘i because knickzones on the western end of the Nāpali coast have a negative water balance (where P - PET <0) which limits the effects of chemical weathering (Chadwick et al., 2003; Porder et al., 2007). This seems like a more probable explanation, than a simple climate dependency on ω_m, as this trend is largely driven by a group of knickzones, with a negative water balance, on the western end of the Nāpali coast (Fig. 3.11B). Presumably, knickzone retreat through weathering and mass wasting is slow enough that these effects may not be detectable in younger regions.

Beyond these explanations, the lack of a clear climate signal preserved by knickzones is provocative given that the Hawaiian islands are often cited as prime location for understanding the role of climate in landscape evolution (Ferrier et al., 2013a; Murphy et al., 2016; Perron, 2017). Ostensibly, this expected signal of climate maybe partially obscured because we can only observe the conditions where knickzones are preserved. This would suggest that knickzones may present an inherent survival bias. In the case of Lānaʻi, which is dominated Pāhoehoe lava flows, a wetter climate would likely prevent the formation of knickzones or knickzones may be short lived and succumb to rapid weathering and collapse. This point is reinforced by the fact that knickzones are conspicuously absent where streams in wet environments have cut into the caldera complex (e.g. West Maui, East Molokaʻi; Fig. 3.2), which predominately consisting of breccias and dike swarms (Stearns and Macdonald, 1942) is presumably weaker rock. In juxtaposition, where knickzones are preserved in the wettest conditions they are associated with the most resistant lava flows. For example, knickzones in the Mt Wailele regions of Kauai, (with mean annual rainfall approaching 10 m/yr; Fig. 3.3) are found in the sub-horizontal and extremely thick flows of the Olokele member of the Waimea Basalt (Fig. 3).

CONCLUSIONS

Our results suggest that the majority of knickzones across the Hawaiian Islands are at a threshold drainage area predicted by conditions where estimates of maximum unit stream power (ω_m) is less than or equal to a critical stream power (ω_c). This is demonstrated by (1) the absence of an influence of island age on drainage area above

knickzones, (2) the development of knickzones in regions without significant base-level fall, (3) the strong dependence of drainage area above knickzones on channel gradient, and (4) the excellent agreement of hanging valleys with the condition $\omega_m \leq \omega_c$. However, this latter condition is not met in the Pololū region where identified complex knickzones clearly exceed ω_c which provides evidence of transient behavior consistent with the region's younger age. Physical explanations for ω_c, in the context of knickzones, is most simply explained by a stream ability to move coarse sediment but may also record information about dominant rock mass properties.

In identifying conditions required for ω_m our analysis shows a clear change in the behavior of the maximum observed discharge with drainage area. The maximum observed discharge, at and below 2km^2, is approximately linear with drainage area, implying a greater sensitivity to changes in drainage area. This behavior may be due to hydrometeorological controls on rainfall-runoff and extreme precipitation events. And though the behavior and speed of knickzone retreat could be sensitive to climate, to the degree that extreme precipitation events are not correlated with mean climate conditions, the location of stable knickzones may not show a clear climate dependence. Indeed, drainage area above knickzones is only slightly correlated with mean annual rainfall. In part this may be due to a survival bias caused by the tendency for knickzone to only be preserved in resistant rock. Only on the island of Kaua'i is there a decrease in ω_m with P, which may be explained by increased mass wasting over long-time scales (~ 4Ma) in regions with a positive water balance.

Importantly, our work here shows that knickzone are more than isolated instances of landscape disequilibrium. Rather they record important hydrometeorological limits with

significant relevance for understanding landscape evolution. Indeed, the presence of knickzones as stabilized features reflect the condition where the stream has failed to incise. Where this happens is inherently dependent on (1) controls on the channel gradient above the knickzone, (2) the maximum possible discharge, and (3) rock mass properties including controls on grain size. Application of the threshold framework developed here may help in further understanding the influence of hydrometrological controls on landscape evolution and the development and preservations of relict landscapes.

FIGURES

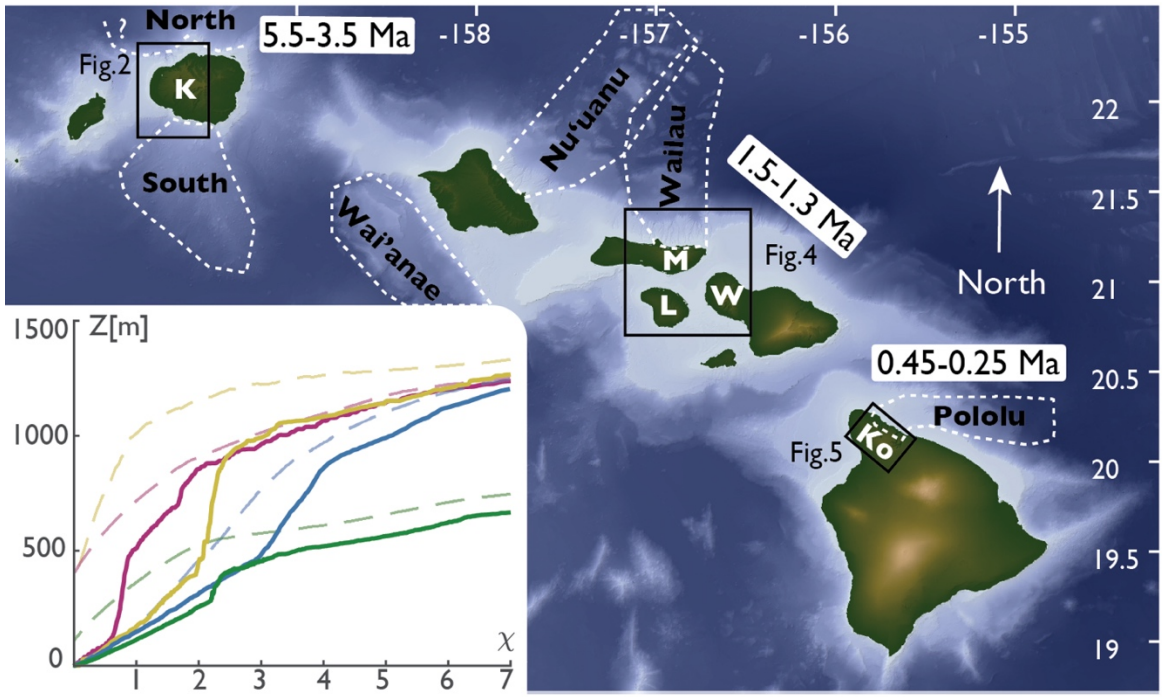

Figure 3.1. Hawaiian Islands and locations studied in Chapter 3. Regions are labeled by white bold letters (K: Kauaʻi , M: East Molokaʻi, W: West Maui, L: Lānaʻi, Ko: Pololū region on the Kohala Peninsula). Dashed white lines demarcate locations of large submarine landslides and are labeled with black bold font. Ages of volcanoes and landslides are shown adjacent to location. Inset plot shows chi-elevation profiles of select knickzones from the Pololū region (red), Lānaʻi (green), West Maui (blue), and Kauaʻi (yellow).

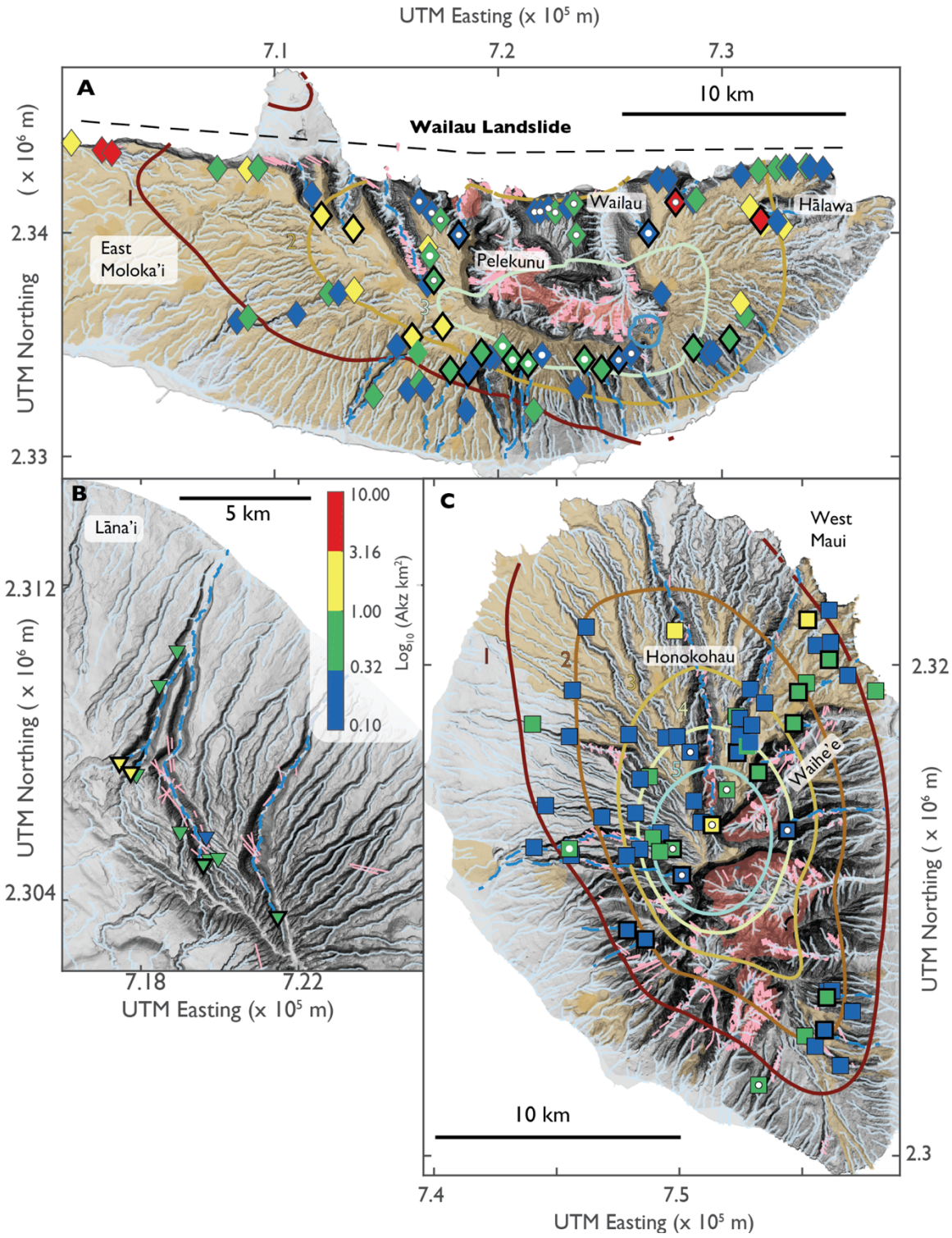

Figure 3.2. Location of Knickzones on Maui Nui: (A) East Molokaʻi (B) Lānaʻi , (C) West Maui. Markers, colored by the $\log_{10}$ of drainage area above knickzones in square kilometers, show the location of knickzones (Lānaʻi , downward pointing triangles; West Maui, squares; East Molokaʻi, Diamonds). Upstream knickzones, defined as knickzones

that have retreated more than 500 m upstream from nearest confluence of stream outlet are outlined in black. The remaining knickzones are defined as fluvial hanging valleys, where the stream network remains elevated above the nearest tributary junction or coast line (Crosby et al., 2007). Knickzones with potential drainage area loss are indicated with white dots. Dashed blue lines indicate the portion of the network associated with upstream knickzones. Colored solid lines are mean annual rainfall contours (m/yr). Pink lines indicate mapped dikes. Light brown region shows extent of post-shield stage flows. Light red regions indicate mapped caldera and dike complexes.

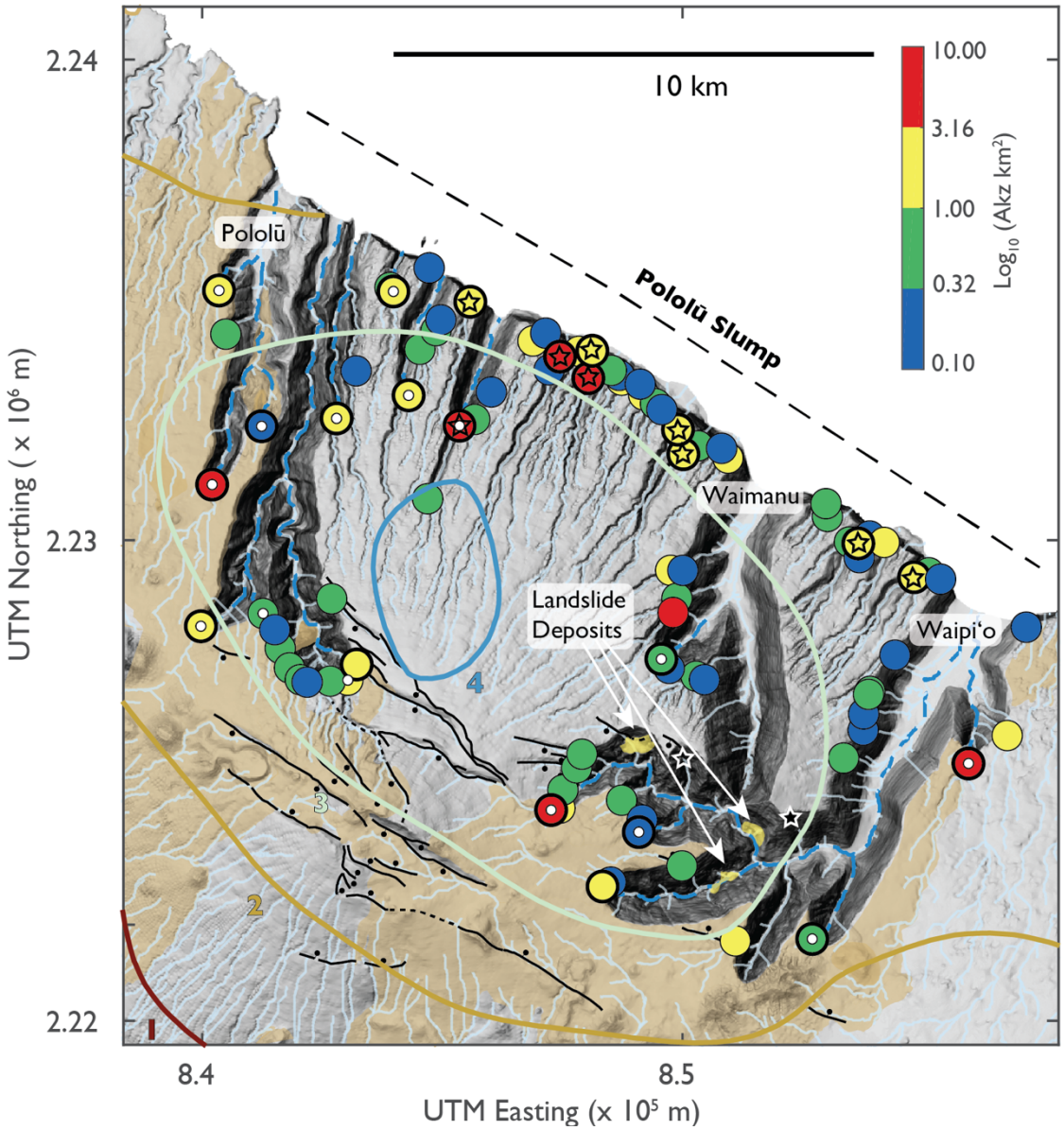

Figure 3.3. Location of Knickzones in the Pololū slump region on the Kohala Peninsula, Hawai'i. Circles indicate mapped knickzones and are colored by the $\log_{10}$ of drainage area above knickzones in square kilometers. Upstream knickzones are outlined in black. Black stars show location of complex knickzones. Knickzones with potential drainage area loss

are indicated with white dot. Colored solid lines are mean annual rainfall contours (m/yr). Dashed blue lines indicate the portion of the network associated with upstream knickzones. Colored solid lines are mean annual rainfall contours (m/yr). Light brown region shows extent of post-shield stage flows. Thin black line shows normal faults with ball and bar on downthrown block (Wolfe and Morris, 1996). White arrows show mapped landslides. White stars show small canyons that cut up-dip of the dominant slope of the volcano. Dashed line emphasizes coastal embayment associated with the Pololū slump.

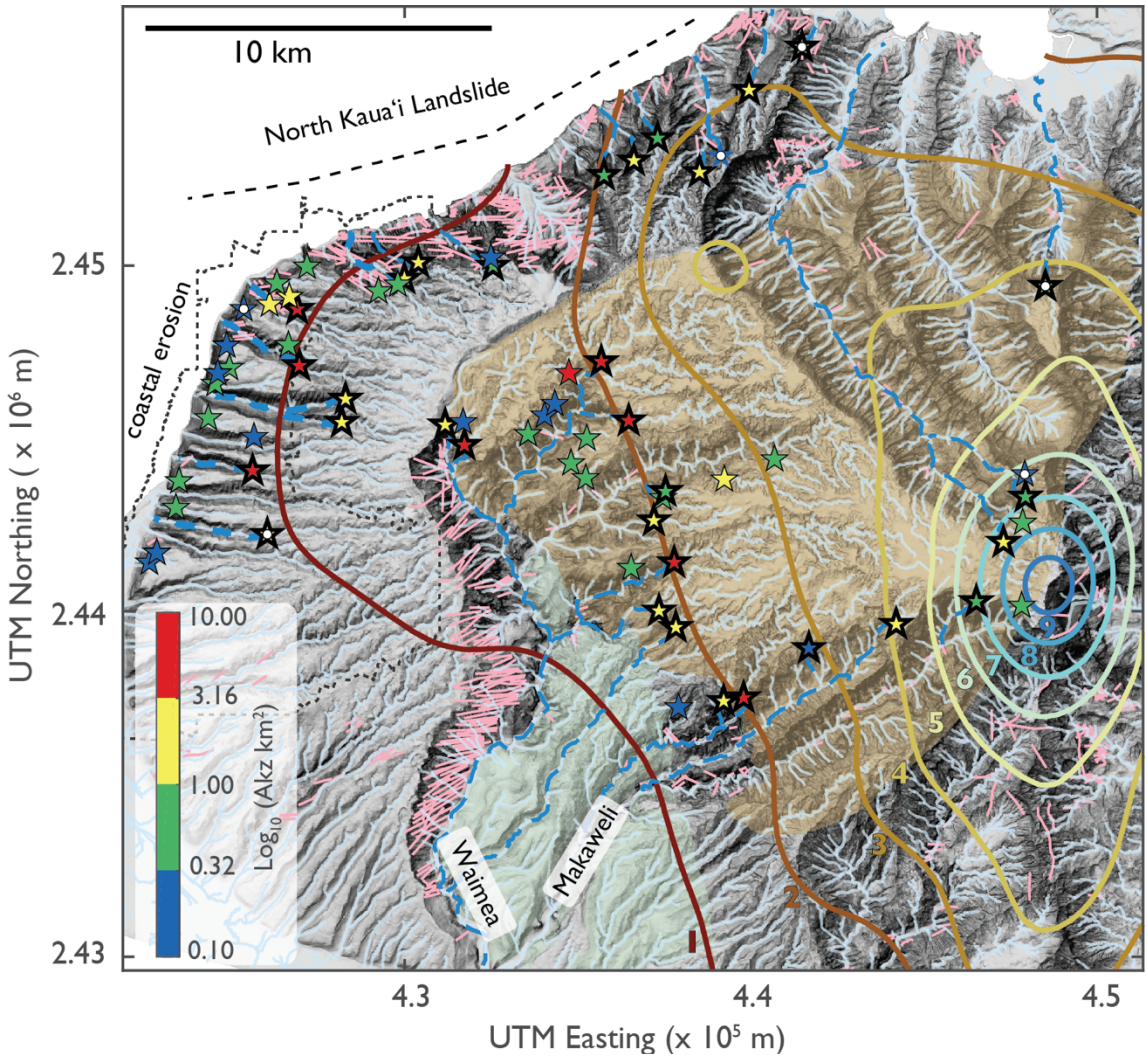

Figure 3.4. Location of Knickzones on Kaua'i. Stars indicate mapped knickzones and are colored by the $\log_{10}$ of drainage area above knickzones in square kilometers. Knickzones with potential drainage area loss are indicated with white circles. Dashed blue lines indicate the portion of the network associated with upstream knickzones. Colored solid lines are mean annual rainfall contours (m/yr). Dark gray dashed line shows extent of lidar used on the western end of the Nā Pali coast. Pink line segments indicated mapped

dikes, green region shows extent of the Makaweli Member of the Nāpali formation. Light brown region shows extent of the Olokele Member of the Nāpali formation.

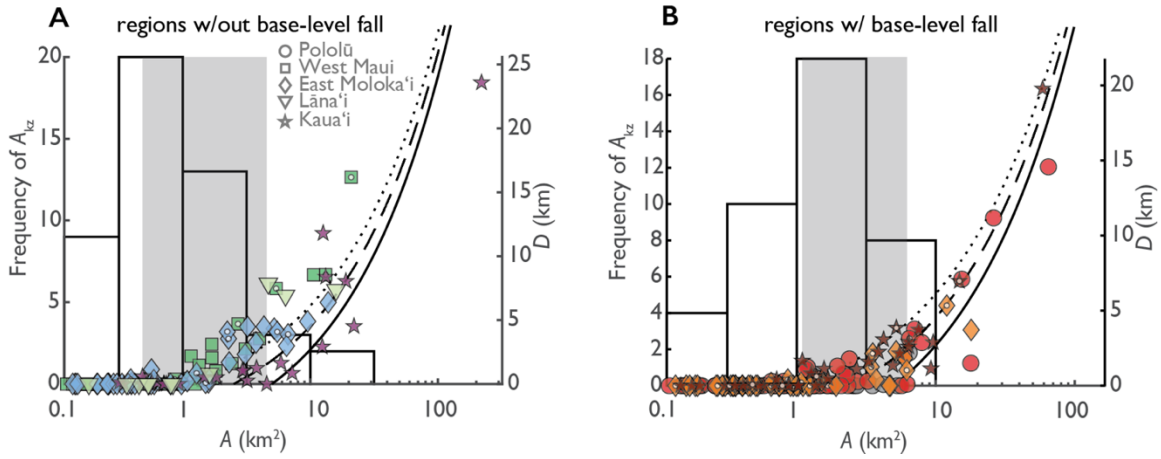

Figure 3.5. Evidence of a threshold drainage area. Scatterplots of total drainage area for each knickzone (A) vs distance from confluence or outlet (D, right y-axis). A and B show regions with and without significant base-level fall, respectively. Hanging valleys are defined as knickzones with values of D<= 0.5 km, while for upstream knickzones D is >0.5km. Gray vertical band indicates overlap between hanging valleys and upstream knickzones, with the lower boundary of box set by the smallest drainage area for upstream knickzones and the upper boundary set by the largest drainage area for hanging valleys. Histograms (with frequency on the left y-axis) show distribution of drainage area above upstream knickzones (A_{kz}). Gray circles in B show complex knickzones for the Pololū region. Note overlap between histogram peak and the transition between hanging valleys and upstream knickzones. Black line shows the predicted trend of a threshold drainage (Eqn. 1A), with solid, dashed, and dotted lines showing threshold drainage areas at 5 km^2, 2.5 km^2, and 1km^2, respectively.

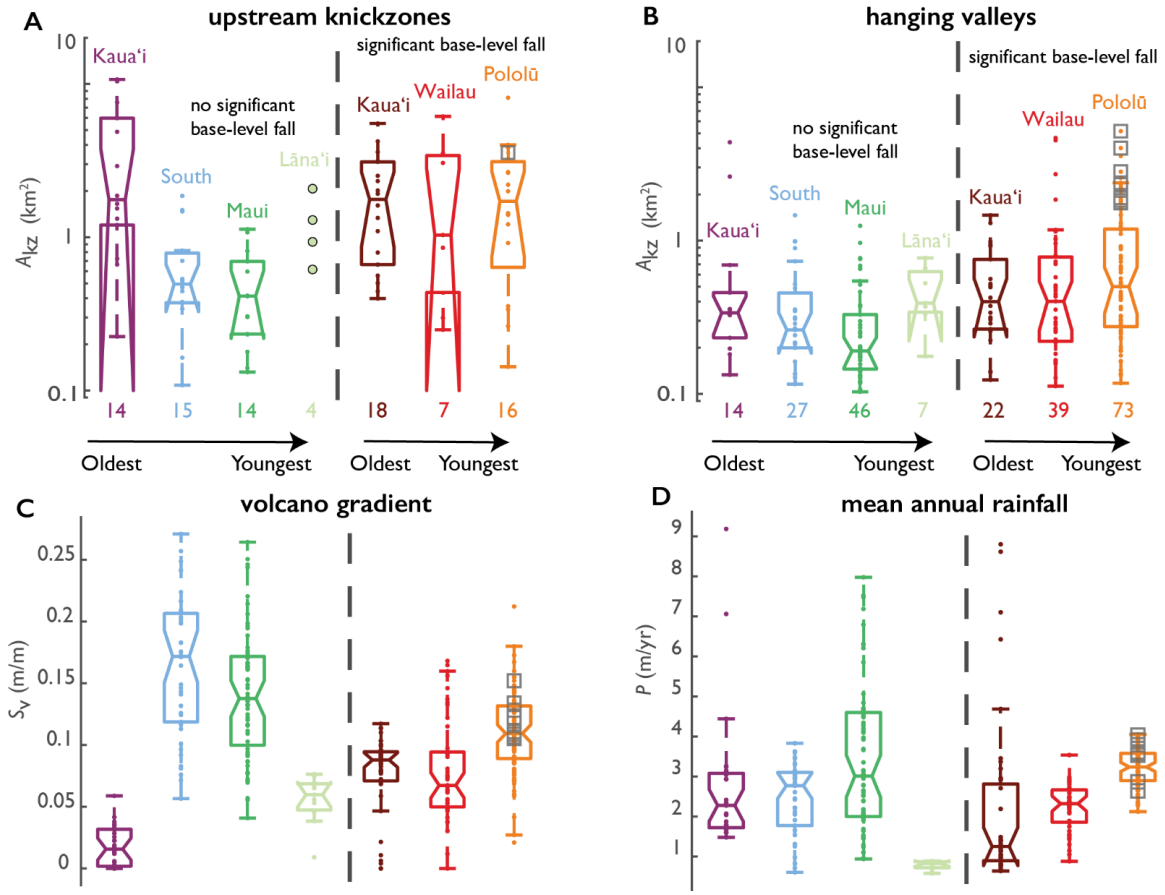

Figure 3.6. Boxplots of drainage area (A_{kz}), volcano gradient (Sv), and mean annual rainfall (P), above knickzones. A: upstream knickzones. B: Hanging valleys. C: volcano gradient. D: and mean annual rainfall. Numbers below boxplots indicate sample size. Gray squares for Pololū region indicate complex knickzones.

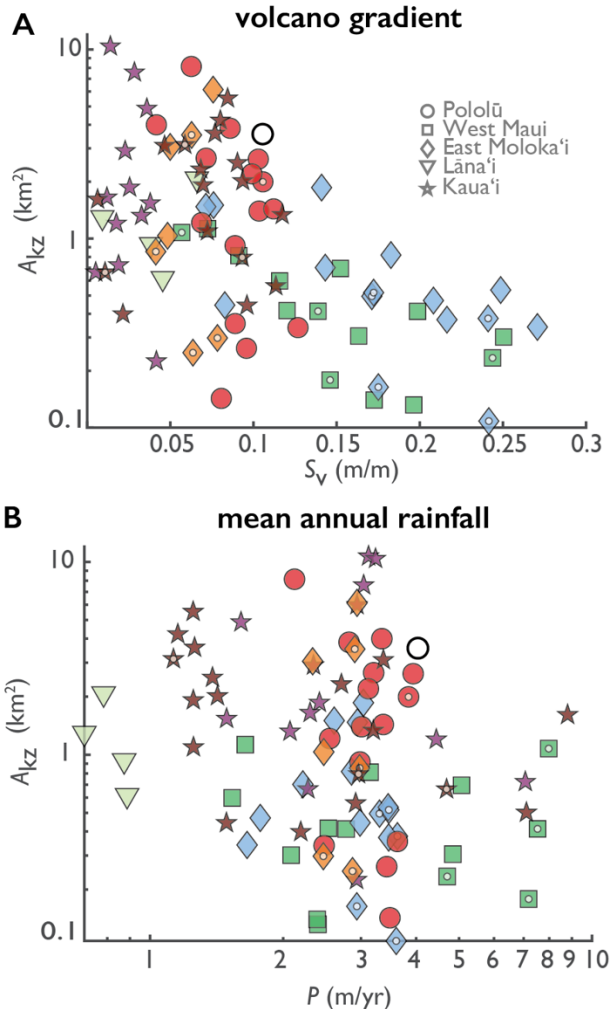

Figure 3.7. Influence of volcano gradient and climate on upstream knickzones. A: Scatterplot of drainage area above knickzones (A_{kz}) against volcano gradient (S_v). B: Scatterplot of A_{kz} against mean annual rainfall (P) for upstream knickzone. Open black circle shows complex knickzone in Pololū region.

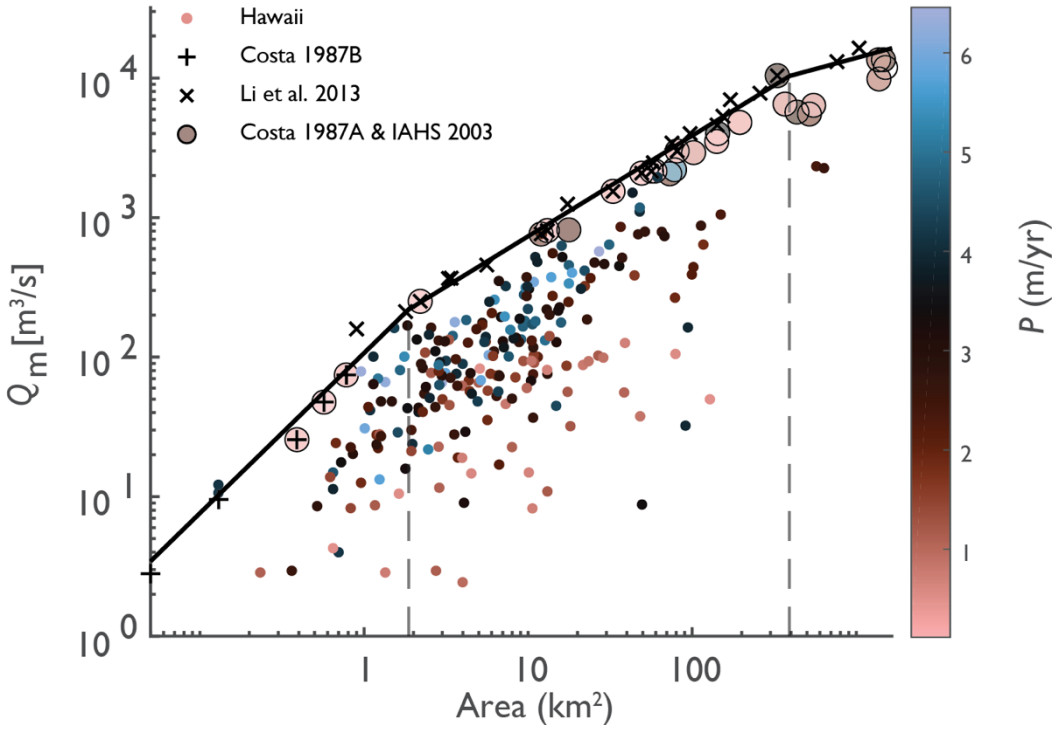

Figure 3.8. Envelope curve for maximum observed floods (Q_m). Data is from global (x, Li et al., 2013) and coterminous US (+,Costa, 1987) flood records. Black solid curve shows best fit line from multiple change point Bayesian regression with dashed vertical lines indicating location of change points centered at ~ 2 and 400 km^2 respectively. Dots show the maximum observed peak annual discharge for natural stream gages in Hawaii (same gages used in local flood regression from Oki et al., 2010). Circles are data from Costa, (1987a) and the International Association of Hydrological Sciences report on maximum observed floods (2003) colored by mean annual precipitation (P).

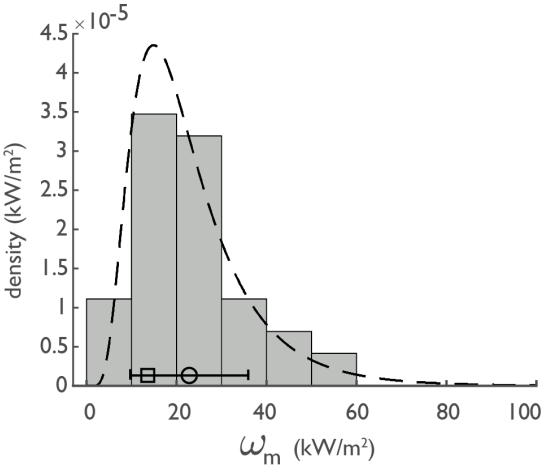

Figure 3.9. Histogram of maximum stream power (ω_m) above upstream knickzones. Data omits the Pololū region and uses a change in discharge-area scaling at ~ 2km^2 with a fitted log-normal distribution shown by the dashed black line. Circle shows the mean

(22.8 kW/m^2) of the log-normal distribution with error bars showing +- one standard deviation from the mean (10.2, 35.9, kW/m^2) . Square shows reference stream power of ~13.6 (kW/m^2) determined from field observations of boulder mobility in extreme conditions, see Discussion for more details.

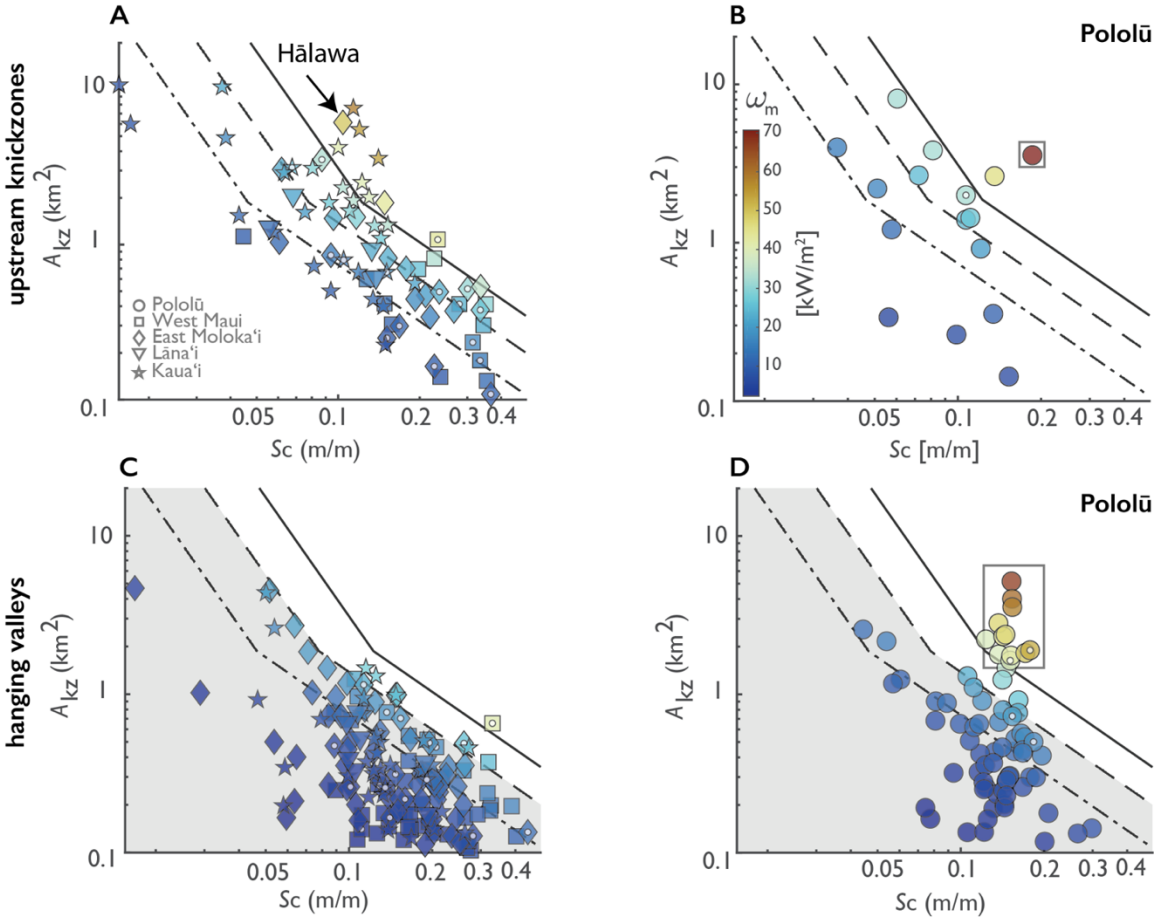

Figure 3.10. Controls on drainage area above knickzones. A-D: Scatter plots of drainage area (A_{kz}) and channel gradient (S_c) above the knickzone colored by estimates of ω_m. Lines show theoretical predictions of A_c as function of S_c incorporating a change in discharge-area scaling at ~2km^2. Solid line shows theoretical prediction with $\omega_c =$ 35.9 (kW/m^2), dashed line with $\omega_c = 22.8$ (kW/m^2) and dashed-dotted lines with $\omega_c =$ 13.6 (kW/m^2). White circles show knickzones with potential drainage area loss. Gray boxes bound valleys with complex response for the Pololū Region in B and D. Gray shading in C and D indicates the theoretical inequality represented by Eqn. 5.

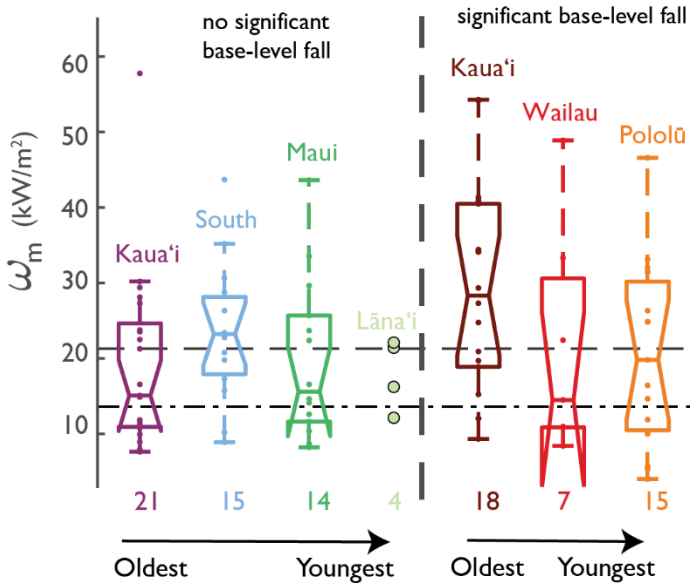

Figure 3.11. Boxplots of maximum stream power (ω_m) for upstream knickzones in each region. Numbers below boxplots indicate sample size. Boxplot of the Pololū region omits one complex knickzone. Dashed horizontal line shows $\omega_m = 22.8$ (kW/m^2) and dashed dotted line shows $\omega_m = 13.6$ (kW/m^2).

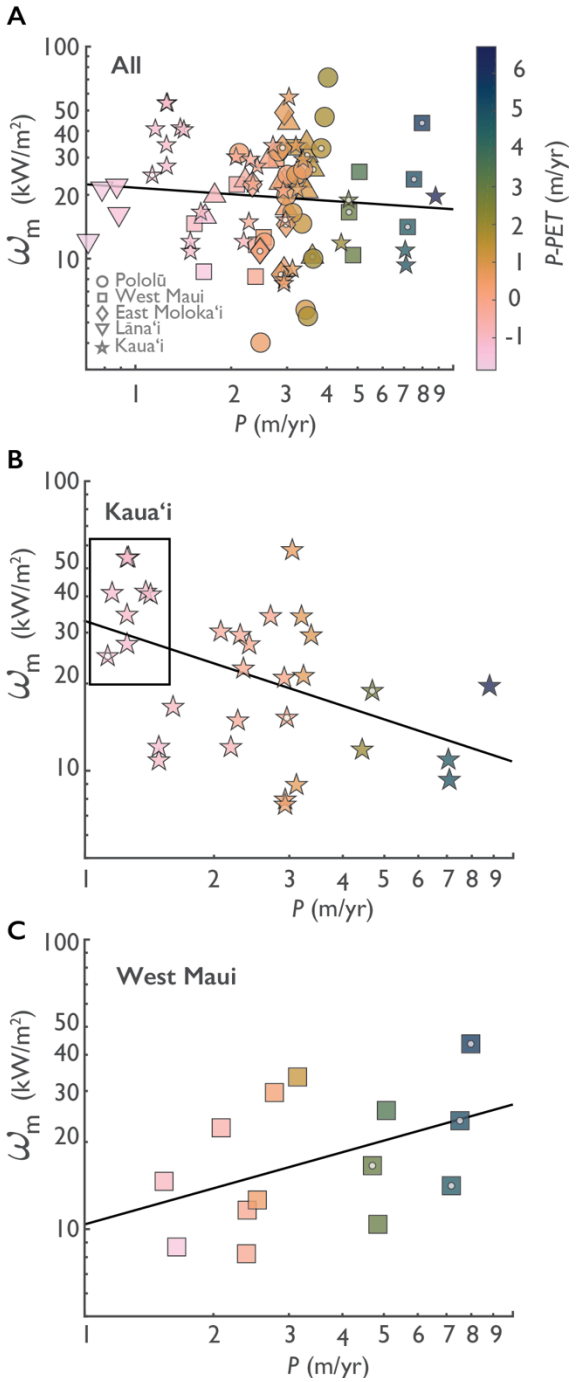

Figure 3.12. Influence of climate on maximum stream power above knickzones. Scatter plots of maximum stream power (ω_m) versus mean annual rainfall (P) with data colored by P – PET, where PET is the mean annual potential evapotranspiration. A: P versus ω_m for all upstream knickzones. B and C: P versus ω_m for upstream knickzones on Kaua'i and West Maui, respectively. Black solid line in each panel show best fit to log-

transformed data of P vs ω_m. Box in B highlights knickzones found along the dry western end of the Nāpali coast that create the observed trend of ω_m with P.

REFERENCES

Akoglu, H., 2018, User's guide to correlation coefficients: Turkish Journal of Emergency Medicine, v. 18, p. 91–93, doi:10.1016/j.tjem.2018.08.001.

Annandale, G.W., 1995, Erodibility: Journal of Hydraulic Research, v. 33, p. 471–494, doi:10.1080/00221689509498656.

Anton, L., Mather, A.E., Stokes, M., Muñoz-Martin, A., and De Vicente, G., 2015, Exceptional river gorge formation from unexceptional floods: Nature Communications, v. 6, p. 7963, doi:10.1038/ncomms8963.

Baynes, E.R.C., Attal, M., Niedermann, S., Kirstein, L.A., Dugmore, A.J., and Naylor, M., 2015, Erosion during extreme flood events dominates Holocene canyon evolution in northeast Iceland: Proceedings of the National Academy of Sciences, v. 112, p. 2355–2360, doi:10.1073/pnas.1415443112.

Baynes, E.R.C., Lague, D., Attal, M., Gangloff, A., Kirstein, L.A., and Dugmore, A.J., 2018, River self-organisation inhibits discharge control on waterfall migration: Scientific Reports, v. 8, p. 2444, doi:10.1038/s41598-018-20767-6.

Berlin, M.M., and Anderson, R.S., 2007, Modeling of knickpoint retreat on the Roan Plateau, western Colorado: Journal of Geophysical Research: Earth Surface, v. 112, p. F03S06, doi:10.1029/2006JF000553.

Bishop, P., Hoey, T.B., Jansen, J.D., and Artza, I.L., 2005, Knickpoint recession rate and catchment area: the case of uplifted rivers in Eastern Scotland: Earth Surface Processes and Landforms, v. 30, p. 767–778, doi:10.1002/esp.1191.

Brocard, G.Y., Willenbring, J.K., Miller, T.E., and Scatena, F.N., 2016, Relict landscape resistance to dissection by upstream migrating knickpoints: Journal of Geophysical Research: Earth Surface, v. 121, p. 1182–1203, doi:10.1002/2015JF003678.

Chadwick, O.A., Gavenda, R.T., Kelly, E.F., Ziegler, K., Olson, C.G., Elliott, W.C., and Hendricks, D.M., 2003, The impact of climate on the biogeochemical functioning of volcanic soils: Chemical Geology, v. 202, p. 195–223, doi:10.1016/j.chemgeo.2002.09.001.

Chatanantavet, P., and Parker, G., 2009, Physically based modeling of bedrock incision by abrasion, plucking, and macroabrasion: Journal of Geophysical Research: Earth Surface, v. 114, doi:10.1029/2008JF001044.

Clague, D.A., and Moore, J.G., 2002, The proximal part of the giant submarine Wailau landslide, Molokai, Hawaii: Journal of Volcanology and Geothermal Research, v. 113, p. 259–287, doi:10.1016/S0377-0273(01)00261-X.

Clague, D.A., and Sherrod, D.R., 2014, Growth and degradation of Hawaiian volcanoes, *in* Characteristics of Hawaiian volcanoes, Professional Paper, US Geological Survey, 1801, p. 97–146.

Cook, K.L., Turowski, J.M., and Hovius, N., 2013, A demonstration of the importance of bedload transport for fluvial bedrock erosion and knickpoint propagation: Earth Surface Processes and Landforms, v. 38, p. 683–695, doi:https://doi.org/10.1002/esp.3313.

Costa, J.E., 1987a, A comparison of the largest rainfall-runoff floods in the United States with those of the People's Republic of China and the world: Journal of Hydrology, v. 96, p. 101–115, doi:10.1016/0022-1694(87)90146-6.

Costa, J.E., 1987b, Hydraulics and basin morphometry of the largest flash floods in the conterminous United States: Journal of Hydrology, v. 93, p. 313–338, doi:10.1016/0022-1694(87)90102-8.

Crosby, B.T., and Whipple, K.X., 2006, Knickpoint initiation and distribution within fluvial networks: 236 waterfalls in the Waipaoa River, North Island, New Zealand: Geomorphology, v. 82, p. 16–38, doi:10.1016/j.geomorph.2005.08.023.

Crosby, B.T., Whipple, K.X., Gasparini, N.M., and Wobus, C.W., 2007, Formation of fluvial hanging valleys: Theory and simulation: Journal of Geophysical Research: Earth Surface, v. 112, doi:https://doi.org/10.1029/2006JF000566.

DiBiase, R.A., Whipple, K.X., Lamb, M.P., and Heimsath, A.M., 2015, The role of waterfalls and knickzones in controlling the style and pace of landscape adjustment in the western San Gabriel Mountains, California: GSA Bulletin, v. 127, p. 539–559, doi:10.1130/B31113.1.

Dubinski, I.M., and Wohl, E., 2013, Relationships between block quarrying, bed shear stress, and stream power: A physical model of block quarrying of a jointed bedrock channel: Geomorphology, v. 180–181, p. 66–81, doi:10.1016/j.geomorph.2012.09.007.

Ferrier, K.L., Huppert, K.L., and Perron, J.T., 2013a, Climatic control of bedrock river incision: Nature, v. 496, p. 206–209, doi:https://doi.org/10.1038/nature11982.

Ferrier, K.L., Perron, J.T., Mukhopadhyay, S., Rosener, M., Stock, J.D., Huppert, K.L., and Slosberg, M., 2013b, Covariation of climate and long-term erosion rates across a steep rainfall gradient on the Hawaiian island of Kaua‘i: GSA Bulletin, v. 125, p. 1146–1163, doi:10.1130/B30726.1.

Frazier, A.G., Giambelluca, T.W., Diaz, H.F., and Needham, H.L., 2016, Comparison of geostatistical approaches to spatially interpolate month-year rainfall for the Hawaiian Islands: International Journal of Climatology, v. 36, p. 1459–1470, doi:10.1002/joc.4437.

Gardner, T.W., 1983, Experimental study of knickpoint and longitudinal profile evolution in cohesive, homogeneous material: GSA Bulletin, v. 94, p. 664–672, doi:10.1130/0016-7606(1983)94<664:ESOKAL>2.0.CO;2.

Gavenda, R.T., 1994, Hawaiian quaternary paleoenvironments: A review of geological, pedological, and botanical evidence., *in* A Natural History of the Hawaiian Islands: Selected Readings II, Honolulu, University of Hawaii Press, A Natural History of the Hawaiian Islands II, p. 118–130.

Gayer, E., Michon, L., Louvat, P., and Gaillardet, J., 2019, Storm-induced precipitation variability control of long-term erosion: Earth and Planetary Science Letters, v. 517, p. 61–70, doi:10.1016/j.epsl.2019.04.003.

Giambelluca, T.W., Chen, Q., Frazier, A.G., Price, J.P., Chen, Y.-L., Chu, P.-S., Eischeid, J.K., and Delparte, D.M., 2012, Online Rainfall Atlas of Hawai‘i: Bulletin of the American Meteorological Society, v. 94, p. 313–316, doi:10.1175/BAMS-D-11-00228.1.

Giambelluca, T.W., Shuai, X., Barnes, M.L., Alliss, R.J., Longman, R.J., Miura, T., Chen, Q., Frazier, A.G., Mudd, R.G., and Cuo, L., 2014, Evapotranspiration of Hawai ‘i: Final report submitted to the US Army Corps of Engineers—Honolulu District, and the Commission on Water Resource Management, State of Hawai ‘i,.

Goode, J.K., and Burbank, D.W., 2009, Numerical study of degradation of fluvial hanging valleys due to climate change: Journal of Geophysical Research: Earth Surface, v. 114, doi:https://doi.org/10.1029/2007JF000965.

Goodrich, D.C., Lane, L.J., Shillito, R.M., Miller, S.N., Syed, K.H., and Woolhiser, D.A., 1997, Linearity of basin response as a function of scale in a semiarid watershed: Water Resources Research, v. 33, p. 2951–2965, doi:https://doi.org/10.1029/97WR01422.

Groh, E.L., and Scheingross, J.S., 2021, Morphologic signatures of autogenic waterfalls: A case study in the San Gabriel Mountains, California: Geology, doi:10.1130/G49320.1.

Hack, J.T., 1957, Studies of longitudinal stream profiles in Virginia and Maryland: U.S. Geological Survey Professional Paper, v. 294-B.

Harris, A.J.L., Rowland, S.K., Villeneuve, N., and Thordarson, T., 2016, Pāhoehoe, ‘a‘ā, and block lava: an illustrated history of the nomenclature: Bulletin of Volcanology, v. 79, p. 7, doi:10.1007/s00445-016-1075-7.

Haviv, I., Enzel, Y., Whipple, K.X., Zilberman, E., Stone, J., Matmon, A., and Fifield, L.K., 2006, Amplified erosion above waterfalls and oversteepened bedrock reaches: Journal of Geophysical Research: Earth Surface, v. 111, doi:10.1029/2006JF000461.

Hayakawa, Y., and Matsukura, Y., 2003, Recession rates of waterfalls in Boso Peninsula, Japan, and a predictive equation: Earth Surface Processes and Landforms, v. 28, p. 675–684, doi:10.1002/esp.519.

Hearty, P.J., Karner, D.B., Renne, P.R., Olson, S.L., and Fletcher, S., 2005, 40Ar/39Ar age of a young rejuvenation basalt flow: Implications for the duration of volcanism and the timing of carbonate platform development during the quaternary on Kaua'i, Hawaiian Islands: New Zealand Journal of Geology and Geophysics, v. 48, p. 199–211, doi:10.1080/00288306.2005.9515110.

Herschy, R.W., 2002, The world's maximum observed floods: Flow Measurement and Instrumentation, v. 13, p. 231–235, doi:10.1016/S0955-5986(02)00054-7.

Holcomb, R.T., 1987, Eruptive history and long-term behavior of Kilauea Volcano, *in* Volcanism In Hawaii, U.S.Geological Survey, v. 1, p. 261–350, https://pubs.usgs.gov/pp/1987/1350/.

Hotchkiss, S., Vitousek, P.M., Chadwick, O.A., and Price, J., 2000, Climate Cycles, Geomorphological Change, and the Interpretation of Soil and Ecosystem Development: Ecosystems, v. 3, p. 522–533, doi:10.1007/s100210000046.

Howard, A.D., and McLane III, C.F., 1988, Erosion of cohesionless sediment by groundwater seepage: Water Resources Research, v. 24, p. 1659–1674, doi:10.1029/WR024i010p01659.

Huppert, K.L., Royden, L.H., and Perron, J.T., 2015, Dominant influence of volcanic loading on vertical motions of the Hawaiian Islands: Earth and Planetary Science Letters, v. 418, p. 149–171, doi:10.1016/j.epsl.2015.02.027.

Izumi, N., Yokokawa, M., and Parker, G., 2017, Incisional cyclic steps of permanent form in mixed bedrock-alluvial rivers: Journal of Geophysical Research: Earth Surface, v. 122, p. 130–152, doi:https://doi.org/10.1002/2016JF003847.

Jackson, E.D., Silver, E.A., and Dalrymple, G.B., 1972, Hawaiian-Emperor Chain and Its Relation to Cenozoic Circumpacific Tectonics: GSA Bulletin, v. 83, p. 601–618, doi:10.1130/0016-7606(1972)83[601:HCAIRT]2.0.CO;2.

Jones, B.L., Chinn, S.S.W., and Brice, J.C., 1984, Olokele rock avalanche, island of Kauai, Hawaii: Geology, v. 12, p. 209–211.

Katz, M.G., and Cashman, K.V., 2003, Hawaiian lava flows in the third dimension: Identification and interpretation of pahoehoe and ′a′a distribution in the KP-1 and

SOH-4 cores: Geochemistry, Geophysics, Geosystems, v. 4, doi:10.1029/2001GC000209.

Kendall, M.G., 1938, A New Measure of Rank Correlation: Biometrika, v. 30, p. 81–93, doi:10.2307/2332226.

Killick, R., Fearnhead, P., and Eckley, I.A., 2012, Optimal Detection of Changepoints With a Linear Computational Cost: Journal of the American Statistical Association, v. 107, p. 1590–1598, doi:10.1080/01621459.2012.737745.

Kirby, E., and Whipple, K.X., 2012, Expression of active tectonics in erosional landscapes: Journal of Structural Geology, v. 44, p. 54–75.

Knapp, K.R., Kruk, M.C., Levinson, D.H., Diamond, H.J., and Neumann, C.J., 2010, The International Best Track Archive for Climate Stewardship (IBTrACS): Unifying Tropical Cyclone Data: Bulletin of the American Meteorological Society, v. 91, p. 363–376, doi:10.1175/2009BAMS2755.1.

Lamb, M.P., and Dietrich, W.E., 2009, The persistence of waterfalls in fractured rock: GSA Bulletin, v. 121, p. 1123–1134, doi:10.1130/B26482.1.

Lamb, M.P., Finnegan, N.J., Scheingross, J.S., and Sklar, L.S., 2015, New insights into the mechanics of fluvial bedrock erosion through flume experiments and theory: Geomorphology, v. 244, p. 33–55, doi:10.1016/j.geomorph.2015.03.003.

Lamb, M.P., and Fonstad, M.A., 2010, Rapid formation of a modern bedrock canyon by a single flood event: Nature Geoscience, v. 3, p. 477–481, doi:10.1038/ngeo894.

Lamb, M.P., Howard, A.D., Dietrich, W.E., and Perron, J.T., 2007, Formation of amphitheater-headed valleys by waterfall erosion after large-scale slumping on Hawai ʻi: GSA Bulletin, v. 119, p. 805–822, doi:https://doi.org/10.1130/B25986.1.

Lapotre, M.G.A., and Lamb, M.P., 2018, Substrate controls on valley formation by groundwater on Earth and Mars: Geology, v. 46, p. 531–534, doi:10.1130/G40007.1.

Li, Y.-H., 1988, Denudation Rates of the Hawaiian Islands by Rivers and Groundwaters:, http://scholarspace.manoa.hawaii.edu/handle/10125/1082 (accessed April 2021).

Li, C., Wang, G., and Li, R., 2013, Maximum observed floods in China: Hydrological Sciences Journal, v. 58, p. 728–735, doi:10.1080/02626667.2013.772299.

Limber, P.W., and Barnard, P.L., 2018, Coastal knickpoints and the competition between fluvial and wave-driven erosion on rocky coastlines: Geomorphology, v. 306, p. 1–12, doi:10.1016/j.geomorph.2017.12.035.

Lindeløv, J.K., 2020, mcp: An R Package for Regression With Multiple Change Points:, doi:10.31219/osf.io/fzqxv.

Macdonald, G.A., Abbott, A.T., and Peterson, F.L., 1983, Volcanoes in the Sea: The Geology of Hawaii: University of Hawaii Press, 558 p.

Macdonald, G.A., Davis, D.A., and Cox, D.C., 1960, Geology and ground-water resources of the island of Kauai, Hawaii: Bulletin Other Government Series 13, http://pubs.er.usgs.gov/publication/70160871 (accessed December 2019).

Mackey, B.H., Scheingross, J.S., Lamb, M.P., and Farley, K.A., 2014, Knickpoint formation, rapid propagation, and landscape response following coastal cliff retreat at the last interglacial sea-level highstand: Kaua‘i, Hawai‘i: GSA Bulletin, v. 126, p. 925–942, doi:10.1130/B30930.1.

Magilligan, F.J., 1992, Thresholds and the spatial variability of flood power during extreme floods: Geomorphology, v. 5, p. 373–390, doi:10.1016/0169-555X(92)90014-F.

McDougall, I., 1979, Age of shield-building volcanism of Kauai and linear migration of volcanism in the Hawaiian island chain: Earth and Planetary Science Letters, v. 46, p. 31–42, doi:10.1016/0012-821X(79)90063-3.

Moore, J.G., and Clague, D.A., 1992, Volcano growth and evolution of the island of Hawaii: Geological Society of America Bulletin, v. 104, p. 1471–1484.

Moore, J.G., Clague, D.A., Holcomb, R.T., Lipman, P.W., Normark, W.R., and Torresan, M.E., 1989, Prodigious submarine landslides on the Hawaiian Ridge: Journal of Geophysical Research: Solid Earth, v. 94, p. 17465–17484, doi:10.1029/JB094iB12p17465.

Morisawa, M.E., 1962, Quantitative Geomorphology of Some Watersheds in the Appalachian Plateau: GSA Bulletin, v. 73, p. 1025–1046, doi:10.1130/0016-7606(1962)73[1025:QGOSWI]2.0.CO;2.

Murphy, B.P., Johnson, J.P.L., Gasparini, N.M., and Sklar, L.S., 2016, Chemical weathering as a mechanism for the climatic control of bedrock river incision: Nature, v. 532, p. 223–227, doi:10.1038/nature17449.

Neely, A.B., and DiBiase, R.A., 2020, Drainage Area, Bedrock Fracture Spacing, and Weathering Controls on Landscape-Scale Patterns in Surface Sediment Grain Size: Journal of Geophysical Research: Earth Surface, v. 125, p. e2020JF005560, doi:https://doi.org/10.1029/2020JF005560.

Oki, D.S., Rosa, S.N., and Yeung, C.W., 2010, Flood-frequency estimates for streams on Kaua’i, O’ahu, Moloka’i, Maui, and Hawai’i, State of Hawai’i: U.S. Geological Survey Scientific Investigations Report 5035, 121 p.

Okubo, C.H., 2004, Rock mass strength and slope stability of the Hilina slump, Kīlauea volcano, Hawai'i: Journal of Volcanology and Geothermal Research, v. 138, p. 43–76, doi:10.1016/j.jvolgeores.2004.06.006.

Ortega, J.A., Wohl, E., and Livers, B., 2013, Waterfalls on the eastern side of Rocky Mountain National Park, Colorado, USA: Geomorphology, v. 198, p. 37–44, doi:10.1016/j.geomorph.2013.05.010.

Palucis, M.C., Ulizio, T., Fuller, B., and Lamb, M.P., 2018, Intense Granular Sheetflow in Steep Streams: Geophysical Research Letters, v. 45, p. 5509–5517, doi:https://doi.org/10.1029/2018GL077526.

Parker, C., Clifford, N.J., and Thorne, C.R., 2011, Understanding the influence of slope on the threshold of coarse grain motion: Revisiting critical stream power: Geomorphology, v. 126, p. 51–65, doi:10.1016/j.geomorph.2010.10.027.

Perron, J.T., 2017, Climate and the Pace of Erosional Landscape Evolution: Annual Review of Earth and Planetary Sciences, v. 45, p. 561–591, doi:10.1146/annurev-earth-060614-105405.

Perron, J.T., and Royden, L., 2013, An integral approach to bedrock river profile analysis: Earth Surface Processes and Landforms, v. 38, p. 570–576, doi:10.1002/esp.3302.

Porder, S., Hilley, G.E., and Chadwick, O.A., 2007, Chemical weathering, mass loss, and dust inputs across a climate by time matrix in the Hawaiian Islands: Earth and Planetary Science Letters, v. 258, p. 414–427, doi:10.1016/j.epsl.2007.03.047.

Prancevic, J.P., and Lamb, M.P., 2015, Unraveling bed slope from relative roughness in initial sediment motion: Journal of Geophysical Research: Earth Surface, v. 120, p. 474–489, doi:10.1002/2014JF003323.

Prancevic, J.P., Lamb, M.P., and Fuller, B.M., 2014, Incipient sediment motion across the river to debris-flow transition: Geology, v. 42, p. 191–194, doi:10.1130/G34927.1.

Price, J.P., and Elliott-Fisk, D., 2004, Topographic History of the Maui Nui Complex, Hawai'i, and Its Implications for Biogeography: Pacific Science, v. 58, p. 27–45, doi:10.1353/psc.2004.0008.

Raming, L.W., and Whipple, K.X., 2022, When knickzones limit upstream transmission of base-level fall: An example from Kaua'i, Hawai'i: Geology, doi:10.1130/G50019.1.

Rigon, R., Rodriguez-Iturbe, I., Maritan, A., Giacometti, A., Tarboton, D.G., and Rinaldo, A., 1996, On Hack's Law: Water Resources Research, v. 32, p. 3367–3374, doi:10.1029/96WR02397.

Roda-Boluda, D.C., D'Arcy, M., McDonald, J., and Whittaker, A.C., 2018, Lithological controls on hillslope sediment supply: insights from landslide activity and grain size distributions: Earth Surface Processes and Landforms, v. 43, p. 956–977, doi:10.1002/esp.4281.

Rodier, J.A., and Roche, M., 1984, World catalogue of maximum observed floods =: Repertoire mondial des crues maximales observees: Wallingford, Oxfordshire, International Association of Hydrological Sciences, IAHS publication no. 143, 354 p.

Rossi, M.W., Whipple, K.X., and Vivoni, E.R., 2016, Precipitation and evapotranspiration controls on daily runoff variability in the contiguous United States and Puerto Rico: Journal of Geophysical Research: Earth Surface, v. 121, p. 128–145, doi:10.1002/2015JF003446.

Rowland, S.K., and Garbeil, H., 2000, Slopes of Oceanic Basalt Volcanoes, *in* Remote Sensing of Active Volcanism, American Geophysical Union (AGU), p. 223–247, doi:10.1029/GM116p0223.

Ryan, A.J., and Whipple, K.X., 2020, Amphitheatre-headed canyons of Southern Utah: Stratigraphic control of canyon morphology: Earth Surface Processes and Landforms, v. 45, p. 3607–3622, doi:doi.org/10.1002/esp.4987.

Sassolas-Serrayet, T., Cattin, R., and Ferry, M., 2018, The shape of watersheds: Nature Communications, v. 9, p. 3791, doi:10.1038/s41467-018-06210-4.

Satake, K., Smith, J.R., and Shinozaki, K., 2002, Three-Dimensional Reconstruction and Tsunami Model of the Nuuanu and Wailau Giant Landslides, Hawaii, *in* Hawaiian Volcanoes: Deep Underwater Perspectives, American Geophysical Union (AGU), p. 333–346, doi:10.1029/GM128p0333.

Scheingross, J.S., and Lamb, M.P., 2017, A Mechanistic Model of Waterfall Plunge Pool Erosion into Bedrock: Journal of Geophysical Research: Earth Surface, v. 122, p. 2079–2104, doi:10.1002/2017JF004195.

Scheingross, J.S., and Lamb, M.P., 2021, Mass balance controls on sediment scour and bedrock erosion in waterfall plunge pools: Geology, doi:10.1130/G48881.1.

Schwanghart, W., and Scherler, D., 2017, Bumps in river profiles: uncertainty assessment and smoothing using quantile regression techniques: Earth Surface Dynamics, v. 5, p. 821–839, doi:https://doi.org/10.5194/esurf-5-821-2017.

Schwanghart, W., and Scherler, D., 2020, Divide mobility controls knickpoint migration on the Roan Plateau (Colorado, USA): Geology, doi:10.1130/G47054.1.

Schwanghart, W., and Scherler, D., 2014, Short Communication: TopoToolbox 2 – MATLAB-based software for topographic analysis and modeling in Earth surface

sciences: Earth Surface Dynamics, v. 2, p. 1–7, doi:https://doi.org/10.5194/esurf-2-1-2014.

Scott, G.A.J., and Street, J.M., 1976, The role of chemical weathering in the formation of Hawaiian Amphitheatre-headed valleys.: Zeitschrift fr Geomorphologie, Annals of geomorphology.,.

Seidl, M.A., Dietrich, W.E., and Kirchner, J.W., 1994, Longitudinal profile development into bedrock: An analysis of Hawaiian channels: Journal of Geology, v. 102, p. 457, doi:10.1086/629686.

Shelef, E., Haviv, I., and Goren, L., 2018, A Potential Link Between Waterfall Recession Rate and Bedrock Channel Concavity: Journal of Geophysical Research: Earth Surface, v. 123, p. 905–923, doi:10.1002/2016JF004138.

Sherrod, D.R., Murai, T., and Tagami, T., 2007, New K–Ar ages for calculating end-of-shield extrusion rates at West Maui volcano, Hawaiian island chain: Bulletin of Volcanology, v. 69, p. 627–642, doi:10.1007/s00445-006-0099-9.

Sherrod, D.R., Sinton, J.M., Watkins, S.E., and Brunt, K.M., 2021, Geologic map of the State of Hawaii: U.S. Geological Survey Scientific Investigations Map USGS Numbered Series 3143, 72 p., doi:10.3133/sim3143.

Shobe, C.M., Tucker, G.E., and Rossi, M.W., 2018, Variable-Threshold Behavior in Rivers Arising From Hillslope-Derived Blocks: Journal of Geophysical Research: Earth Surface, v. 123, p. 1931–1957, doi:10.1029/2017JF004575.

Sinton, J.M., Eason, D.E., and Duncan, R.A., 2017, Volcanic evolution of Moloka‘i, Hawai‘i: Implications for the shield to postshield transition in Hawaiian volcanoes: Journal of Volcanology and Geothermal Research, v. 340, p. 30–51, doi:10.1016/j.jvolgeores.2017.04.011.

Sklar, L.S., and Dietrich, W.E., 2004, A mechanistic model for river incision into bedrock by saltating bed load: Water Resources Research, v. 40, doi:10.1029/2003WR002496.

Small, E.E., Blom, T., Hancock, G.S., Hynek, B.M., and Wobus, C.W., 2015, Variability of rock erodibility in bedrock-floored stream channels based on abrasion mill experiments: Journal of Geophysical Research: Earth Surface, v. 120, p. 1455–1469, doi:10.1002/2015JF003506.

Stearns, H.T., and Macdonald, G.A., 1942, General geology and ground-water resources of the island of Maui, Hawaii: Advertiser Publishing Co.

Stearns, H.T., Macdonald, G.A., and Swartz, J.H., 1940, Geology and ground-water resources of the islands of Lanai and Kahoolawe, Hawaii: Advertiser Publishing Co.

Vehtari, A., Gelman, A., and Gabry, J., 2017, Practical Bayesian model evaluation using leave-one-out cross-validation and WAIC: Statistics and Computing, v. 27, p. 1413–1432, doi:10.1007/s11222-016-9696-4.

Veneziano, D., and Niemann, J.D., 2000, Self-similarity and multifractality of fluvial erosion topography: 2. Scaling properties: Water Resources Research, v. 36, p. 1937–1951, doi:https://doi.org/10.1029/2000WR900054.

Verdian, J.P., Sklar, L.S., Riebe, C.S., and Moore, J.R., 2020, Sediment size on talus slopes correlates with fracture spacing on bedrock cliffs: Implications for predicting initial sediment size distributions on hillslopes: Earth Surface Dynamics Discussions, p. 1–23, doi:https://doi.org/10.5194/esurf-2020-54.

Voigtlander, J.V., Clark, M.K., Zekkos, D., Greenwood, W.W., Anderson, S.P., Anderson, R.S., and Godt, J.W., 2018, Strong variation in weathering of layered rock maintains hillslope-scale strength under high precipitation: Earth Surface Processes and Landforms, v. 43, p. 1183–1194, doi:doi.org/10.1002/esp.4290.

Weissel, J.K., and Seidl, M.A., 1997, Influence of rock strength properties on escarpment retreat across passive continental margins: Geology, v. 25, p. 631–634, doi:10.1130/0091-7613(1997)025<0631:IORSPO>2.3.CO;2.

Wentworth, C.K., 1928, Principles of Stream Erosion in Hawaii: The Journal of Geology, v. 36, p. 385–410.

Wentworth, C.K., and Macdonald, G.A., 1953, Structures and Forms of Basaltic Rocks in Hawaii: USGS Bulletin USGS Numbered Series 994, doi:10.3133/b994.

Whipple, K.X., DiBiase, R.A., Crosby, B., and Johnson, J.P.L., 2022, 6.40 - Bedrock Rivers, *in* Shroder, J. (Jack) F. ed., Treatise on Geomorphology (Second Edition), Oxford, Academic Press, p. 865–903, doi:10.1016/B978-0-12-818234-5.00101-2.

White, S.E., 1949, Processes of erosion on steep slopes of oahu, Hawaii: American Journal of Science, v. 247, p. 168–186, doi:10.2475/ajs.247.3.168.

Wobus, C.W., Crosby, B.T., and Whipple, K.X., 2006, Hanging valleys in fluvial systems: Controls on occurrence and implications for landscape evolution: Journal of Geophysical Research: Earth Surface, v. 111, doi:10.1029/2005JF000406.

Wolfe, E.W., and Morris, J., 1996, Geologic map of the island of Hawaii: US Geological Survey, 2524-A.

CHAPTER 4

THRESHOLDS AND CLIMATE IN LANDSCAPE EVOLUTION OF THE HAWAIIAN ISLANDS

ABSTRACT

Feedbacks between climate and bedrock river incision have the potential to directly alter and regulate the Earth's surface. Thresholds in bedrock river incision hold an important key in determining where these feedbacks may be present. In this analysis we examine how thresholds in bedrock river incision influence patterns of incision on the Hawaiian Islands (which span a globally representative range of mean annual rainfall rates) and test for a potential climate-threshold interaction on these patterns of incision. Geological, topographical, and field observations show that bedrock river channels on the Hawaiian Islands are likely at threshold conditions, where rivers can incise 100s to a 1000 plus meters in a short period of time (100ka-1Ma) followed by long periods of quiescence. Theoretical derivations demonstrate that the commonly used channel steepness metric (k_{sn}) can record threshold conditions and that geometric constraints set by (1) shield volcano gradient, (2) sea-cliff height, and (3) k_{sn} , determine incision depth. Using this foundation, we automate identification of uniform k_{sn} segments in canyons on volcanoes that range over an order of magnitude in age (~ 4ma to 0.4 ma). We find that the maximum incision depth for deeply incised canyons (with depths > 300 m) show comparable depths of incision (~ 700m) from the youngest volcano (Kohala) to the oldest volcano (Kaua‘i) in our analysis. In part, these patterns of incision may be explained by coastal erosion through sea-cliff retreat and landslides and the influence of volcano

gradient and channel length. However, we demonstrate that k_{sn} exerts a fundamental and detectable control on incision depth and importantly identify a clear correlation between k_{sn} and mean annual rainfall (P), where $k_{sn} \propto P^{-0.36}$. This relationship appears to be stronger on Kaua‘i then on other volcanoes in the analysis and there remains some uncertainty in what causes the observed relationship (or lack thereof) between k_{sn} and P. Regardless, our results show that patterns of incision are well explained by threshold conditions on the Hawaiian Islands, and demonstrate that the role of climate, as recorded by the landscape, is to determine the maximum incision depth.

INTRODUCTION

The influence of climate in driving landscape evolution is as provocative as it is elusive. Where increases in rainfall translate to an increase in erosional efficiency, there is the potential for direct coupling between local climate conditions and tectonic processes (Willett, 1999) , which through accelerated drawdown of carbon dioxide (Raymo, 1991) can impact the Earth’s climate as a whole (Raymo and Ruddiman, 1992; Macdonald et al., 2019). However, wetter climates do not necessarily translate to increased erosion rates (e.g. Burbank et al., 2003; von Blanckenburg, 2005) and field data unambiguously supporting the intuitive paradigm that increased rainfall should lead to increased erosion rates largely remains elusive. In addressing this problem significant focus has been placed on understanding how bedrock rivers, which control the overall pace of landscape response to external forcing (Whipple and Tucker, 1999), respond to different climate regimes (Burbank et al., 2003; Thiede et al., 2004; Bookhagen et al.,

2005; Bookhagen and Strecker, 2012; Carretier et al., 2013; Adams et al., 2020; Forte et al., 2022). One of the clearest examples linking mean annual rainfall to bedrock river incision is provided by Ferrier et al. (2013), where they document that river incision depth and thus time-averaged incision rate increases with mean annual rainfall and argue that time-averaged incision rate scales linearly with stream power. The interpreted linear dependence of incision rate on mean annual rainfall is surprising given the expected non-linearity associated with the role of thresholds in bedrock river incision (Tucker, 2004; Lague et al., 2005; DiBiase and Whipple, 2011) that are almost certainly important in decaying post-orogenic landscapes (e.g. Baldwin et al., 2003; Thaler and Covington, 2016).

A threshold in bedrock river incision at the simplest level is set by a stream's ability to mobilize coarse sediment armoring the river bed (e.g. Lague, 2014). In the absence of bedrock river incision thresholds, the influence of climate on bedrock river incision is straightforward as wetter climates with more frequent or larger floods will increase the rate at which bedrock is detached, resulting in increased incision rates (e.g. Ferrier et al., 2013). However, most mountainous streams are typically armored by coarse sediment ranging from decimeter to meter scales (Wohl and Merritt, 2008). The presence of coarse sediments set the requirement that bedrock river incision can only occur for a range of floods capable of moving this material (Snyder et al., 2003; Tucker, 2004; Lague et al., 2005; DiBiase and Whipple, 2011; Deal et al., 2018). These threshold conditions can potentially decouple mean annual rainfall from bedrock river incision (Forte et al., 2022), which are only related to the degree that mean annual rainfall rates scale with the range of geomorphically effective floods.

Though the impact of this threshold behavior on bedrock river incision is well documented (DiBiase and Whipple, 2011; Scherler et al., 2017; Campforts et al., 2020; Forte et al., 2022), how thresholds of sediment entrainment manifest across a wide range of climate conditions remains relatively unknown. Tectonically inactive regions are attractive for study of this problem because signals of climate may be recorded with greater fidelity given the simpler history and boundary conditions. Following Ferrier et al. (2013a), we focus on the Hawaiian Islands, which span a globally representative range of mean annual rainfall rates that range from 0.2 to 10 m/yr (Giambelluca et al., 2012; Frazier et al., 2016) and are largely uninfluenced by tectonic activity, to ask the questions: (1) How are bedrock river incision thresholds manifest on the Hawaiian islands and (2) what are the implications of thresholds in understanding the role of climate in landscape evolution? To answer these questions, we present a combination of topographic and field observations that demonstrate deeply incised canyons have cut down to a threshold state where net incision is stalled or greatly reduced. We then test the hypothesis, using a simplified geometric model, that patterns of incision depth are consistent with a normalized channel steepness index (k_{sn}) representative of a critical stream power required to mobilize coarse sediment. From these results we find evidence that incision depth does exhibit a climate dependency directly controlled by k_{sn}, with implications that the influence of climate on patterns of incision is to control the ultimate depth of incision and that channel profiles may not reflect information about incision rate in tectonically inactive landscapes where thresholds dominate.

GEOLOGICAL SETTINGS AND BACKGROUND

The Hawaiian Islands: Evolution and Climate

The Hawaiian Islands are a sequence of shield volcanoes created from the migration of the pacific plate over the Hawaii hotspot (Figure 1; Jackson et al., 1972). The ages of the islands range from ~ 4-5 Ma to the present with ongoing shield building on the island of Hawai'i (Sherrod et al., 2021). Shield volcanoes can be characterized by a series of relatively predictable evolutionary stages (Clague and Sherrod, 2014). These stages are defined on a chemical basis and the transitions between the stages are typically gradational in nature. The shield building stage consists of tholeiitic lava flows and is responsible for emplacing the majority of the volcanic mass (80-95%, Clague and Sherrod, 2014). The post-shield stage is characterized by a transition to more alkalic lava flows (Clague and Sherrod, 2014) with localized eruptions of ʻaʻā flows occurring from vents and cinder cones (e.g. Sinton et al., 2017). At the end of the shield/post shield stages, isostatic subsidence significantly decreases and is followed by a period of marginal uplift caused by the flexural bulge from nearby shield building (Watts and Brink, 1989; Huppert et al., 2015). Once a volcano is past the flexural bulge, the final stage of a volcanic island is characterized by slow thermal driven subsidence (Huppert et al., 2015).

Although the shield volcanoes of the Hawaiian Islands consist of lithologically homogenous rock (i.e. basalt), physical differences between ʻaʻā and pāhoehoe lava flows result in significant variability of rock mass properties (Okubo, 2004; Raming and Whipple, 2022). Pāhoehoe flows are less viscous and tend to produce thinner lava flows (less than a meter to only a couple of meters) which are characterized by a ropey and

bulbous texture (Wentworth and Macdonald, 1953). Whereas ʻaʻā lava flows are more viscous and are generally thicker ranging from centimeters to 10s-of-meters thick (Wentworth and Macdonald, 1953; Macdonald et al., 1960; Sinton et al., 2017). ʻAʻā flows are characterized by a rubbly and clastic exterior denoted as clinker (Harris et al., 2016) and a massive and dense core, which presents significant resistance to incision (Raming and Whipple, 2022). Distributions of ʻaʻā and pāhoehoe flows are spatially correlated with topography and proximity to vents and rift zones (Holcomb, 1987). ʻAʻā flows are found in steeper regions, areas affected by post-shield stage events, and in regions distal to the main caldera, whereas, pāhoehoe flows are found in less steep regions and are associated with the shield building stage (Katz and Cashman, 2003).

The Hawaiian islands exhibit some of the strongest mean annual rainfall gradients on Earth (Giambelluca et al., 2012). These rainfall gradients originate from the interaction of moist surface air from the northeast trade-winds with local topography and the dry descending air of the Hadley cell resulting in a trade-wind inversion (Leopold, 1949; Giambelluca and Nullet, 1991; Giambelluca et al., 2012). The inversion develops on a daily basis and amplifies rainfall along the windward side of islands below 2 km, and as a consequence, the windward sides of the islands are notably wetter than the leeward sides. The magnitude of mean annual rainfall has likely changed through time (Hotchkiss et al., 2000), yet orographic rainfall patterns driven by the trade-winds are thought to have remained relatively stable (Gavenda, 1994; Ferrier et al., 2013b).

Regions analyzed

In this analysis we focus on regions with significant river incision, this includes

the majority of Kauaʻi, East Molokaʻi, West Maui, and the Kohala peninsula on Hawaiʻi. We avoid the island of Oʻahu as flexural uplift (McMurtry et al., 2010) has lengthened streams and subsequently resulted in significant aggradation (Sherrod et al., 2021). The volcanoes analyzed cover a wide range of mean annual rainfall (~0.4 -10 m/yr) and ages. Kauaʻi is the oldest island in this study (~ 4 Ma; McDougall, 1979) with a complex geologic history recording the presence of a younger shield volcano emplaced on the collapsed flank of an older one (Holcomb et al., 1997; Sherrod et al., 2021). Here we focus on the older relatively well-preserved western portion of Kauaʻi consisting of the Nāpali member (5.5-4 Ma) and the larger canyons draining the Olokele (~ 4Ma) and Makaweli (4-3.5Ma) members of the Waimea canyon basalts (Figure 4.2; Sherrod et al., 2021). Submarine landslides and coastal erosion drive base-level fall on Kauaʻi (Seidl et al., 1994; Mackey et al., 2014). Large submarine landslides likely occurred shortly after shield building on both the north and southern portions of the island (Moore et al., 1989). The Nāpali coast and Mana Plain have also experienced significant base-level fall due to coastal erosion which predominantly occurred prior to 2Ma (Seidl et al., 1994; Hearty et al., 2005; Mackey et al., 2014).

East Molokaʻi (Figure 4.3) and West Maui (Figure 4.4) are similar in age. Subaerial shield building for East Molokaʻi began around 1.75 Ma followed by a transition to the post-shield stage around 1.49 Ma which was active until 1.35 Ma (Sinton et al., 2017; Sherrod et al., 2021). Shield building on West Maui is thought to begin as early as 2 Ma with a transition to the post-shield stage from 1.3 to 1.1 Ma (Sherrod et al., 2021). Significant base-level fall is largely absent on West Maui, whereas the north side of East Molokaʻi is clearly defined by large sea-cliffs that are related to the Wailau

landslide (Figure 4.3) which is thought to have occurred around the end of the post-shield stage, ca. 1.5 – 1.3 Ma (Clague and Moore, 2002).

The Kohala peninsula of Hawai‘i is the youngest region in this analysis with exposed lava flows all younger than 0.78 Ma (Figure 4.5; Dalrymple, 1971; Sherrod et al., 2021). The shield stage of the Kohala Peninsula is defined by the Pololū volcanics with the majority of flows dated between 0.45 to 0.32Ma (Sherrod et al., 2021). In turn, the post-shield stage is defined by the Hāwī volcanics, which range in age from 0.26 to 0.14 Ma with the youngest flows dating to 0.12Ma (Sherrod et al., 2021). Similar to East Moloka'i anomalously high sea-cliffs along the north east coast of Kohala potentially demarcate the head scarp of the Pololū slump, a large landslide that extended 20km wide and traveled over a distance of 130km (Figure 4.1, Moore et al., 1989). Timing of the Pololū slump is constrained by the absence of the Hāwī volcanics and a preserved submarine volcanic terrace, with the most probable timing of the slump bracketed between 0.39 to 0.17 Ma (Lamb et al., 2007).

Surface Processes and Landscape Evolution on the Hawaiian Islands

The simple geometry of shield volcanoes and preservation of uneroded surfaces, along with the range of island ages and climate, make the Hawaiian Islands an excellent natural laboratory for understanding dominant controls on landscape evolution. Landscape evolution studies of the Hawaiian Islands have predominantly focused on the formation of amphitheater headed valleys. Amphitheater headed valleys are thought to have formed because of variably resistant rock mass (Hinds, 1925; Stearns and Vaksvik, 1935) and a combination of fluvial (Stearns and Vaksvik, 1935; Howard et al., 1994;

Lamb et al., 2007), chemical (Wentworth, 1928; White, 1949; Scott and Street, 1976), and seepage erosion (Kochel and Piper, 1986). In addition, reduction in rock strength through faulting may also play an important role in the development of amphitheater headed valleys (Bishop, 2018). The previous chapter in this dissertation built on this work and showed that waterfalls and knickzones associated with amphitheater headed valleys, for all except a subset of knickzones on Kohala, could be identified with a threshold critical stream power where bedrock river incision is no longer operable. Stearns and Vaksvik (1935), similarly identified a threshold behavior where amphitheater headed valleys do not form on O'ahu anywhere the original volcano flank had a gradient less than 5%.

The role of chemical weathering is an important area of focus on the Hawaiian islands (e.g. Chadwick et al., 2003) and though many of the studies are framed in terms of a bio-geochemical framework (Vitousek et al., 2009, 2016) the implications of chemical weathering on landscape evolution, especially in terms of climate, are equally important (Scott and Street, 1976; Han et al., 2014; Murphy et al., 2016; Dixon et al., 2018). Climate is directly tied to chemical weathering with notable threshold behaviors. On Kohala a step change in the rate of weathering (Porder et al., 2007) is observed where mean annual rainfall exceeds mean annual potential evapotranspiration (Chadwick et al., 2003). This threshold, however, appears to be sensitive to lava flow age (Porder et al., 2007; Vitousek et al., 2016). This shift with age may simply reflect the gradual influence of weathering across all substrates or may be representative of past climatic conditions (Hotchkiss et al., 2000; Vitousek et al., 2016). Chemical weathering is also directly relevant to the physical processes that shape the Hawaiian Islands and may play an

important role in determining the overall sediment flux or sediment grainsize distribution for a given volcano. For example, Scott and Street (1976) showed that soil avalanches, which are thought to play an important role in valley widening, do not appear to occur in regions with a mean annual rainfall less than 1.4 m/yr. A value that coincidentally, describes a change in vegetation cover from non-photosynthetic plant material to photosynthetic plant material (Asner et al., 2005) and also coincides with a threshold for increased weathering on Kohala (Chadwick et al., 2003). Even in bedrock channels, chemical weathering may reduce rock strength (Murphy, 2016) or the caliber of coarse bed material and thus the incision threshold, and thereby increase the efficiency of long-term bedrock river incision. Additionally, at a reach scale, weathering is accelerated disproportionally along channel boundaries relative to the thalweg (Small et al., 2015) suggesting weathering may also have important impact on channel width. However, the effects of weathering do appear to be sensitive to lava flow types, which may explain why significant relief can be maintained in wetter areas (Voigtlander et al., 2018).

Hypothesis

Sklar and Dietrich (2006) proposed that the gradient of a channel at steady state (S_s) consists of the sum of three distinct components,

$$S_s = S_c + \Delta S_{Qs} + \Delta S_I, \qquad (1)$$

where S_c is the gradient required to exceed a threshold of motion set by the dominant grainsize, ΔS_{Qs} is the additional gradient to maintain sediment transport at the rate of sediment supply, and ΔS_I is the additional gradient required to incise the channel bed. We hypothesize that channel segments for deeply incised canyons on the Hawaiian Island are

no longer incising such that $\Delta S_I = 0$. Consequently, the slope of a channel segment will be dominated by either S_c (Howard, 1980; Stock et al., 2005) and or ΔS_{Qs} (Finnegan et al., 2017; Pfeiffer et al., 2017). The influence of climate is then recorded by channel gradient to the degree that wetter climates produce larger and more frequent floods (e.g. Molnar et al., 2006) capable of exceeding thresholds of motion. Importantly this implies: (1) where S_c is dominant, a linear dependence on unit-stream power is also expected—providing an alternative explanation to Ferrier et al. (2013a) and (2) that the depth of incision on the Hawaiian Islands, and consequently the influence of climate, may not necessarily reflect any information about the rates of bedrock river incision.

Relevant observations

There are a number of important observations that suggest physical thresholds in bedrock incision play a critical role on the Hawaiian Islands and for at least deeply incised canyon incision rates are negligible:

(1) Deep canyons are cut into young volcanoes (Stearns and Macdonald, 1942, 1946; Lamb et al., 2007) with incision depths comparable to the canyons observed on older islands like Kaua‘i. In some places these canyons have been deeply incised and re-filled or partially filled with volcanic material (Stearns and Macdonald, 1946, 1942). On Kaua‘i, inset Koloa volcanics in the Wainiha valley (Macdonald et al., 1960; Clague and Dalrymple, 1988; Sherrod et al., 2021) constrain the age of incision. These constraints show that the lower reaches of the Wainiha valley

reached their full incision depth by ~2.6 Ma (Figure 4.6). A similar situation is observed on Kohala, where inset Hāwī volcanics show that the deeply incised portions of the Pololu Valley (400-500 m) date back to 0.15 Ma (McDougall and Swanson, 1972) and have incised little since.

(2) In Hawaiian rivers and streams coarse sediment is ubiquitous (Figure 4.7; Wentworth, 1928; White, 1949). The presence of coarse sediment provides a simple mechanism for a threshold in bedrock river incision. Additionally, linearized longitudinal stream profiles (inset plot in Figure 4.1; Harkins et al., 2007; Kirby and Whipple, 2012; Perron and Royden, 2013) show a constant channel steepness which in the absence of tectonic forcing is strongly suggestive of a threshold in bedrock river incision.

(3) For virtually all volcanoes, regardless of age, intact portions of the shield volcano preserve its initial shape. Deeply incised canyons only form in regions with steep slopes or where significant base-level fall has occurred through coastal erosion via sea-cliff retreat and landslides (Stearns and Vaksvik, 1935; Lamb et al., 2007; Mackey et al., 2014).

(4) Fluvial hanging valleys and knickzones on the Hawaiian Islands can inhibit bedrock river incision. Where knickzones form or stall is consistent with thresholds in sediment mobility (Raming and Whipple, 2022).

Theoretical Background and Controls on Incision Depth

The above observations suggest that thresholds for bedrock river incision play an important role on the Hawaiian Islands. Once this threshold is exceeded bedrock river incision can occur rapidly, resulting in deeply incised canyons over a short period of time (Figure 4.6). However, as uplift and subsidence rates on the Hawaiian Islands are limited after the period of initially rapid subsidence, tectonic forcing is minimized, and a channel's slope at steady state ($S_{s;}$ Equation 1) will be dominated by thresholds of sediment motion (S_c) and or controls on sediment flux (ΔS_{Qs}). Here we do not attempt to distinguish between the signals of S_c and ΔS_{Qs} , rather we focus on the cessation of rapid bedrock incision and consider the implications of climate and thresholds at the spatial and temporal scales characteristic of most geomorphic transport laws (Dietrich et al., 2003). Previous studies have utilized this approach (e.g. Ferrier et al., 2013; Murphy, 2016), to identify how climate is incorporated into the rate coefficient of the broadly used stream power model (Howard, 1994; Whipple and Tucker, 1999). We build on this work by considering endmember behavior of the stream power model at threshold conditions which appears most relevant for the Hawaiian Islands given the key observations described above.

The stream power model assumes that bedrock river incision is a detachment limited process and that vertical incision rate (I) is proportional to the rate of energy expenditure from geomorphically effective floods (Howard, 1994; Whipple and Tucker, 1999). This is expressed as,

$$I = K\left(\frac{\gamma QS}{W} - \omega_c\right)^a, \qquad (2),$$

where K is an erodibility coefficient and a is an exponent that captures the nonlinear nature of bedrock river incision (Whipple and Tucker, 1999). Within the parentheses of Equation (2) the left hand term is unit stream power (ω), where γ is the specific weight of water, Q is river discharge, W is channel width , and S is the channel gradient which is a proxy for energy loss along the stream bed (Annandale, 1995) and the right hand term, ω_c, is the critical unit stream power below which $I = 0$.

Notably, Q is a stochastic variable often described by either an inverse gamma distribution or a Weibull distribution (Lague et al., 2005; DiBiase and Whipple, 2011; Rossi et al., 2016; Forte et al., 2022). This additional complexity can be added to the stream power model by expressing the incision rate over a given time period as the incision done by the weighted average of all discharges above a critical discharge that exceeds ω_c (Campforts et al., 2020; Deal et al., 2018; DiBiase and Whipple, 2011; Forte et al., 2022; Lague et al., 2005; Scherler et al., 2017; Tucker, 2004). However, if a channel has truly reached threshold conditions such that $I = 0$ for all discharges, then this complexity is reduced and Equation (2) can be expressed as,

$$\omega_c = \frac{\gamma Q_m S}{W_m}, \qquad (3),$$

where Q_m is the maximum possible discharge (Deal et al., 2018; Lague et al., 2005) and W_m is the channel width associated with Q_m.

In attempts to link metrics of climate to discharge and to allow for testable predictions, Equation (3) can be adapted to spatial and temporal scales of landscape

evolution. Both W_m and Q_m can be described as power functions of drainage area (Leopold and Maddock Jr., 1953; Herschy, 2002; Li et al., 2013) which can be directly substituted into Equation (3). There are, however, challenges to this approach. Indeed, there is significant uncertainty of how W_m scales with discharge and drainage area. In the absence of direct observations between large floods and channel width, channel width can instead be described by a power-law dependence on drainage area and here we assume $Wm = k_w A^b$ where k_w is a scaling coefficient and b is an exponent that ranges from 0.3 to 0.5 (Montgomery and Gran, 2001; Wohl and Merritt, 2008; Whipple et al., 2022). Furthermore, though estimates of Q_m can be made with a reasonable level of confidence (Costa, 1987b) and expressed as the power function $Q_m = k_q A^c$ where A is a drainage area and k_q and c are empirically identified parameters (e.g. Li et al., 2013), the controls on Q_m remain relatively unclear. This is especially true, in terms of understanding how and if Q_m relates to mean annual precipitation, as extreme rainfall events associated with large floods do not necessarily correlate with mean annual rainfall (Gayer et al., 2019). In spite of this uncertainty, a number of studies (Finlayson et al., 2002; Bookhagen and Strecker, 2012; Ferrier et al., 2013b; Rossi et al., 2016; Adams et al., 2020) have found that weighting drainage area by mean annual rainfall (P) provides increased predictive power on the effective flood size, including Ferrier et al. (2013a) where they show on Kaua‘i that floods with probabilities up to the 5-year recurrence interval exhibit a linear relationship with drainage area weighted by mean annual rainfall.

In addition to the challenges determining the influence of climate on Q_m, it is also unclear if Q_m truly needs to be at a maximum flood size. Gravel bedded rivers tend to adjust channel width and depth to near threshold conditions of sediment transport (e.g.

Parker et al., 2007; Phillips and Jerolmack, 2019, 2016). As consequence the discharge size associated with the development of threshold condition may be distinctly less than Q_m. To addresses this challenge, we redefine Q_m as the threshold setting flood as described by Phillips and Jerolmack (2016) but acknowledge that Q_m may potentially represent an extreme floods approaching the maximum limit on flood size.

Notwithstanding these challenges, with this background we can predict how threshold conditions act to limit incision depth and exert a first order control on patterns of incision across the islands. This effect can be captured to first order using Equation (3) by substituting the derivative of elevation with respect to distance for *S*, and then rearranging and integrating for river bed elevation (z) in a manner analogous to results for steady state river profiles (Harkins et al., 2007; Kirby and Whipple, 2012; Perron and Royden, 2013). This is shown by the following equation:

$$z(x) = z_0 + \frac{\omega_c \, k_w}{\gamma \, k_q} \chi, \qquad (4)$$

where z_0 is the elevation of the stream's outlet and $\chi = \int_{x_o}^{x} \left(\frac{\mathrm{A_0}}{A(\mathrm{x})}\right)^{c-b} dx$, with drainage area normalized by the reference drainage area $\mathrm{A_0}$, here set equal to one. Importantly, $k_{sn} = \frac{\omega_c \, k_w}{\gamma \, k_q}$ where k_{sn} it the commonly used normalized channel steepness index which can be directly measured from the topography. Here we assume c-b = 0.45, which is consistent with the range of values reported for both *c* (Herschy, 2002; Li et al., 2013) and *b* (Whipple et al., 2021; Wohl and Merritt, 2008) and is comparable to the commonly employed reference concavity used in other settings (Kirby and Whipple, 2012).

Assuming the original volcanic surface can be described by an average gradient (S_v), then the depth of incision (I) for a given location in river channel can be expressed as,

$$I = C + S_v L - k_{sn}\chi, \qquad (5)$$

where C is sea-cliff height if present, L is stream length, and z_0 equals zero as all catchments in our study drain to sea-level (Figure 4.8). Notably, this expression shows that incision depth is controlled by both the initial conditions of the original volcano slope, the presence and magnitude of sea-cliff height, channel length, and k_{sn}. In this formulation we do not explicitly account for influence of mean annual rainfall (P) on k_{sn}, however, if $Q_m \propto AP$ and $W_m \propto Q_m^{0.5}$ then we may expect that $k_{sn} \propto P^{-0.5}$.

METHODS

In this analysis we evaluate spatial patterns of incision, longitudinal stream profiles, and mean annual rainfall. We obtained gridded estimates of mean annual rainfall from the Rainfall Atlas of Hawaii (Frazier et al., 2016). To analyze longitudinal stream profiles, we used TopoToolbox (Schwanghart and Scherler, 2014) and extracted stream networks from a USGS 10 m DEM with a threshold drainage area of 2 km^2. Along the western end of Kaua‘i, in place of the USGS 10 m DEM, where available we used a resampled 5m lidar to avoid artificial oversteepening in particularly narrow canyons found along the Nāpali coast. Oversteepening in the USGS 10m DEM appears to occur in narrow canyons where channel elevation is averaged over knickzones. Traditionally, most stream networks are extracted with a minimum drainage area of ~1km^2 in order to

avoid reaches dominated by colluvial processes (Montgomery and Foufoula-Georgiou, 1993; Stock and Dietrich, 2003), however, as shown by Costa (1987) and as identified in the previous chapter, extreme floods can exhibit a clear change in the discharge-area exponent at ~ 2 km^2. To avoid this complication, we use the more conservative value of 2 km^2. We also truncated the stream network to the base of all major knickzones, where we identified the base of the knickzone, as outlined in chapter 2, by where the average channel gradient exceeds 40%. This value was chosen as experimental and theoretical work (Prancevic et al., 2014; Palucis and Lamb, 2017) suggest that sediment in channels with gradients in excess of 40% are prone to failure resulting in in-channel debris flows, suggesting these segments of the stream network should be predominately exposed bedrock.

To identify stream segments with near uniform k_{sn} we used an automated approach. We did this by using the Pruned Exact Linear Time (PELT) algorithm (Killick et al., 2012). The PELT algorithm identifies change points in a data array if the sum of the outputs from the cost functions plus a threshold value is less than the output from the cost function for fitting the whole data set. In our analysis we focus on changes in gradient (i.e. k_{sn}) along χ-elevation transformed profiles, where the cost function is set by the root-mean squared error of a linear model. We use a threshold value of 5000 to avoid overfitting k_{sn} segments to noise within the DEM and to ensures that uniform k_{sn} segments are of a reasonable length. In a few instances on the volcano of Kohala, where the uniform k_{sn} segment was less than 1 km in length, we excluded that segment. Additionally, to avoid instances where k_{sn} is associated with floodplains and alluvial fans, we evaluated the fraction that a k_{sn} segment overlaid either geologically mapped alluvial

deposits and or water (Sherrod et al., 2021). We only excluded k_{sn} segments with more than 90% mapped alluvium as visual inspection indicated these segments were located in flood plains and alluvial fans.

To identify patterns of incision we reconstructed the initial surface of each shield volcano. We fit convex hulls to elevation contours spaced 50 m apart starting from 600 to 200m below sea level to the highest point on the volcano. We used a 10 m USGS DEM and for bathymetric data we used a 50 m resolution DEM obtained from Main Hawaiian Islands Multibeam Bathymetry Synthesis (http://www.soest.hawaii.edu/hmrg/multibeam/index.php) at the School of Ocean and Earth Science and Technology, University of Hawaii at Manoa. We then applied a thin plate spline to the elevation points extracted from the convex hull to interpolate the reconstructed volcanic surface. In our analysis we focus on the maximum depth of incision (I_{max}) for each uniform k_{sn} segment, which we identified as the maximum difference between the reconstructed surface and the current topography. We obtained estimates of S_v by taking the slope from the best fit linear regression of elevation extracted from the reconstructed volcanic surface against the current stream length. We estimated sea-cliff height (C) as the difference between the reconstructed surface and the current topography at the outlet of a given catchment.

RESULTS

Patterns of incision and ksn

Here we present results from our analysis on patterns of incision for each identified uniform k_{sn} segment (Figures 4.2-5). Across each volcano the maximum depth

of incision (I_{max}) shows a bimodal distribution. This is illustrated in Figure 4.9 where both the probability density and the empirical cumulative distribution of I_{max} indicate a distinct transition at approximately 300 m. Using this transition as a cutoff value we classify segments with a maximum incision depth in excess of 300 m as deeply incised, whereas segments that do not exceed 300 m are classified as lightly incised. For the remainder of this analysis we predominately focus on deeply incised canyons as they have likely incised to a threshold slope, whereas lightly incised canyons may be below threshold conditions and dominated by weathering or could still be actively incising. This transition does appear to be sensitive to island age. On Kohala, the transition between lightly and deeply incised segments occur at the ~80th percentile (and would be even higher if we had selected all streams on the Kohala peninsula), whereas on East Moloka'i, West Maui, and Kaua'i this transition occurs at the 70th, 60th, and 40th percentile respectively (Figure 4.9). Maximum incision depth (I_{max}) for deeply incised k_{sn} segments across the volcanoes show a wide range from the minimum threshold value at 300 m to ~1200 m on East Moloka'i (Figure 4.10). The median value of I_{max} is near-constant across all volcanoes and ranges from slightly less than 700 m (West Maui) to more than 800m on East Moloka'i (midline in box, Figure 4.10), whereas the maximum values of I_{max} (upper whiskers, Figure.10) do show an increase from 950m on Kohala to 1150m on West Maui but appears unchanged across East Moloka'i and Kaua'i. These findings indicate that on the older islands incision depth remains relatively constant for deeply incised canyons, but with island age there does appear to be an increase in the number of canyons that exceed a maximum incision depth of 300m.

Normalized channel steepness index values (k_{sn}) for individual segments vary from approximately 10 to 160, with a mean value of ~70. For deeply incised segments both the minimum and the mean k_{sn} increase to 34 and 91 respectively. Analysis of variance of deeply incised segments suggest that there is significant evidence (p-value = 0.03) against the null hypothesis that the mean value of k_{sn} is approximately the same for each region, with evidence that the mean value of k_{sn} for West Maui and Kohala are statistically distinct from each other. West Maui does exhibit the lowest mean k_{sn} at 78 whereas Kohala exhibits the highest mean k_{sn} at 100 and mean k_{sn} values for Kaua'i and East Moloka'i are 85 and 96, respectively. We did test for correlation of climate controls on individual k_{sn} segments and the associated I_{max} . These results are presented in the supplementary material, as we are predominately focused on trends of k_{sn}, climate, and I_{max} at a catchment scale, which we explore in the following section.

Controls on incision depth and the influence of climate

Here we explore how volcano gradient (S_v), valley length (L), and sea-cliff height (C) can determine incision depth for a valley and test for a climate influence on k_{sn} and maximum incision depth (I_{max}). For some regions, controls on maximum incision depth do appear to be dominated by volcano gradient and sea-cliff height (Figure 4.11). This is demonstrated by controls on the maximum potential for incision depth (Z_{max}) as measured from the reconstructed volcanic surface at the point of I_{max}. As expected I_{max} and Z_{max} are clearly related (Figure 4.11) with a clear impact of cliff height (C), volcano slope (S_v), and catchment length (L) on I_{max} (Figure 4.11). Where these controls dominate, it remains unclear if the maximum incision depth is sensitive enough to record signals of climate

through climatic control of $k_{sn.}$ for threshold channels. To test for the sensitivity of incision depth to k_{sn} we developed a simple geometric model (Figure 8) from Equation (4) and use individual measurements of L, $S_{v,}$ and C, while keeping k_{sn} fixed at an average value of 84 for deeply incised catchments on Kaua‘i, East Moloka‘i, and West Maui. We do omit valleys from Kohala in this portion of our analysis as evidence presented above (Figure 4.9 and Figure 4.10) and in previous work (Chapter 2) suggests that the region is actively incising. We also omit any catchment with more than 90% of the stream network mapped as alluvium and on Kaua‘i we omit the 3 largest valleys on the southern flank as they clearly cannot be described by a single averaged volcano gradient. Results from this analysis show that incision depth in most cases can be well predicted by setting k_{sn} to the mean value of 84 (Figure 4.12) with a median absolute difference between the modeled and observed maximum incision depth at ~100m, in a few cases there is a significant difference between modeled and observed incision depth with the maximum absolute difference of ~560m. However, as demonstrated by Figure 4.12B, the differences between modeled and observed I_{max} show a dependency on k_{sn} and intriguingly indicate k_{sn} may record signals of mean annual precipitation as dryer valleys tend to over predict I_{max} whereas wetter valleys under predict I_{max} (Figure 4.12).

Correlation between the catchment averaged k_{sn} and P is present across all of the volcanoes analyzed (Figure 4.13). Though much of that correlation ($r^2 = 0.34$) is driven by catchments on Kaua’i as the best fit coefficient and exponent on P is nearly identical to the fit for individual uniform k_{sn} segments (see Appendix: Chapter 4 Supplementary). and no other region spans as large of a range of mean annual rainfall. Omitting Kaua’i from the regression increases the exponent on P from 0.36 to 0.43, but the overall

correlation decreases significantly ($r^2 = 0.14$) and most of this correlation is driven by East Moloka'i as there appears to be virtually no relationship between P and k_{sn} on West Maui (see Appendix: Chapter 4 Supplementary). These results suggest that climate may be recorded by the topography through the correlation of P with k_{sn} as indicated by Equation (4) and shown in Figure 4.12. To test this, we evaluate whether the performance of the geometric model increases by employing the theoretical prediction $k_{sn} \sim P^{-0.5}$ with an empirically constrained prefactor of 100 (Figure 4.13). Results from this test show a decrease in the median absolute difference between the modeled and observed maximum incision depth at ~70m, which is approximately 30% less than the difference for using a constant k_{sn} (Figure 4.14), and importantly eliminates the dependence of k_{sn} shown in Figure 4.12.

The dependence of maximum incision depth on climate is directly observed in the topography (Figure 4.15A), though it is somewhat obscured by data from West Maui. This maybe expected as there is no detectable trend between P and k_{sn} on West Maui (see Appendix: Chapter 4 Supplementary). Furthermore, there may be spurious correlation of precipitation with incision depth where sea-cliff height, length of a catchment, or volcano gradient covary with mean annual rainfall. To remove the effects of these additional controls and to further isolate a climate control directly influenced by k_{sn} we used the normalized incision metric I^*, where $I^* = \frac{I_{\max}}{S\nu L + C}$. Testing for a power-law relationship between I_{max}, I^*, and P we exclude data from West Maui. These results show that in both instances there is a decent correlation with P (Figure 4.15), with a small but notable difference on the exponent of P. Intriguingly, I^* vs P yields a near identical exponent

(0.36) as k_{sn} vs P (Figure 4.15B and Figure 4.13), whereas the exponent on P vs I_{max} is 0.56.

DISCUSSION

At the beginning of this paper, we set out to answer two questions: (1) How are bedrock river incision thresholds manifest on the Hawaiian Islands and (2) what are the implications of thresholds in understanding the role of climate in landscape evolution? Our results show that thresholds play an important role in determining where incision has occurred on the islands, though, the overall patterns of incision are also influenced by sea-cliff height, volcano gradient, and channel length (Figure 4.11). Nonetheless we demonstrate that maximum incision depths are dependent on k_{sn} (Figure 4.12 and Figure 14) reflecting the dominance of thresholds in bedrock river incision. Fundamentally, thresholds manifest on the Hawaiian Islands by their influence on the overall incision depth of rivers even when accounting for other dominant controls. Consequently, the role of climate manifest by its interaction with k_{sn}, with the notable impact that k_{sn} is reduced with wetter climates (Figure 4.13). This trend may be explained by the fact that wetter climates do tend to produce larger floods, such that for the same threshold of motion, wetter climates will have an overall lower channel gradient. Importantly this implies that although climate undoubtedly influences the rates at which rivers incise, ultimately what is recorded in the topography is the influence of climate in determining the maximum incision depth.

These findings have critical implications for inferring incision rates from the topography on the Hawaiian Islands. This is demonstrated by the fact that as a channel

approaches a threshold slope, Equation (1), the range of floods capable of doing work is reduced, indicating an increase in the time between periods of active river incision. An increase in the time between periods of incision result in a clear inverse dependency of time averaged incision rates on the time scale over which they are measured (Nativ and Turowski, 2020). This effect which is documented in other settings (Finnegan et al., 2014) is clearly present on the Hawaiian islands as the average maximum incision depth for deeply incised canyons is nearly constant (~ 700 m) across the volcanos analyzed (Figure 4.10). For this reason, when interpreted as a time averaged incision rate there is a clear dependence of incision rate on island age (Figure 4.16). This implies that the slower incision rates on older islands largely reflects a longer period of stasis in terms of net river incision. Furthermore, the presence of thresholds have direct implications for understanding where rapid incision on the Hawaiian islands is likely to occur and conversely can explain why portions of even the oldest volcanoes remain in a relatively youthful stage. Consistent with the seminal work of Stearns and Vaksvik, (1935), our findings show that volcano gradient, in conjunction with drainage area, plays a fundamental role in determining where deeply incised canyons can form on the Hawaiian Islands. Indeed, weighting the original volcano gradient by drainage area (so as to be comparable to k_{sn}) shows that deeply incised canyons that formed in the absence of significant coastal erosion are clearly distinct from lightly incised canyons (Figure 4.17). Furthermore, deeply incised canyons either originally covered a range of drainage area and slope that greatly exceeds mean observed k_{sn} values or they show a comparable range of drainage area and slope to mean observed k_{sn} values but are associated with significant base-level fall associated with landsliding and/or coastal erosion. Whereas the majority of

lightly incised canyons have a range of drainage area and slope comparable to mean observed k_{sn} values (Figure 4.17). This suggests that deeply incised canyons can either form in response to significant base-level fall or where the original channel steepness was likely much greater than mean observed k_{sn} values. Conversely, it appears that the majority of lightly incised canyon have persisted at or below threshold conditions.

The enigma of climate in landscape evolution of the Hawaiian Islands

Though the role of climate in bedrock river incision has been proposed to be recorded in the landscape through its influence on river discharge (Ferrier et al., 2013) our findings suggest that this is clearly not the case for West Maui. Furthermore, the observed trends of k_{sn} and P is relatively consistent with the theoretical prediction that $k_{sn} \propto P^{-0.5}$ (Figure 4.13); however, our analysis consistently shows a lower dependency on P with a value of 0.36 (Figure 4.13), a value that is also recovered from the influence of climate on incision depth, when normalizing for additional controls on incision (Figure 4.15B). Even though it is a small discrepancy, it does suggest that the proposed dependency of Q_m on P maybe weaker than expected. It may simply be the case that $Q_m \propto W_m^{0.3}$ or the weaker dependence on climate maybe expressed through other means.

One possible explanation for this decreased signal of P relates to how P is correlated with extreme floods. Work by Chu et al., (2009) shows that extreme rainfall events tend to occur locally and mainly on the wet windward slopes of the volcanoes (Fig. 4.1). Intriguingly, Chu et al. (2009) also show that the western side of West Maui exhibits the clearest departure of mean annual rainfall from patterns of extreme rainfall events. If P is uncorrelated with extreme but geomorphically effective floods, this could

explain why there is a lack of correlation between k_{sn}, I_{max}, and P on West Maui (Figure 4.13 & Figure 4.15), which may also explain why West Maui has systematically lower values of k_{sn}. Historical tropical cyclone tracks (Knapp et al., 2010) do show that at least the dry southern side of Kaua'i is periodically prone to large storm systems that could produce extreme floods and thus other islands may exhibit the same decoupling between extreme events and mean annual precipitation. If this is the case another explanation for the clear influence of P on k_{sn} on Kaua'i would be required. On the other hand, the frequency of extreme floods may also play an important role. Though dry climates may be capable of generating extreme floods comparable in magnitude to wetter climates, the frequency at which these floods occur relative to the influx of sediment from hillslopes may play an important role in determining whether the channel gradient is dominated by thresholds in sediment mobility (Sc) or controls on sediment supply (ΔS_{Qs}).

Indeed, it is possible that ΔS_{Qs}, the additional gradient required to balance sediment flux, is a dominant control in recording signals of climate in the landscape. Under this hypothesis, it may be unsurprising that Kaua'i exhibits the strongest climate signals given that weathering on the islands in general is age dependent (Porder et al., 2007; Vitousek et al., 2016) and for the fact mean annual rainfall rates for a significant portion of Kaua'i exceed the climate threshold of 1.4 m/yr (Scott and Street 1976) required for soil avalanches—a mechanism that may play an important role in transferring sediment from valley walls to channels. Furthermore, Kaua'i is distinctly different than East Moloka'i and West Maui as it has already experienced the period of marginal uplift due to shield building of the Maui Nui complex, which was sustained for ~ 1-1.5 million years, and now is experiencing thermally induced subsidence (Hearty et

al., 2005). Uplift on the islands has the effect of lengthening streams and buffering sea-cliffs from coastal erosion (Mackey et al., 2014), and potentially may drive aggradation as observed on O‘ahu (Sherrod et al., 2021). Though Kaua‘i has been exposed to renewed coastal erosion after 0.5 Ma (Hearty et al., 2005; Mackey et al., 2014) and channels have since incised through alluvial deposits and very well could be at threshold conditions, it remains unclear if the greater age and complex base-level history of Kaua‘i helps explain why channels on Kaua‘i record the strongest signals of climate.

Influence of lava flow properties

The variability of rock mass properties in lava flows may also directly impact the observed patterns of climate, k_{sn}, and incision. Specifically, lava flows with wider joint spacing will produce larger blocks and result in a higher threshold. The best evidence for this behavior can be seen on Kaua’i where rivers and streams have carved valleys into the thick and sub-horizontal lava flows of the Olokele formation. Figure 4.2 (and Supplementary Figure 1) shows that there is a clear increase in k_{sn} for channel that incise into the Olokele formation. In contrast, on West Maui and East Moloka’i a subset of channels has tapped into what is mapped as a caldera complex. Opposed to the caldera filling lava flows of the Olokele formation, these rocks are extremely fractured and predominately consist of breccias and dike swarms (Stearns and Macdonald, 1942). Yet, on West Maui the caldera is dominated by landslides (Stearns and Macdonald, 1942), and on Kohala some stream segments are clearly incising into mapped landslide deposits (Wolfe and Morris, 1996). Higher values of k_{sn} in these regions may reflect either transient behavior where streams are actively incising landslide deposits or where they

have stalled due to the ample amount of coarse sediment associated with landslides (Ouimet et al., 2007). Conversely, if the propensity for generating large coarse sediment is inversely correlated with patterns of climate it is possible that climate signals in k_{sn} may be obscured by an increase in grain size. Steeper constructional volcano flanks and post-shield volcanics are often associated with an increase in the abundance of ‘a‘ā flows (Katz and Cashman, 2003; Sinton et al., 2017) which are attributed to the production of coarse sediment that armor channel beds on the Hawaiian Islands (Raming and Whipple, 2022). Both of these controls of lava flows are present on West Maui (Figure 4.4), though their influence remains unclear. The lowest values of I^* ($I^* < 0.5$, Figure 4.15 B) on West Maui do all occur on the northern flank of the volcano where post-shield stage volcanics are dominate and may explain some of the higher k_{sn} values at that range of P (2.5-4 m/yr, Figure 4.13). This hypothesis may be simply tested with field data, with a clear prediction that these channels are dominated with larger grain sizes than the other channels in a similar range of rainfall.

CONCLUSIONS

Here we have demonstrated that thresholds in bedrock river incision play a fundamental role in determining patterns of incision depth on the Hawaiian Island. The influence of climate in determining these patterns of incision is consistent with the theoretical prediction that wetter climates produce deeper incision depths. This likely occurs with a near-constant threshold because wetter climates generate larger and more frequent floods and thereby reach a lower threshold channel gradient. We do, however, find that most of the climate signal recorded by these threshold conditions is dominated

by channels on Kaua'i, with a less clear signal observed on East Moloka'i and West Maui, indicating the influence of climate on landscape evolution of the Hawaiian Islands maybe more complex than expected. Regardless, this work highlights the importance of threshold conditions in general in determining where rapid bedrock river incision can occur and suggests caution in interpreting controls on erosion efficiency from time-averaged incision rates from the topography in landscapes potentially dominated by thresholds.

FIGURES

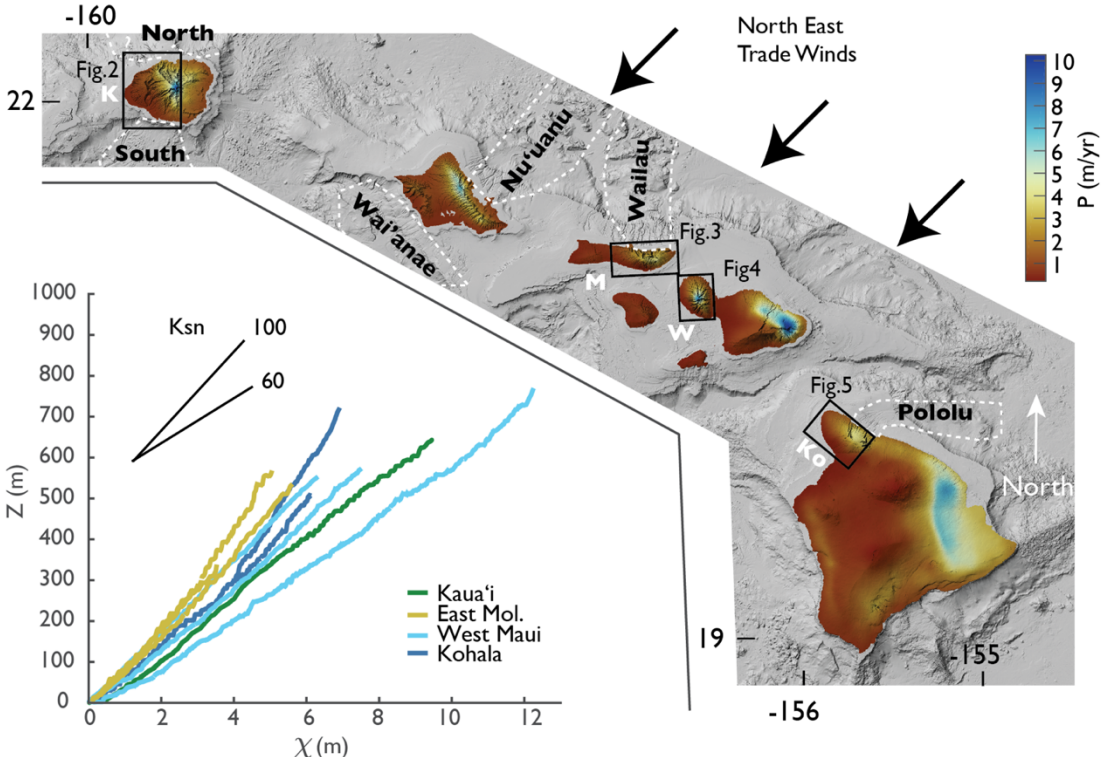

Figure 4.1. Hawaiian Islands and Locations Studied in This Analysis. Hillshade is colored by mean annual precipitation (*P*) for the subaerial portion of the islands. Regions analyzed in this study are labeled by white bold letters (K: Kaua'i , M: East Moloka'i, W: West Maui, Ko: Kohala Peninsula). Dashed white lines demarcate locations of large submarine landslides and are labeled with black bold font. Inset plot shows examples of χ-transformed stream profiles with nearly uniform channel steepness characteristic of steady state stream profiles (e.g. Perron and Royden, 2013).

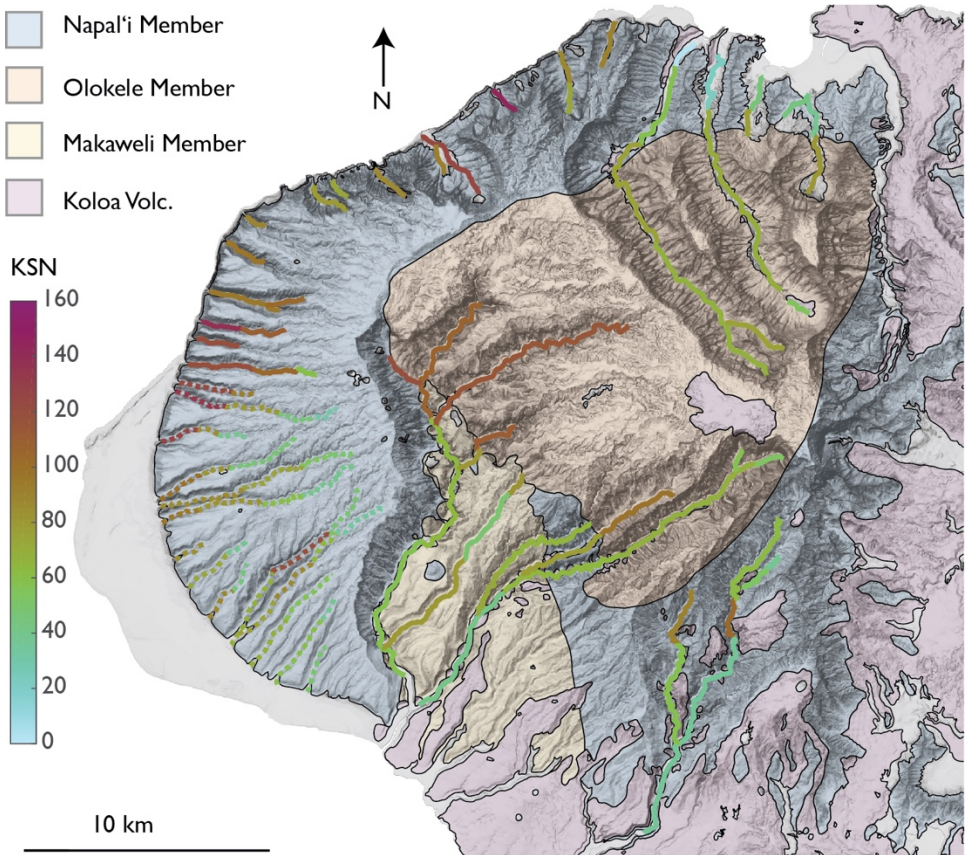

Figure 4.2. Spatial Patterns of Channel Steepness (k_{sn}) For Streams on Kaua'i. k_{sn} segments shown by solid and dashed lines. Dashed lines indicate uniform k_{sn} segment with a maximum incision depth less than 300 m.

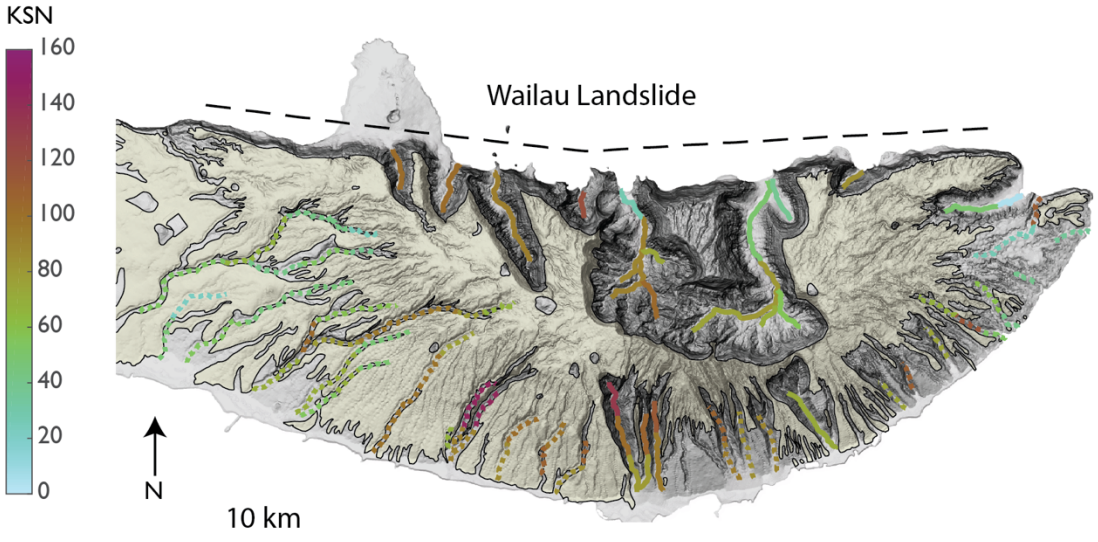

Figure 4.3. Spatial Patterns of Channel Steepness (k_{sn}) for Streams on East Moloka'i. Dashed lines indicate uniform k_{sn} segment with a maximum incision depth less than 300 m. Outlined yellow shading indicates locations of post-shield flows.

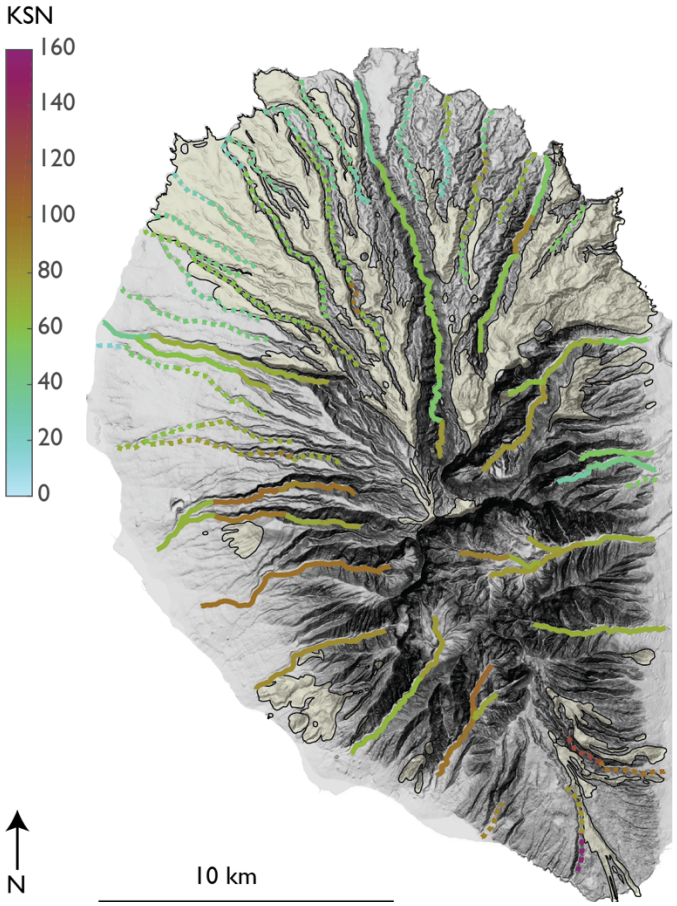

Figure 4.4. Spatial Patterns of Channel Steepness (k_{sn}) for Streams on West Maui. Dashed lines indicate uniform k_{sn} segment with a maximum incision depth less than 300 m. Outlined yellow shading indicates locations of post-shield flows.

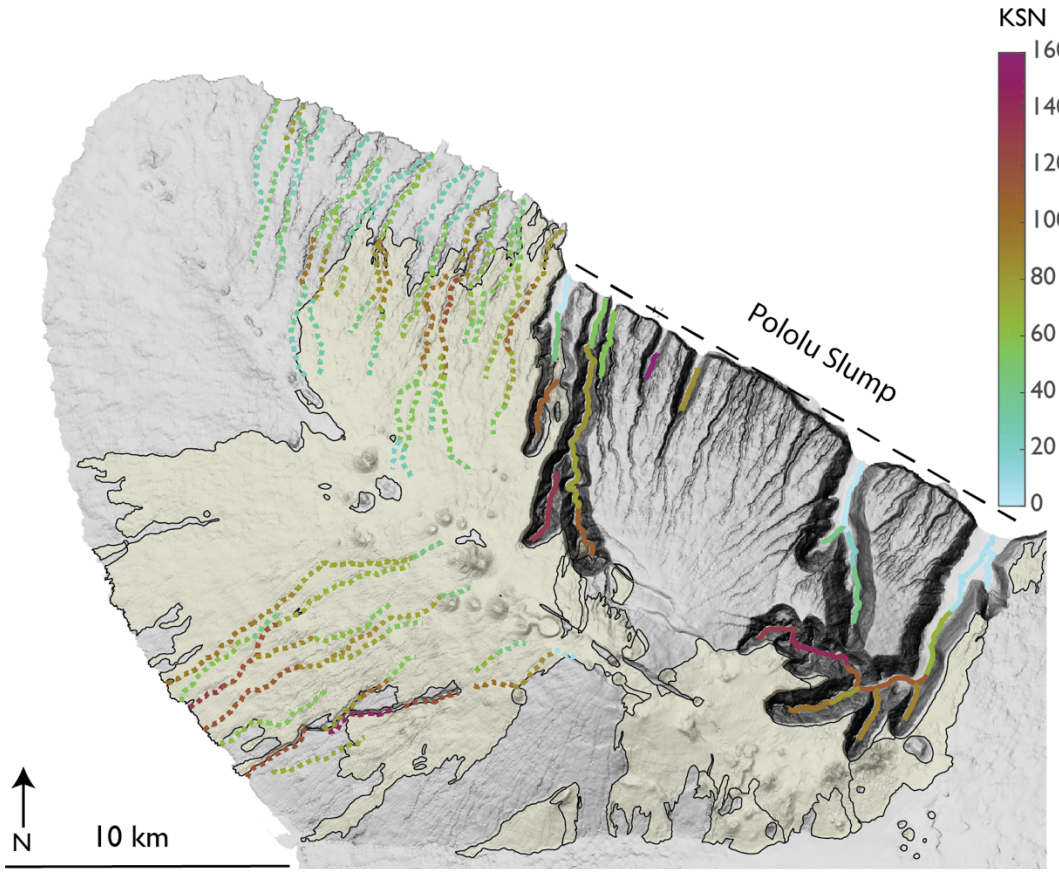

Figure 4.5. Spatial Patterns of Channel Steepness (k_{sn}) for Streams on Kohala. k_{sn} segments shown by solid and dashed lines. Dashed lines indicate uniform k_{sn} segment with a maximum incision depth less than 300 m. Outlined yellow shading indicates locations of post-shield flows

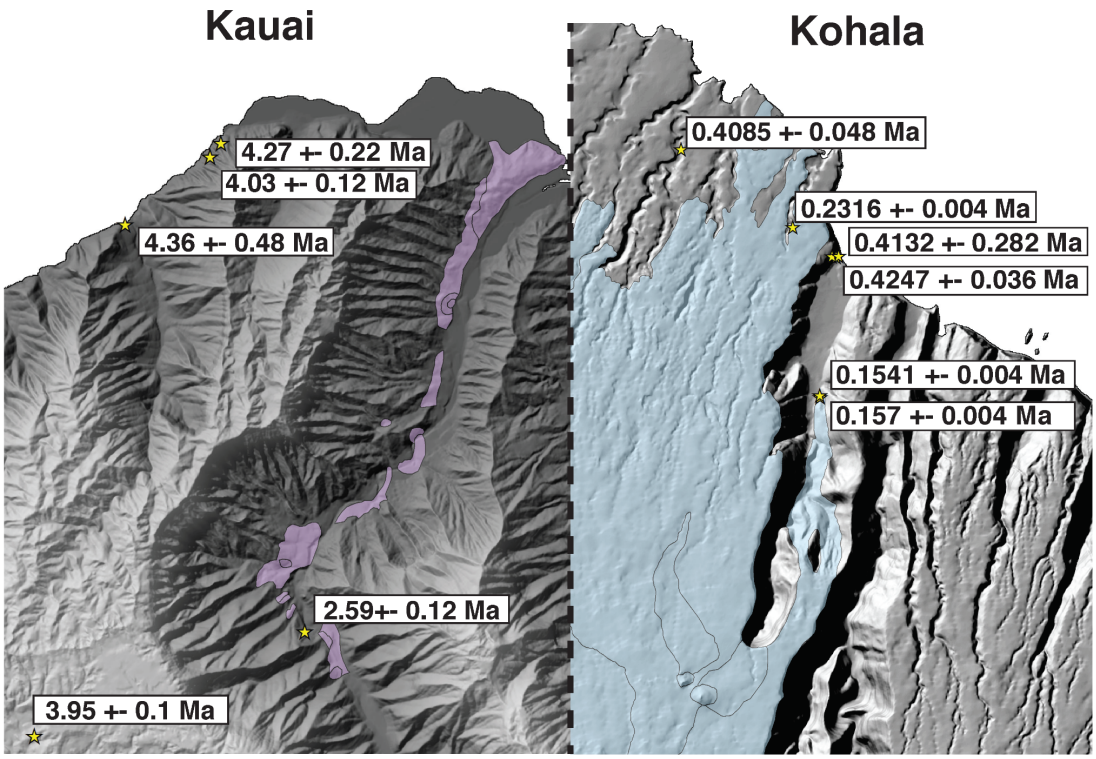

Figure 4.6. Evidence of Rapid Incision. Hillshade of the north coast of Kauaʻi and Kohala with rejuvenated volcanics shown by purple shading and post-shield volcanics shown by blue shading. Stars indicate radiometric dates of the shield stage, post-shield stage, and rejuvenated stage (Sherrod et al. 2021). Note both canyons are deeply incised (> 500m on Kohala and > 1km on Kauaʻi) which occurred relatively early after the shield building stage.

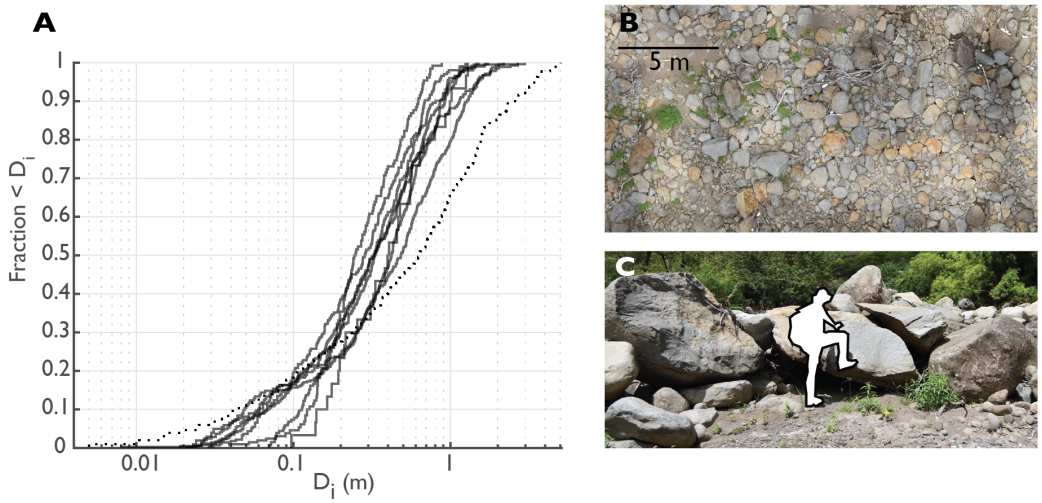

Figure 4.7. Bed Material Sediment Size on the Hawaiian Islands. A: Cumulative distribution of grain size from reach scale (solid line) and catchment scale (dotted line; data from Waiklou Valley, East Moloka'i courtesy of the Pacific Island Network Inventory and Monitoring Program) surveys. B: Photo mosaic of coarse bed material in Honokohau Valley, West Maui. C: Example of large boulders found in Waihee Valley, West Maui. Outline of person is ~ 2m.

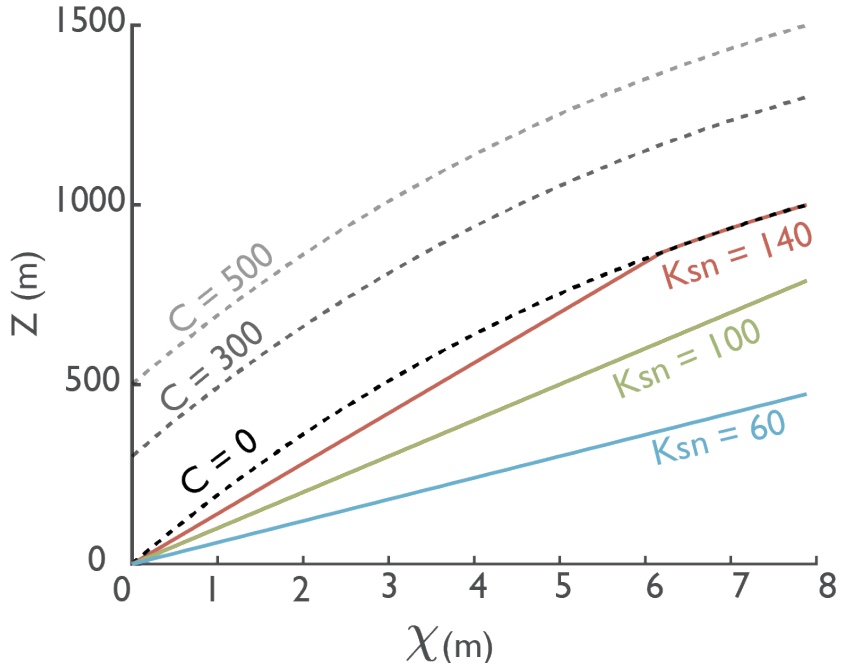

Figure 4.8. Conceptual Model of Controls on Incision Depth. Solid colored lines show χ transformed stream profiles with associated k_{sn}. Dotted lines show the initial volcano surface, with the gray and lighter gray lines showing the effect of a sea-cliff (C) on

incision depth. The maximum incision depth is then identified as the maximum difference between the initial volcano surface and the current stream profile. Other controls not explicitly shown is this figure are the influence of channel length (L) and volcano slope (S_v). In this example L = 10km and S_v = 0.1.

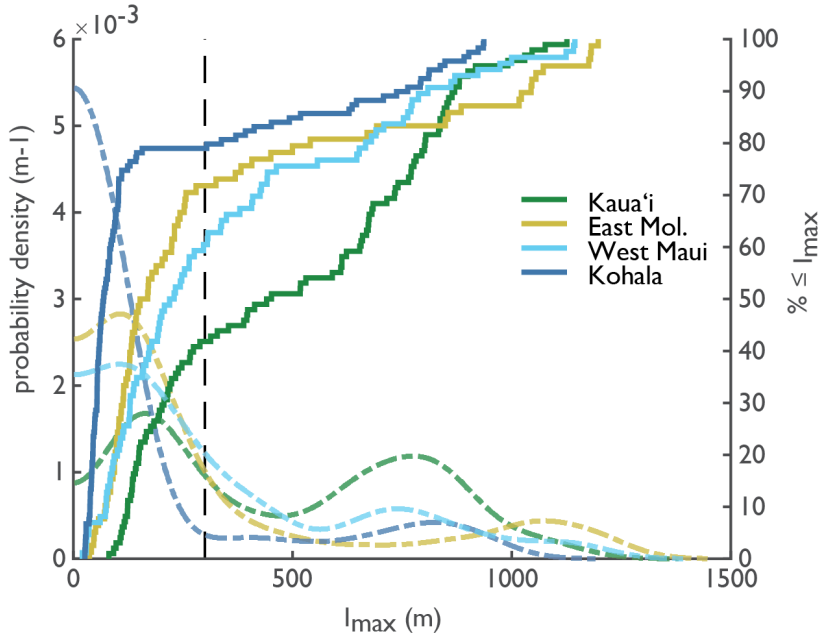

Figure 4.9. Bimodal Distributions of Maximum Incision Depths. Kernel density estimation (left y-axis) and cumulative distributions (right y-axis) of maximum incision depth (I_{max}) for uniform k_{sn} segment identified on Kaua'i (green), East Moloka'i (yellow), West Maui (light blue), and Kohala (dark blue). There are two separate distributions for each volcano, as demonstrated by the bimodal nature of kernel density estimation and by the change in the slope of the cumulative distribution of I_{max}. Vertical dashed line shows cutoff value of 300m which we use to separate lightly incised valleys from deeply incised valleys.

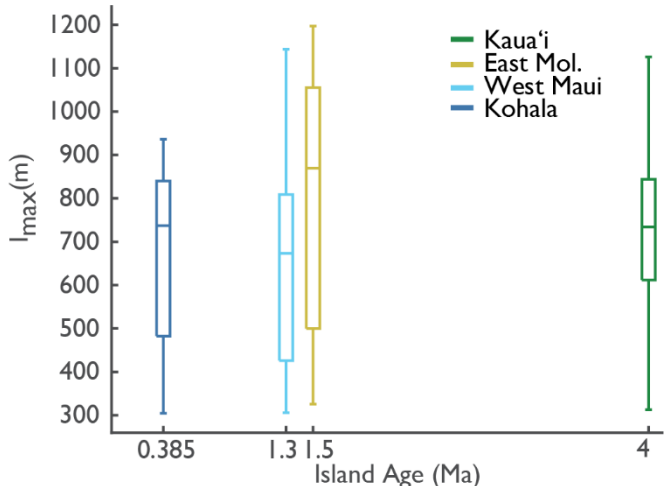

Figure 4.10. Comparison of Maximum Incision Depth Against Volcano Age. For each volcano the data is summarized by box and whiskers, with the lower and upper bounds of

the box showing the 25th and 75th percentile (i.e. interquartile range), and the horizontal line showing the median. The median value across the volcanos is near constant, whereas there is a step increase in the maximum value (upper whisker) from Kohala to West Maui but the maximum value appears to stay constant with the older islands.

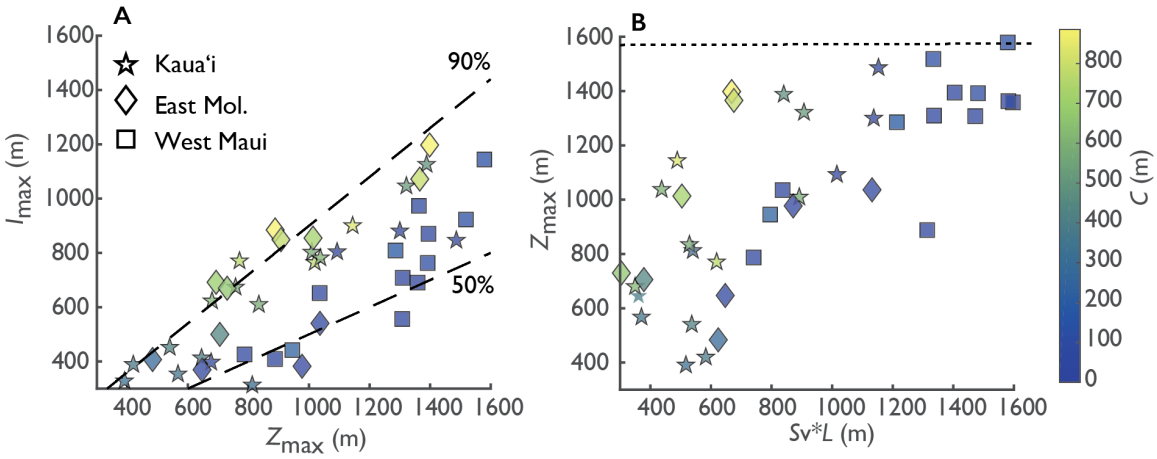

Figure 4.11. Major Controls on Maximum Incision Depths. A: Shows a scatter plot of the maximum potential depth of incision (Z_{max}) against the observed maximum depth of incision (I_{max}). Symbols are colored by sea-cliff height (C) and dashed lines show where I_{max} is 50% and 90% of Z_{max}. B: Shows Z_{max}as a function of average volcano slope (S_v) and catchment length (L). Symbols are also colored by sea-cliff and dotted line showsthe approximate maximum elevation of Kaua'i and East Moloka'i, whereas the maximum elevation of West Maui is ~1700m and outside the range of the y-axis.

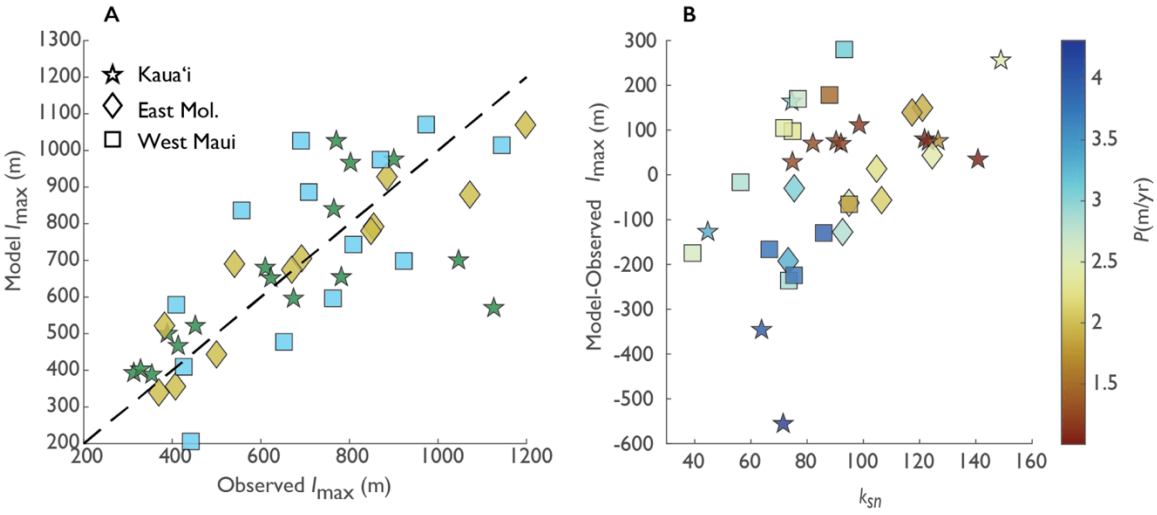

Figure 4.12. Modeled Vs Observed Maximum Incision Depth with Fixed k_{sn}. k_{sn} is fixed at the mean value of 84. A: Scatter plot of modeled vs observed I_{max}, with dashed line showing a 1:1 relationship. Note cluster of outliers for Kaua'i at the observed I_{max} of 800 m deviate from the predicted incision depth as these canyons are clearly not described by

a single volcano gradient (S_v). B: Scatter plot of the difference between modeled and observed I_{max} against k_{sn}, with symbols colored by mean annual rainfall (P).

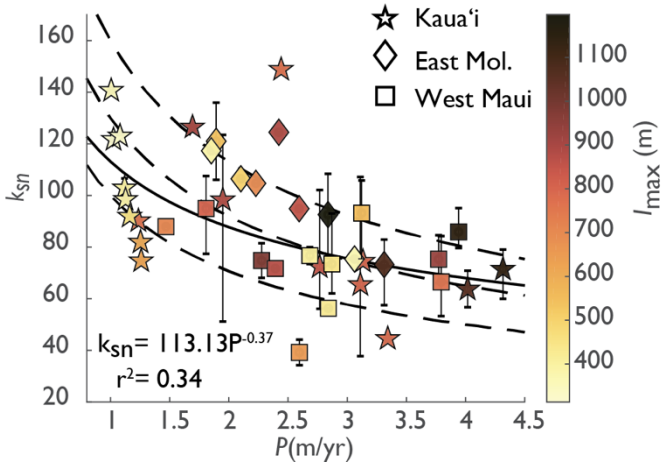

Figure 4.13. Climatic Influence on Channel Steepness. Error bars show range of k_{sn} within a given valley and dashed line indicate best fit power-law relationship. Dashed lines shows the theoretical predictions that $k_{sn} \propto P^{-0.5}$ with the upper lines showing a ~1.2 and 1.4 times increase in the threshold-setting grain size.

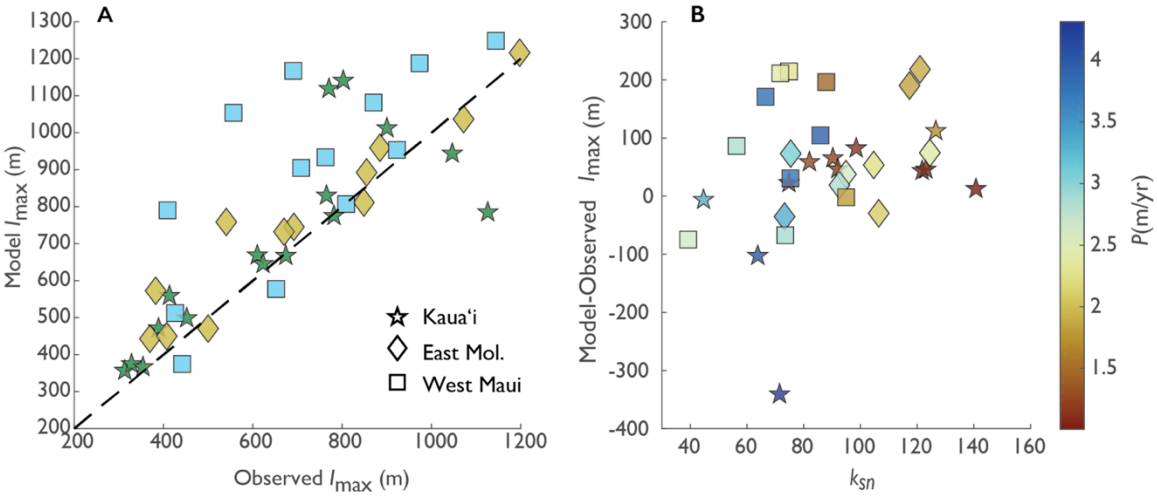

Figure 4.14. Modeled Vs Observed Maximum Incision Depth with $k_{sn} = 100P^{-0.5}$ A: Scatter plot of modeled vs observed Imax, with dashed line showing a 1:1 relationship. Note cluster of outliers for Kaua'i at the observed I_{max} of 800m deviate from the predicted incision depth as these canyons are clearly not described by a single volcano gradient (S_v). B: Scatter plot of the difference between modeled and observed I_{max} against k_{sn}, with symbols colored by mean annual rainfall (P).

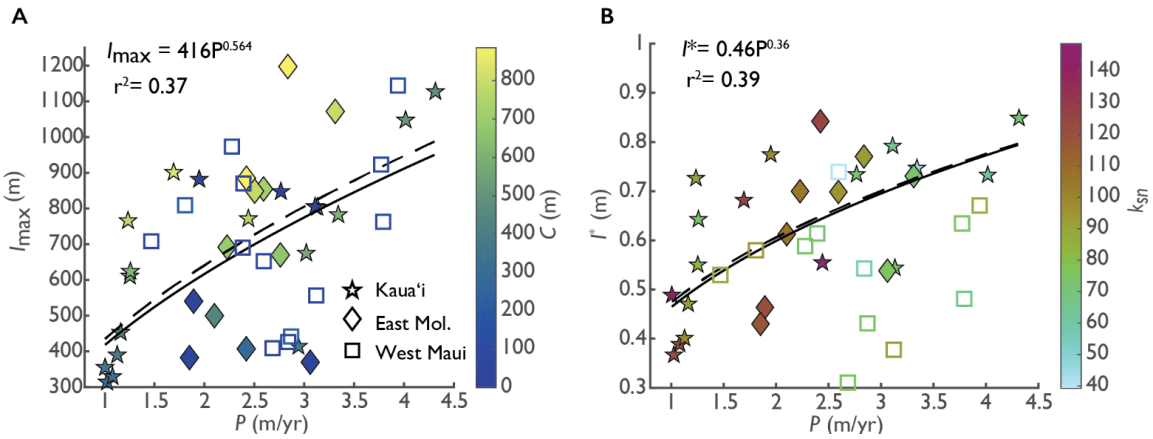

Figure 4.15. Climate Signals Recorded by Incision Depth. A: Scatter plot of I_{max} vs mean annual rainfall (P) with symbols colored by cliff height (C). Dashed line show fit to Kaua'i data, solid line show fit to Kaua'i data and East Moloka'i, regression results in figure are reported for the latter fit. B: Scatter plot of the normalized maximum incision depth I^*, where $I^* = \frac{I_{max}}{S_v L + C}$ where S_v is volcano gradient, L is channel length, and C is sea-cliff height. Lines are the same as in A. Normalizing by other potential controls on I_{max} does not considerably improve the overall fit, however, the dependency on P is clearly decreased and consistent with the empirical trend of P vs k_{sn} in Figure 14.

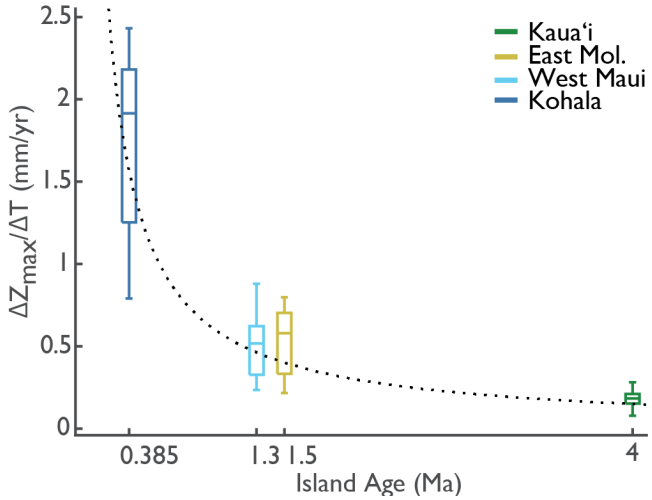

Figure 4.16. Time Averaged Incision Rates (mm/yr) as Function of Island Age. For each volcano the data is summarized by box and whiskers, with the lower and upper bounds of the box showing the 25th and 75th percentile (i.e. interquartile range), and the horizontal line showing the median. Dotted line shows the average maximum incision depth (~ 700) from all volcanoes divided by volcano age.

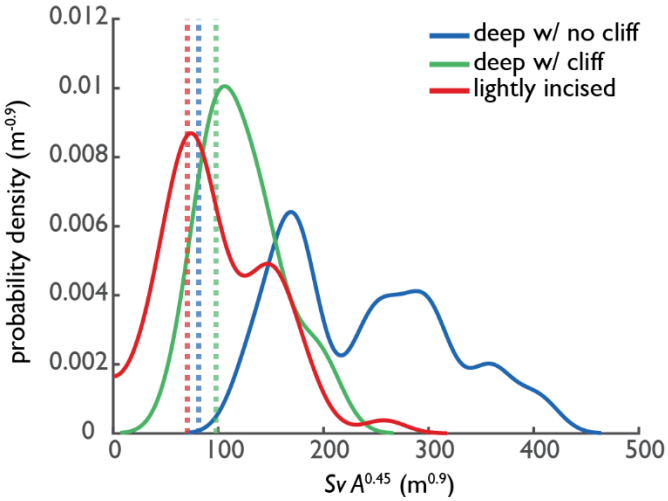

Figure 4.17. Controls on Rapid Incision. Kernel probability density estimate (bandwidth = 100) of catchment average reconstructed volcano gradient (S_V) weighted by catchment drainage area (A) raised to the 0.45 (solid lines) and mean catchment averaged k_{sn} (dotted lines). Data is categorized according to depth of incision and the presence of sea-cliffs. Red lines show lightly incised catchments (I_{max} < 300m), green lines show deeply incised (I_{max} > 300 m) catchments where significant sea-cliffs (sea-cliff height > 270 m—a cutoff reflecting the largest sea-cliffs found on West Maui) are present and the blue lines show deeply incised catchments (I_{max} > 300 m) where no sea-cliffs are present. This figure shows (1) that deeply incised canyons likely form where the initial channel steepness greatly exceeded the current channel steepness, or (2) that deeply incised canyons formed due to coastal erosion and/or flank collapse landslides, and (3) that there is little difference between lightly incised catchments and current k_{sn} indicating the majority may have persistently been at threshold conditions.

REFERENCES

Adams, B.A., Whipple, K.X., Forte, A.M., Heimsath, A.M., and Hodges, K.V., 2020, Climate controls on erosion in tectonically active landscapes: Science Advances, v. 6, p. eaaz3166, doi:10.1126/sciadv.aaz3166.

Annandale, G.W., 1995, Erodibility: Journal of Hydraulic Research, v. 33, p. 471–494, doi:10.1080/00221689509498656.

Asner, G.P., Elmore, A.J., Flint Hughes, R., Warner, A.S., and Vitousek, P.M., 2005, Ecosystem structure along bioclimatic gradients in Hawai'i from imaging spectroscopy: Remote Sensing of Environment, v. 96, p. 497–508, doi:10.1016/j.rse.2005.04.008.

Baldwin, J.A., Whipple, K.X., and Tucker, G.E., 2003, Implications of the shear stress river incision model for the timescale of postorogenic decay of topography:

Journal of Geophysical Research: Solid Earth, v. 108, doi:10.1029/2001JB000550.

Bishop, K.M., 2018, Landslide Interpretation of the Northeast Flank of Kohala Volcano, Hawaii: Environmental and Engineering Geoscience, v. 24, p. 187–205, doi:10.2113/EEG-1961.

von Blanckenburg, F., 2005, The control mechanisms of erosion and weathering at basin scale from cosmogenic nuclides in river sediment: Earth and Planetary Science Letters, v. 237, p. 462–479, doi:10.1016/j.epsl.2005.06.030.

Bookhagen, B., and Strecker, M.R., 2012, Spatiotemporal trends in erosion rates across a pronounced rainfall gradient: Examples from the southern Central Andes: Earth and Planetary Science Letters, v. 327, p. 97–110.

Bookhagen, B., Thiede, R.C., and Strecker, M.R., 2005, Late Quaternary intensified monsoon phases control landscape evolution in the northwest Himalaya: Geology, v. 33, p. 149–152.

Burbank, D.W., Blythe, A.E., Putkonen, J., Pratt-Sitaula, B., Gabet, E., Oskin, M., Barros, A., and Ojha, T.P., 2003, Decoupling of erosion and precipitation in the Himalayas: Nature, v. 426, p. 652–655, doi:10.1038/nature02187.

Campforts, B., Vanacker, V., Herman, F., Vanmaercke, M., Schwanghart, W., Tenorio, G.E., Willems, P., and Govers, G., 2020, Parameterization of river incision models requires accounting for environmental heterogeneity: insights from the tropical Andes: Earth Surface Dynamics, v. 8, p. 447–470, doi:https://doi.org/10.5194/esurf-8-447-2020.

Carretier, S. et al., 2013, Slope and climate variability control of erosion in the Andes of central Chile: Geology, v. 41, p. 195–198, doi:10.1130/G33735.1.

Chadwick, O.A., Gavenda, R.T., Kelly, E.F., Ziegler, K., Olson, C.G., Elliott, W.C., and Hendricks, D.M., 2003, The impact of climate on the biogeochemical functioning of volcanic soils: Chemical Geology, v. 202, p. 195–223, doi:10.1016/j.chemgeo.2002.09.001.

Chu, P.-S., Zhao, X., Ruan, Y., and Grubbs, M., 2009, Extreme Rainfall Events in the Hawaiian Islands: Journal of Applied Meteorology and Climatology, v. 48, p. 502–516, doi:10.1175/2008JAMC1829.1.

Clague, D.A., and Dalrymple, G.B., 1988, Age and petrology of alkalic postshield and rejuvenated-stage lava from Kauai, Hawaii: Contributions to Mineralogy and Petrology, v. 99, p. 202–218, doi:10.1007/BF00371461.

Clague, D.A., and Moore, J.G., 2002, The proximal part of the giant submarine Wailau landslide, Molokai, Hawaii: Journal of Volcanology and Geothermal Research, v. 113, p. 259–287, doi:10.1016/S0377-0273(01)00261-X.

Clague, D.A., and Sherrod, D.R., 2014, Growth and degradation of Hawaiian volcanoes, *in* Characteristics of Hawaiian volcanoes, Professional Paper, US Geological Survey, 1801, p. 97–146.

Costa, J.E., 1987, Hydraulics and basin morphometry of the largest flash floods in the conterminous United States: Journal of Hydrology, v. 93, p. 313–338, doi:10.1016/0022-1694(87)90102-8.

Dalrymple, G.B., 1971, Potassium-Argon Ages from the Pololu Volcanic Series, Kohala Volcano, Hawaii: GSA Bulletin, v. 82, p. 1997–2000, doi:10.1130/0016-7606(1971)82[1997:PAFTPV]2.0.CO;2.

Deal, E., Braun, J., and Botter, G., 2018, Understanding the Role of Rainfall and Hydrology in Determining Fluvial Erosion Efficiency: Journal of Geophysical Research: Earth Surface, v. 123, p. 744–778, doi:10.1002/2017JF004393.

DiBiase, R.A., and Whipple, K.X., 2011, The influence of erosion thresholds and runoff variability on the relationships among topography, climate, and erosion rate: Journal of Geophysical Research: Earth Surface, v. 116, http://onlinelibrary.wiley.com/doi/10.1029/2011JF002095/full (accessed June 2016).

Dietrich, W.E., Bellugi, D.G., Sklar, L.S., Stock, J.D., Heimsath, A.M., and Roering, J.J., 2003, Geomorphic Transport Laws for Predicting Landscape form and Dynamics, *in* Prediction in Geomorphology, American Geophysical Union (AGU), p. 103–132, doi:10.1029/135GM09.

Dixon, J.L., Chadwick, O.A., and Pavich, M.J., 2018, Climatically controlled delivery and retention of meteoric 10Be in soils: Geology, v. 46, p. 899–902, doi:10.1130/G45176.1.

Ferrier, K.L., Huppert, K.L., and Perron, J.T., 2013a, Climatic control of bedrock river incision: Nature, v. 496, p. 206–209, doi:https://doi.org/10.1038/nature11982.

Ferrier, K.L., Perron, J.T., Mukhopadhyay, S., Rosener, M., Stock, J.D., Huppert, K.L., and Slosberg, M., 2013b, Covariation of climate and long-term erosion rates across a steep rainfall gradient on the Hawaiian island of Kaua‘i: GSA Bulletin, v. 125, p. 1146–1163, doi:10.1130/B30726.1.

Finlayson, D.P., Montgomery, D.R., and Hallet, B., 2002, Spatial coincidence of rapid inferred erosion with young metamorphic massifs in the Himalayas: Geology, v. 30, p. 219–222, doi:10.1130/0091-7613(2002)030<0219:SCORIE>2.0.CO;2.

Finnegan, N.J., Klier, R.A., Johnstone, S., Pfeiffer, A.M., and Johnson, K., 2017, Field evidence for the control of grain size and sediment supply on steady-state bedrock river channel slopes in a tectonically active setting: Earth Surface Processes and Landforms, v. 42, p. 2338–2349, doi:10.1002/esp.4187.

Finnegan, N.J., Schumer, R., and Finnegan, S., 2014, A signature of transience in bedrock river incision rates over timescales of 104-107 years: Nature, v. 505, p. 391–394.

Forte, A.M., Leonard, J.S., Rossi, M.W., Whipple, K.X., Heimsath, A.M., Sukhishvili, L., Godoladze, T., and Kadirov, F., 2022, Low variability runoff inhibits coupling of climate, tectonics, and topography in the Greater Caucasus: Earth and Planetary Science Letters, v. 584, p. 117525, doi:10.1016/j.epsl.2022.117525.

Frazier, A.G., Giambelluca, T.W., Diaz, H.F., and Needham, H.L., 2016, Comparison of geostatistical approaches to spatially interpolate month-year rainfall for the Hawaiian Islands: International Journal of Climatology, v. 36, p. 1459–1470, doi:10.1002/joc.4437.

Gavenda, R.T., 1994, Hawaiian quaternary paleoenvironments: A review of geological, pedological, and botanical evidence., *in* A Natural History of the Hawaiian Islands: Selected Readings II, Honolulu, University of Hawaii Press, A Natural History of the Hawaiian Islands II, p. 118–130.

Gayer, E., Michon, L., Louvat, P., and Gaillardet, J., 2019, Storm-induced precipitation variability control of long-term erosion: Earth and Planetary Science Letters, v. 517, p. 61–70, doi:10.1016/j.epsl.2019.04.003.

Giambelluca, T.W., Chen, Q., Frazier, A.G., Price, J.P., Chen, Y.-L., Chu, P.-S., Eischeid, J.K., and Delparte, D.M., 2012, Online Rainfall Atlas of Hawai‘i: Bulletin of the American Meteorological Society, v. 94, p. 313–316, doi:10.1175/BAMS-D-11-00228.1.

Giambelluca, T.W., and Nullet, D., 1991, Influence of the trade-wind inversion on the climate of a leeward mountain slope in Hawaii: Climate Research, v. 1, p. 207–216.

Han, J., Gasparini, N.M., Johnson, J.P.L., and Murphy, B.P., 2014, Modeling the influence of rainfall gradients on discharge, bedrock erodibility, and river profile evolution, with application to the Big Island, Hawai’i: Journal of Geophysical Research: Earth Surface, v. 119, p. 1418–1440, doi:10.1002/2013JF002961.

Harkins, N., Kirby, E., Heimsath, A., Robinson, R., and Reiser, U., 2007, Transient fluvial incision in the headwaters of the Yellow River, northeastern Tibet, China: Journal of Geophysical Research: Earth Surface, v. 112, doi:https://doi.org/10.1029/2006JF000570.

Harris, A.J.L., Rowland, S.K., Villeneuve, N., and Thordarson, T., 2016, Pāhoehoe, ʻaʻā, and block lava: an illustrated history of the nomenclature: Bulletin of Volcanology, v. 79, p. 7, doi:10.1007/s00445-016-1075-7.

Hearty, P.J., Karner, D.B., Renne, P.R., Olson, S.L., and Fletcher, S., 2005, 40Ar/39Ar age of a young rejuvenation basalt flow: Implications for the duration of volcanism and the timing of carbonate platform development during the quaternary on Kaua'i, Hawaiian Islands: New Zealand Journal of Geology and Geophysics, v. 48, p. 199–211, doi:10.1080/00288306.2005.9515110.

Herschy, R.W., 2002, The world's maximum observed floods: Flow Measurement and Instrumentation, v. 13, p. 231–235, doi:10.1016/S0955-5986(02)00054-7.

Hinds, N.E., 1925, Amphitheater valley heads: The Journal of Geology, v. 33, p. 816–818.

Holcomb, R.T., 1987, Eruptive history and long-term behavior of Kilauea Volcano, *in* Volcanism In Hawaii, U.S.Geological Survey, v. 1, p. 261–350, https://pubs.usgs.gov/pp/1987/1350/.

Holcomb, R.T., Reiners, P.W., Nelson, B.K., and Sawyer, N.-L.E., 1997, Evidence for two shield volcanoes exposed on the island of Kauai, Hawaii: Geology, v. 25, p. 811–814, doi:10.1130/0091-7613(1997)025<0811:EFTSVE>2.3.CO;2.

Hotchkiss, S., Vitousek, P.M., Chadwick, O.A., and Price, J., 2000, Climate Cycles, Geomorphological Change, and the Interpretation of Soil and Ecosystem Development: Ecosystems, v. 3, p. 522–533, doi:10.1007/s100210000046.

Howard, A.D., 1994, A detachment-limited model of drainage basin evolution: Water Resources Research, v. 30, p. 2261–2285, doi:10.1029/94WR00757.

Howard, A.D., 1980, Thresholds in river regimes, *in* The Concept of Geomorphic Thresholds, Binghamton, N.Y., Allen and Unwin, p. 227–258.

Howard, A.D., Dietrich, W.E., and Seidl, M.A., 1994, Modeling fluvial erosion on regional to continental scales: Journal of Geophysical Research: Solid Earth, p. 13971–13986, doi:10.1029/94JB00744@10.1002/(ISSN)2169-9356.TECTOP1.

Huppert, K.L., Royden, L.H., and Perron, J.T., 2015, Dominant influence of volcanic loading on vertical motions of the Hawaiian Islands: Earth and Planetary Science Letters, v. 418, p. 149–171, doi:10.1016/j.epsl.2015.02.027.

Jackson, E.D., Silver, E.A., and Dalrymple, G.B., 1972, Hawaiian-Emperor Chain and Its Relation to Cenozoic Circumpacific Tectonics: GSA Bulletin, v. 83, p. 601–618, doi:10.1130/0016-7606(1972)83[601:HCAIRT]2.0.CO;2.

Katz, M.G., and Cashman, K.V., 2003, Hawaiian lava flows in the third dimension: Identification and interpretation of pahoehoe and ′a′a distribution in the KP-1 and SOH-4 cores: Geochemistry, Geophysics, Geosystems, v. 4, doi:10.1029/2001GC000209.

Killick, R., Fearnhead, P., and Eckley, I.A., 2012, Optimal Detection of Changepoints With a Linear Computational Cost: Journal of the American Statistical Association, v. 107, p. 1590–1598, doi:10.1080/01621459.2012.737745.

Kirby, E., and Whipple, K.X., 2012, Expression of active tectonics in erosional landscapes: Journal of Structural Geology, v. 44, p. 54–75.

Knapp, K.R., Kruk, M.C., Levinson, D.H., Diamond, H.J., and Neumann, C.J., 2010, The International Best Track Archive for Climate Stewardship (IBTrACS): Unifying Tropical Cyclone Data: Bulletin of the American Meteorological Society, v. 91, p. 363–376, doi:10.1175/2009BAMS2755.1.

Kochel, R.C., and Piper, J.F., 1986, Morphology of large valleys on Hawaii: Evidence for groundwater sapping and comparisons with Martian valleys: Journal of Geophysical Research: Solid Earth, v. 91, p. E175–E192, doi:https://doi.org/10.1029/JB091iB13p0E175.

Lague, D., 2014, The stream power river incision model: evidence, theory and beyond: Earth Surface Processes and Landforms, v. 39, p. 38–61, doi:10.1002/esp.3462.

Lague, D., Hovius, N., and Davy, P., 2005, Discharge, discharge variability, and the bedrock channel profile: Journal of Geophysical Research: Earth Surface, v. 110, p. F04006, doi:10.1029/2004JF000259.

Lamb, M.P., Howard, A.D., Dietrich, W.E., and Perron, J.T., 2007, Formation of amphitheater-headed valleys by waterfall erosion after large-scale slumping on Hawai ‘i: GSA Bulletin, v. 119, p. 805–822, doi:https://doi.org/10.1130/B25986.1.

Leopold, L.B., 1949, THE INTERACTION OF TRADE WIND AND SEA BREEZE, HAWAII: Journal of the Atmospheric Sciences, v. 6, p. 312–320, doi:10.1175/1520-0469(1949)006<0312:TIOTWA>2.0.CO;2.

Leopold, L.B., and Maddock Jr., T., 1953, The hydraulic geometry of stream channels and some physiographic implications: Professional Paper Report 252, 64 p., doi:10.3133/pp252.

Li, C., Wang, G., and Li, R., 2013, Maximum observed floods in China: Hydrological Sciences Journal, v. 58, p. 728–735, doi:10.1080/02626667.2013.772299.

Macdonald, G.A., Davis, D.A., and Cox, D.C., 1960, Geology and ground-water resources of the island of Kauai, Hawaii: Bulletin Other Government Series 13, http://pubs.er.usgs.gov/publication/70160871 (accessed December 2019).

Macdonald, F.A., Swanson-Hysell, N.L., Park, Y., Lisiecki, L., and Jagoutz, O., 2019, Arc-continent collisions in the tropics set Earth's climate state: Science, v. 364, p. 181–184, doi:10.1126/science.aav5300.

Mackey, B.H., Scheingross, J.S., Lamb, M.P., and Farley, K.A., 2014, Knickpoint formation, rapid propagation, and landscape response following coastal cliff retreat at the last interglacial sea-level highstand: Kaua'i, Hawai'i: GSA Bulletin, v. 126, p. 925–942, doi:10.1130/B30930.1.

McDougall, I., 1979, Age of shield-building volcanism of Kauai and linear migration of volcanism in the Hawaiian island chain: Earth and Planetary Science Letters, v. 46, p. 31–42, doi:10.1016/0012-821X(79)90063-3.

McDougall, I., and Swanson, D.A., 1972, Potassium-Argon Ages of Lavas from the Hawi and Pololu Volcanic Series, Kohala Volcano, Hawaii: GSA Bulletin, v. 83, p. 3731–3738, doi:10.1130/0016-7606(1972)83[3731:PAOLFT]2.0.CO;2.

McMurtry, G.M., Campbell, J.F., Fryer, G.J., and Fietzke, J., 2010, Uplift of Oahu, Hawaii, during the past 500 k.y. as recorded by elevated reef deposits: Geology, v. 38, p. 27–30, doi:10.1130/G30378.1.

Molnar, P., Anderson, R.S., Kier, G., and Rose, J., 2006, Relationships among probability distributions of stream discharges in floods, climate, bed load transport, and river incision: Journal of Geophysical Research: Earth Surface, v. 111, doi:10.1029/2005JF000310.

Montgomery, D.R., and Foufoula-Georgiou, E., 1993, Channel network source representation using digital elevation models: Water Resources Research, v. 29, p. 3925–3934, doi:https://doi.org/10.1029/93WR02463.

Montgomery, D.R., and Gran, K.B., 2001, Downstream variations in the width of bedrock channels: Water Resources Research, v. 37, p. 1841–1846, doi:https://doi.org/10.1029/2000WR900393.

Moore, J.G., Clague, D.A., Holcomb, R.T., Lipman, P.W., Normark, W.R., and Torresan, M.E., 1989, Prodigious submarine landslides on the Hawaiian Ridge: Journal of Geophysical Research: Solid Earth, v. 94, p. 17465–17484, doi:10.1029/JB094iB12p17465.

Murphy, B.P., Johnson, J.P.L., Gasparini, N.M., and Sklar, L.S., 2016, Chemical weathering as a mechanism for the climatic control of bedrock river incision: Nature, v. 532, p. 223–227, doi:10.1038/nature17449.

Nativ, R., and Turowski, J.M., 2020, Site Dependence of Fluvial Incision Rate Scaling With Timescale: Journal of Geophysical Research: Earth Surface, v. 125, p. e2020JF005808, doi:https://doi.org/10.1029/2020JF005808.

Okubo, C.H., 2004, Rock mass strength and slope stability of the Hilina slump, Kīlauea volcano, Hawai'i: Journal of Volcanology and Geothermal Research, v. 138, p. 43–76, doi:10.1016/j.jvolgeores.2004.06.006.

Ouimet, W.B., Whipple, K.X., Royden, L.H., Sun, Z., and Chen, Z., 2007, The influence of large landslides on river incision in a transient landscape: Eastern margin of the Tibetan Plateau (Sichuan, China): GSA Bulletin, v. 119, p. 1462–1476, doi:10.1130/B26136.1.

Palucis, M.C., and Lamb, M.P., 2017, What controls channel form in steep mountain streams? Geophysical Research Letters, v. 44, p. 2017GL074198, doi:10.1002/2017GL074198.

Parker, G., Wilcock, P.R., Paola, C., Dietrich, W.E., and Pitlick, J., 2007, Physical basis for quasi-universal relations describing bankfull hydraulic geometry of single-thread gravel bed rivers: Journal of Geophysical Research: Earth Surface, v. 112, doi:10.1029/2006JF000549.

Perron, J.T., and Royden, L., 2013, An integral approach to bedrock river profile analysis: Earth Surface Processes and Landforms, v. 38, p. 570–576, doi:10.1002/esp.3302.

Pfeiffer, A.M., Finnegan, N.J., and Willenbring, J.K., 2017, Sediment supply controls equilibrium channel geometry in gravel rivers: Proceedings of the National Academy of Sciences, v. 114, p. 3346–3351, doi:10.1073/pnas.1612907114.

Phillips, C.B., and Jerolmack, D.J., 2019, Bankfull Transport Capacity and the Threshold of Motion in Coarse-Grained Rivers: Water Resources Research, v. 55, p. 11316–11330, doi:10.1029/2019WR025455.

Phillips, C.B., and Jerolmack, D.J., 2016, Self-organization of river channels as a critical filter on climate signals: Science, v. 352, p. 694–697, doi:10.1126/science.aad3348.

Porder, S., Hilley, G.E., and Chadwick, O.A., 2007, Chemical weathering, mass loss, and dust inputs across a climate by time matrix in the Hawaiian Islands: Earth and Planetary Science Letters, v. 258, p. 414–427, doi:10.1016/j.epsl.2007.03.047.

Prancevic, J.P., Lamb, M.P., and Fuller, B.M., 2014, Incipient sediment motion across the river to debris-flow transition: Geology, v. 42, p. 191–194, doi:10.1130/G34927.1.

Raming, L.W., and Whipple, K.X., 2022, When knickzones limit upstream transmission of base-level fall: An example from Kauaʻi, Hawaiʻi: Geology, doi:10.1130/G50019.1.

Raymo, M.E., 1991, Geochemical evidence supporting T. C. Chamberlin's theory of glaciation: Geology, v. 19, p. 344–347, doi:10.1130/0091-7613(1991)019<0344:GESTCC>2.3.CO;2.

Raymo, M.E., and Ruddiman, W.F., 1992, Tectonic forcing of late Cenozoic climate: Nature, v. 359, p. 117–122, doi:10.1038/359117a0.

Rossi, M.W., Whipple, K.X., and Vivoni, E.R., 2016, Precipitation and evapotranspiration controls on daily runoff variability in the contiguous United States and Puerto Rico: Journal of Geophysical Research: Earth Surface, v. 121, p. 128–145, doi:10.1002/2015JF003446.

Scherler, D., DiBiase, R.A., Fisher, G.B., and Avouac, J.-P., 2017, Testing monsoonal controls on bedrock river incision in the Himalaya and Eastern Tibet with a stochastic-threshold stream power model: Journal of Geophysical Research: Earth Surface, v. 122, p. 1389–1429, doi:10.1002/2016JF004011.

Schwanghart, W., and Scherler, D., 2014, Short Communication: TopoToolbox 2 – MATLAB-based software for topographic analysis and modeling in Earth surface sciences: Earth Surface Dynamics, v. 2, p. 1–7, doi:https://doi.org/10.5194/esurf-2-1-2014.

Scott, G.A.J., and Street, J.M., 1976, The role of chemical weathering in the formation of Hawaiian Amphitheatre-headed valleys.: Zeitschrift fr Geomorphologie, Annals of geomorphology.,.

Seidl, M.A., Dietrich, W.E., and Kirchner, J.W., 1994, Longitudinal profile development into bedrock: An analysis of Hawaiian channels: Journal of Geology, v. 102, p. 457, doi:10.1086/629686.

Sherrod, D.R., Sinton, J.M., Watkins, S.E., and Brunt, K.M., 2021, Geologic map of the State of Hawaii: U.S. Geological Survey Scientific Investigations Map USGS Numbered Series 3143, 72 p., doi:10.3133/sim3143.

Sinton, J.M., Eason, D.E., and Duncan, R.A., 2017, Volcanic evolution of Molokaʻi, Hawaiʻi: Implications for the shield to postshield transition in Hawaiian volcanoes: Journal of Volcanology and Geothermal Research, v. 340, p. 30–51, doi:10.1016/j.jvolgeores.2017.04.011.

Sklar, L.S., and Dietrich, W.E., 2006, The role of sediment in controlling steady-state bedrock channel slope: Implications of the saltation–abrasion incision model: Geomorphology, v. 82, p. 58–83, doi:10.1016/j.geomorph.2005.08.019.

Small, E.E., Blom, T., Hancock, G.S., Hynek, B.M., and Wobus, C.W., 2015, Variability of rock erodibility in bedrock-floored stream channels based on abrasion mill experiments: Journal of Geophysical Research: Earth Surface, v. 120, p. 1455–1469, doi:10.1002/2015JF003506.

Snyder, N.P., Whipple, K.X., Tucker, G.E., and Merritts, D.J., 2003, Importance of a stochastic distribution of floods and erosion thresholds in the bedrock river incision problem: Journal of Geophysical Research: Solid Earth, v. 108, p. 2117, doi:10.1029/2001JB001655.

Stearns, H.T., and Macdonald, G.A., 1942, General geology and ground-water resources of the island of Maui, Hawaii: Advertiser Publishing Co.

Stearns, H.T., and Macdonald, G.A., 1946, Geology and ground-water resources of the island of Hawaii: Honolulu Advertising 9, https://pubs.er.usgs.gov/publication/70160867 (accessed August 2022).

Stearns, H.T., and Vaksvik, K.N., 1935, Geology and ground-water resources of the island of O ʻahu, Hawai ʻi. Hawai ʻi Division of Hydrography: Bulletin, v. 1, p. 479.

Stock, J., and Dietrich, W.E., 2003, Valley incision by debris flows: Evidence of a topographic signature: Water Resources Research, v. 39, doi:10.1029/2001WR001057.

Stock, J.D., Montgomery, D.R., Collins, B.D., Dietrich, W.E., and Sklar, L., 2005, Field measurements of incision rates following bedrock exposure: Implications for process controls on the long profiles of valleys cut by rivers and debris flows: GSA Bulletin, v. 117, p. 174–194, doi:10.1130/B25560.1.

Thaler, E.A., and Covington, M.D., 2016, The influence of sandstone caprock material on bedrock channel steepness within a tectonically passive setting: Buffalo National River Basin, Arkansas, USA: Journal of Geophysical Research: Earth Surface, v. 121, p. 1635–1650, doi:10.1002/2015JF003771.

Thiede, R.C., Bookhagen, B., Arrowsmith, J.R., Sobel, E.R., and Strecker, M.R., 2004, Climatic control on rapid exhumation along the Southern Himalayan Front: Earth and Planetary Science Letters, v. 222, p. 791–806, doi:10.1016/j.epsl.2004.03.015.

Tucker, G.E., 2004, Drainage basin sensitivity to tectonic and climatic forcing: implications of a stochastic model for the role of entrainment and erosion thresholds: Earth Surface Processes and Landforms, v. 29, p. 185–205, doi:10.1002/esp.1020.

Vitousek, P., Asner, G.P., Chadwick, O.A., and Hotchkiss, S., 2009, Landscape-level variation in forest structure and biogeochemistry across a substrate age gradient in Hawaii: Ecology, v. 90, p. 3074–3086, doi:10.1890/08-0813.1.

Vitousek, P., Dixon, J.L., and Chadwick, O.A., 2016, Parent material and pedogenic thresholds: observations and a simple model: Biogeochemistry, v. 130, p. 147–157, doi:10.1007/s10533-016-0249-x.

Voigtlander, J.V., Clark, M.K., Zekkos, D., Greenwood, W.W., Anderson, S.P., Anderson, R.S., and Godt, J.W., 2018, Strong variation in weathering of layered rock maintains hillslope-scale strength under high precipitation: Earth Surface Processes and Landforms, v. 43, p. 1183–1194, doi:doi.org/10.1002/esp.4290.

Watts, A.B., and Brink, U.S.T., 1989, Crustal structure, flexure, and subsidence history of the Hawaiian Islands: J. Geophys. Res, p. 863–870.

Wentworth, C.K., 1928, Principles of Stream Erosion in Hawaii: The Journal of Geology, v. 36, p. 385–410.

Wentworth, C.K., and Macdonald, G.A., 1953, Structures and Forms of Basaltic Rocks in Hawaii: USGS Bulletin USGS Numbered Series 994, doi:10.3133/b994.

Whipple, K.X., DiBiase, R.A., Crosby, B., and Johnson, J.P.L., 2022, 6.40 - Bedrock Rivers, *in* Shroder, J. (Jack) F. ed., Treatise on Geomorphology (Second Edition), Oxford, Academic Press, p. 865–903, doi:10.1016/B978-0-12-818234-5.00101-2.

Whipple, K.X., and Tucker, G.E., 1999, Dynamics of the stream-power river incision model: Implications for height limits of mountain ranges, landscape response timescales, and research needs: Journal of Geophysical Research: Solid Earth, v. 104, p. 17661–17674.

White, S.E., 1949, Processes of erosion on steep slopes of oahu, Hawaii: American Journal of Science, v. 247, p. 168–186, doi:10.2475/ajs.247.3.168.

Willett, S.D., 1999, Orogeny and orography: The effects of erosion on the structure of mountain belts: Journal of Geophysical Research: Solid Earth, v. 104, p. 28957–28981, doi:10.1029/1999JB900248.

Wohl, E., and Merritt, D.M., 2008, Reach-scale channel geometry of mountain streams: Geomorphology, v. 93, p. 168–185, doi:https://doi.org/10.1016/j.geomorph.2007.02.014.

Wolfe, E.W., and Morris, J., 1996, Geologic map of the island of Hawaii: US Geological Survey, 2524-A.

CHAPTER 5

SYNTHESIS

This dissertation is centered on the landscape evolution of the Hawaiian Islands, with emphasis on the role of threshold bedrock river incision. Below I summarize key findings from this work and highlight opportunities for future research.

WATERFALLS AND KNICKZONES

Chapter 2 and Chapter 3 focus on the role of waterfalls and knickzones in the landscape evolution of the Hawaiian Islands. A number of studies (Seidl et al., 1994, 1997; Howard et al., 1994; Stock and Montgomery, 1999; De Young, 2000; Chatanantavet and Parker, 2005; Lamb et al., 2007; Mackey et al., 2014) have previously focused on the processes that drive knickzone retreat on the Hawaiian Islands and their role in transmitting signals of base-level fall in response to coastal erosion. Virtually, all of these studies assumed that the variability in rock mass properties associated with the different lava flow types is so wide spread as to be inconsequential to where knickzone form and or stall. Chapter 2 relaxes this assumption and furthermore challenges the paradigm that knickzones on the Nāpali Coast of Kaua'i are in fact actively retreating (e.g. Seidl et al., 1994; Mackey et al., 2014). From the analysis in Chapter 2 we present observations that strong and massive ‘a‘ā flows and or dikes crop out at the lip of every knickzone visited in the field. We then compare canyons with knickzones to canyons without knickzones to demonstrate that the effect of knickzones on the Nāpali coast is to limit bedrock river incision and the upstream transmission of base-level fall. The inhibiting nature of knickzones is further reinforced, as we show a clear correlation

between knickzone and sea-cliff height—with some knickzones accruing more than 450m of base-level fall that occurred prior to 1.5 Ma. We use these observations to motivate the question why do knickzones, including fluvial hanging valleys which are defined as waterfalls that remain elevated above the nearest tributary junction or coast line (Wobus et al., 2006; Crosby et al., 2007), appear to stall at a threshold drainage area (Crosby and Whipple, 2006)? To answer this question, we use a stochastic distribution of peak annual floods from a local stream gauge to demonstrate that channel conditions above knickzones have rapidly decreasing probabilities of mobilizing coarse sediment above knickzones, with probabilities of exceeding thresholds of motion approaching near zero at approximately 1 km^2. A drainage area consistent with where most fluvial hanging valleys form or stall.

Chapter 3 builds on the findings from Chapter 2 by extending a similar analysis to a larger fraction of the volcanos on the Hawaiian Islands. Our findings show that virtually all of the knickzones identified are consistent with a threshold drainage area—albeit with quite a wide range from 0.1 to 10 km^2. Topographic analysis reveals that in part the range in drainage area may be explained by a dependency on volcano slope, indicating that where knickzone stall or form is consistent with a near-constant critical unit stream power. Motivated by these observations we tested the hypothesis that knickzones represent a physical limit in bedrock river incision, where even the largest possible floods are unable to drive incision. To test this hypothesis, we developed an envelope curve for the largest observed floods across the world, with a subtle but important break where the discharge-area power-law exponent changes from ~1 to 0.7 at 2km^2. Using this estimate of the maximum observed flood we then estimate the

maximum unit stream power possible above each knickzone. From this analysis we found that hanging valleys can be well described by the conditions $\omega_m \leq \omega_c$, where $\omega_c \cong 21$ (kW/m^2), a value that is close to the critical stream power required to mobilize some of the largest observed boulders mobilized in extreme floods on the Hawaiian Islands. The majority of knickzones that have retreated or formed upstream of tributaries or the coast also generally follow the same patterns as hanging valleys though with slightly higher values of ω_m. Importantly, in this analysis the observed break in discharge-area scaling with the maximum observed flood appears to be expressed in the relationship of drainage area above knickzones against measured channel gradient and is consistent with theoretical predictions. Additionally, through this framework, our analysis does show that a handful knickzones in the Pololū Slump region on Kohala are clearly above the critical unit stream power and likely incising and or retreating, an interpretation that is consistent with the region's younger age.

THRESHOLD CHANNELS

Where Chapter 2 and 3 focus on limits of bedrock river incision above waterfalls and knickzones—Chapter 4 examines how thresholds in channels below waterfalls act to limit bedrock river incision and how thresholds influence our understanding of the role of climate in landscape evolution of the Hawaiian Islands. Specifically, we build on the work of other studies that have examined how climate influences bedrock river incision on the Hawaiian Islands (Ferrier et al., 2013a; Han et al., 2014; Ward and Galewsky, 2014; Murphy et al., 2016) but focus on the importance of thresholds in determining the overall patterns of incision. The importance of thresholds on the Hawaiian Islands can be

demonstrated by the observations: (1) that the majority of channels on the Hawaiian islands are heavily armored by large boulders, (2) inset volcanics constrain where in the landscape canyons have cut rapidly into the edifice of the shield volcano and demonstrate that the majority of incision (500-1000+ m) can occur within a relatively short period of time (0.15-1.5 Ma), and (3) longitudinal stream profiles in the majority of canyons exhibit nearly uniform channel steepness demonstrating that rivers and streams exhibit a near uniform shear stress or stream power—a condition in tectonically active landscapes that would be interpreted as representing steady state conditions where uplift balances erosion. However, on the Hawaiian Islands, where tectonic signals are limited, the only other explanation for this observed pattern is that rivers are at a threshold steady state limited by thresholds in sediment motion and or sediment flux.

Motivated by these observations, we show that the influence of climate on patterns of incision on the Hawaiian Islands is to determine the depth of incision—but we cannot infer, at least from the topography, how climate influences incision rate. In our analysis we automatically identify uniform normalized channel steepness (k_{sn}) segments and classify valleys as either deeply incised (> 300 m) or lightly incised (< 300 m). We then show for deeply incised canyons that although sea-cliff height, volcano slope, and catchment length play an important role in determining incision depth, critically it is through k_{sn} that signals of climate are encoded into incision depth. Specifically, we find that the influence of k_{sn} on mean annual rainfall (P) is relatively consistent with the theoretical prediction that $k_{sn} \sim P^{-0.5}$ (though our best fit showed a slightly lower dependency at $P^{-0.36}$, a value that maybe more consistent with $W \propto Q^{0.3}$), and that by

normalizing for the other dominant factors of incision the same dependency on P is recovered from patterns of incision.

FUTURE RESEARCH

The Hawaiian Islands provide an excellent natural laboratory for understanding how climate and surface processes interact to influence landscape evolution. The work presented in this dissertation provides only a hint at the full potential of the Hawaiian Islands in informing our understanding of how climate, thresholds, and coastal erosion exert dominant controls in surface processes and landscape evolution. Below I outline key areas of research that deserve further attention. I start with work that will improve upon the findings presented in this analysis and then I outline key observations that need further explanations and may play important role in understanding how coastal erosion and climate drive landscape evolution on the Hawaiian Islands.

The majority of the work presented in this dissertation relies on simple theoretical predictions that can be easily tested from medium resolution topography (10m DEM). Perhaps the biggest assumption in my work is how channel width scales with discharge and or drainage area. Ferrier et al (2013) found that floods with the probability of a 90-day recurrence interval, exhibit a power-law scaling with the square root of discharge. In other mountainous settings power-law scaling of channel width with drainage area or discharge show a lower dependency with a predicted exponent around 0.3 (Wohl and Merritt, 2008; Whipple et al., 2022). The latter is more consistent with our findings; however, it remains uncertain whether the decreased dependency of k_{sn} on P results from the relationship between channel width and drainage area, or because there is just a

weaker than predicted dependence on climate. Regardless, channel width remains one of the most important controls on unit stream power (Baker and Costa, 1987) and because weathering has the potential role to be a dominate factor in bedrock river incision on the Hawaiian Islands (Murphy et al., 2016), there may be important signals of weathering preserved by channel width. The best evidence for this is presented by Small et al. (2015), where they show that basalt on Hawai'i and Maui exhibit preferential weathering on channel perimeters relative to the thalweg. This influence of weathering in conjunction with variability in rock mass properties due to variation in lava flows may provide a mechanism where channel widening may significantly reduce unit stream power. This may be one mechanism that explains the range of values for ω_m estimated in Chapter 3.

Beyond channel width, the influence of grain size clearly plays an important predicted role in setting threshold conditions. A key thread, common to all the chapters in my dissertation focus on how ʻaʻā and pāhoehoe lava flows produce distinct rock mass properties and to some degree can be associated with the topography and shield stage (Katz and Cashman, 2003; Sinton et al., 2017). Importantly because rock mass properties such as fracture density determine the size of sediment delivered from hillslopes to channels (Neely and DiBiase, 2020; Verdian et al., 2020) there is reason to suspect that the threshold setting grain size should vary considerably across the Hawaiian Islands. Future research focused on the field collection of data on grain size and channel width will clearly be valuable and may aid in explaining the range in ω_m above knickzones and variations in k_{sn}.

One of the last major areas flagged for potential research that is directly relevant to the work presented in this dissertation is better understanding of how extreme precipitation events and mean climate conditions differ. In particular, we hypothesize that the weak to absent signal of mean annual rainfall associated with knickzones may be a result of decoupling between extreme rainfall events and mean annual rainfall rates. With the advent of new climate data sets (e.g. Huang et al., 2022) it should now be possible to evaluate the degree to which mean climate conditions and extreme events are decoupled. Furthermore, the duration and intensity of rainfall may have a direct impact on the discharge-area scaling break of $2km^2$ for maximum observed floods. Consequently, pairing these observations with the influence of topography on extreme events (Foster et al., 2003) maybe beneficial to understanding controls on extreme floods and how they impact landscape evolution.

Outside of bedrock channels, one of the more impressive and notable features of the Hawaiian Islands is the presence of thin ridge lines that protrude from valleys walls resulting in a corrugated appearance of the valley walls at a catchment scale. These features have likely developed in response to soil avalanches (Scott and Street, 1976) which are only thought to occur above 1.4 m/yr. This rainfall rate is also associated with a step wise increase in weathering on Kohala (Chadwick et al., 2003) and changes in the dominance of non-photosynthetic vegetation to photosynthetic vegetation (Asner et al., 2005). Furthermore, even the influence of climate recorded on drainage area above knickzones appears to be largely driven by a step change in drainage area for knickzones on Kaua'i that are dryer than 1.4 m/yr (Fig. 3.12). It is possible that the alignment of these different observation with a mean annual rainfall rate 1.4 m/yr is a coincidence. However,

evidence suggests that a whole suite of processing driven by weathering and possibly related to vegetation, begin to operate at the threshold value of 1.4 m/yr, which is associated with a positive water balance (Chadwick et al., 2003). Fut.
ure work linking these behaviors to weathering and the physical processes that ensue has the potential to transform our understanding of how climate drives landscape evolution.

Another important area needing additional research, is on the coupling between coastal processes and channel dynamics. The western end of the Nāpali coast on Kaua'i exhibits a wide range of channel steepness. Examination of the topography from lidar shows that the where the highest channel steepness values occur is associated with the current coastline where the Mana Plain meets the cliffs of the Nāpali coast (Fig. 2.1), with channels that have narrowed and evacuated the majority of their alluvial fill. Furthermore, direct coupling between submarine canyons and terrestrial canyons on the Hawaiian Islands occurs in several locations. Whether and how this coupling influences evolution of the terrestrial canyon is unclear, but in places (i.e. Kalalau Valley on Kaua‘i) there is evidence to suggest that coupled submarine-terrestrial canyons may experience higher rates of erosion. Research on understanding how fluvial and colluvial processes respond to changes in boundary conditions at the coastline have important implications for understanding how previous and future high stands impact the landscape.

REFERENCES

Asner, G.P., Elmore, A.J., Flint Hughes, R., Warner, A.S., and Vitousek, P.M., 2005, Ecosystem structure along bioclimatic gradients in Hawai’i from imaging spectroscopy: Remote Sensing of Environment, v. 96, p. 497–508, doi:10.1016/j.rse.2005.04.008.

Baker, V.R., and Costa, J.E., 1987, Flood power, *in* Catastrophic Flooding, Routledge, 21 p.

Chadwick, O.A., Gavenda, R.T., Kelly, E.F., Ziegler, K., Olson, C.G., Elliott, W.C., and Hendricks, D.M., 2003, The impact of climate on the biogeochemical functioning of volcanic soils: Chemical Geology, v. 202, p. 195–223, doi:10.1016/j.chemgeo.2002.09.001.

Chatanantavet, P., and Parker, G., 2005, Modeling the bedrock river evolution of western Kaua'i, Hawai'i, by a physically-based incision model based on abrasion, *in* Tunnelling. A Decade of Progress. GeoDelft 1995-2005, p. 99–110.

Crosby, B.T., and Whipple, K.X., 2006, Knickpoint initiation and distribution within fluvial networks: 236 waterfalls in the Waipaoa River, North Island, New Zealand: Geomorphology, v. 82, p. 16–38, doi:10.1016/j.geomorph.2005.08.023.

Crosby, B.T., Whipple, K.X., Gasparini, N.M., and Wobus, C.W., 2007, Formation of fluvial hanging valleys: Theory and simulation: Journal of Geophysical Research: Earth Surface, v. 112, doi:https://doi.org/10.1029/2006JF000566.

De Young, N., 2000, Modeling the Geomorphic Evolution of Western Kauai, Hawaii: A study of surface processes in a basaltic terrain. [Masters]: Dalhousie University, 157 p., https://www.collectionscanada.gc.ca/obj/s4/f2/dsk1/tape4/PQDD_0018/MQ57281.pdf (accessed December 2019).

Ferrier, K.L., Huppert, K.L., and Perron, J.T., 2013, Climatic control of bedrock river incision: Nature, v. 496, p. 206–209, doi:https://doi.org/10.1038/nature11982.

Foster, J., Bevis, M., Chen, Y.-L., Businger, S., and Zhang, Y., 2003, The Ka‘ storm (November 2000): Imaging precipitable water using GPS: Journal of Geophysical Research: Atmospheres, v. 108, doi:10.1029/2003JD003413.

Han, J., Gasparini, N.M., Johnson, J.P.L., and Murphy, B.P., 2014, Modeling the influence of rainfall gradients on discharge, bedrock erodibility, and river profile evolution, with application to the Big Island, Hawai'i: Journal of Geophysical Research: Earth Surface, v. 119, p. 1418–1440, doi:10.1002/2013JF002961.

Howard, A.D., Dietrich, W.E., and Seidl, M.A., 1994, Modeling fluvial erosion on regional to continental scales: Journal of Geophysical Research: Solid Earth, p. 13971–13986, doi:10.1029/94JB00744@10.1002/(ISSN)2169-9356.TECTOP1.

Huang, Y.-F., Gayte, M., Tsang, Y., Longman, R.J., Nugent, A.D., Kodama, K., Lucas, M.P., and Giambelluca, T.W., 2022, Hourly rainfall data from rain gauge networks and weather radar up to 2020 across the Hawaiian Islands: Scientific Data, v. 9, p. 334, doi:10.1038/s41597-022-01430-2.

Katz, M.G., and Cashman, K.V., 2003, Hawaiian lava flows in the third dimension: Identification and interpretation of pahoehoe and ′a′a distribution in the KP-1 and SOH-4 cores: Geochemistry, Geophysics, Geosystems, v. 4, doi:10.1029/2001GC000209.

Lamb, M.P., Howard, A.D., Dietrich, W.E., and Perron, J.T., 2007, Formation of amphitheater-headed valleys by waterfall erosion after large-scale slumping on Hawai ʻi: GSA Bulletin, v. 119, p. 805–822, doi:https://doi.org/10.1130/B25986.1.

Mackey, B.H., Scheingross, J.S., Lamb, M.P., and Farley, K.A., 2014, Knickpoint formation, rapid propagation, and landscape response following coastal cliff retreat at the last interglacial sea-level highstand: Kauaʻi, Hawaiʻi: GSA Bulletin, v. 126, p. 925–942, doi:10.1130/B30930.1.

Murphy, B.P., Johnson, J.P.L., Gasparini, N.M., and Sklar, L.S., 2016, Chemical weathering as a mechanism for the climatic control of bedrock river incision: Nature, v. 532, p. 223–227, doi:10.1038/nature17449.

Neely, A.B., and DiBiase, R.A., 2020, Drainage Area, Bedrock Fracture Spacing, and Weathering Controls on Landscape-Scale Patterns in Surface Sediment Grain Size: Journal of Geophysical Research: Earth Surface, v. 125, p. e2020JF005560, doi:https://doi.org/10.1029/2020JF005560.

Scott, G.A.J., and Street, J.M., 1976, The role of chemical weathering in the formation of Hawaiian Amphitheatre-headed valleys.: Zeitschrift fr Geomorphologie, Annals of geomorphology.,.

Seidl, M.A., Dietrich, W.E., and Kirchner, J.W., 1994, Longitudinal profile development into bedrock: An analysis of Hawaiian channels: Journal of Geology, v. 102, p. 457, doi:10.1086/629686.

Seidl, M.A., Finkel, R.C., Caffee, M.W., Hudson, G.B., and Dietrich, W.E., 1997, Cosmogenic Isotope Analyses Applied to River Longitudinal Profile Evolution: Problems and Interpretations: Earth Surface Processes and Landforms, v. 22, p. 195–209, doi:10.1002/(SICI)1096-9837(199703)22:3<195::AID-ESP748>3.0.CO;2-0.

Sinton, J.M., Eason, D.E., and Duncan, R.A., 2017, Volcanic evolution of Molokaʻi, Hawaiʻi: Implications for the shield to postshield transition in Hawaiian volcanoes: Journal of Volcanology and Geothermal Research, v. 340, p. 30–51, doi:10.1016/j.jvolgeores.2017.04.011.

Small, E.E., Blom, T., Hancock, G.S., Hynek, B.M., and Wobus, C.W., 2015, Variability of rock erodibility in bedrock-floored stream channels based on abrasion mill experiments: Journal of Geophysical Research: Earth Surface, v. 120, p. 1455–1469, doi:10.1002/2015JF003506.

Stock, J.D., and Montgomery, D.R., 1999, Geologic constraints on bedrock river incision using the stream power law: Journal of Geophysical Research: Solid Earth, v. 104, p. 4983–4993, doi:10.1029/98JB02139.

Verdian, J.P., Sklar, L.S., Riebe, C.S., and Moore, J.R., 2020, Sediment size on talus slopes correlates with fracture spacing on bedrock cliffs: Implications for predicting initial sediment size distributions on hillslopes: Earth Surface Dynamics Discussions, p. 1–23, doi:https://doi.org/10.5194/esurf-2020-54.

Ward, D.J., and Galewsky, J., 2014, Exploring landscape sensitivity to the Pacific Trade Wind Inversion on the subsiding island of Hawaii: Journal of Geophysical Research: Earth Surface, v. 119, p. 2014JF003155, doi:10.1002/2014JF003155.

Whipple, K.X., DiBiase, R.A., Crosby, B., and Johnson, J.P.L., 2022, 6.40 - Bedrock Rivers, *in* Shroder, J. (Jack) F. ed., Treatise on Geomorphology (Second Edition), Oxford, Academic Press, p. 865–903, doi:10.1016/B978-0-12-818234-5.00101-2.

Wobus, C.W., Crosby, B.T., and Whipple, K.X., 2006, Hanging valleys in fluvial systems: Controls on occurrence and implications for landscape evolution: Journal of Geophysical Research: Earth Surface, v. 111, doi:10.1029/2005JF000406.

Wohl, E., and Merritt, D.M., 2008, Reach-scale channel geometry of mountain streams: Geomorphology, v. 93, p. 168–185, doi:https://doi.org/10.1016/j.geomorph.2007.02.014.

REFERENCES

Adams, B.A., Whipple, K.X., Forte, A.M., Heimsath, A.M., and Hodges, K.V., 2020, Climate controls on erosion in tectonically active landscapes: Science Advances, v. 6, p. eaaz3166, doi:10.1126/sciadv.aaz3166.

Akoglu, H., 2018, User's guide to correlation coefficients: Turkish Journal of Emergency Medicine, v. 18, p. 91–93, doi:10.1016/j.tjem.2018.08.001.

Annandale, G.W., 1995, Erodibility: Journal of Hydraulic Research, v. 33, p. 471–494, doi:10.1080/00221689509498656.

Anton, L., Mather, A.E., Stokes, M., Muñoz-Martin, A., and De Vicente, G., 2015, Exceptional river gorge formation from unexceptional floods: Nature Communications, v. 6, p. 7963, doi:10.1038/ncomms8963.

Asner, G.P., Elmore, A.J., Flint Hughes, R., Warner, A.S., and Vitousek, P.M., 2005, Ecosystem structure along bioclimatic gradients in Hawai'i from imaging spectroscopy: Remote Sensing of Environment, v. 96, p. 497–508, doi:10.1016/j.rse.2005.04.008.

Baker, V.R., and Costa, J.E., 1987, Flood power, *in* Catastrophic Flooding, Routledge, 21 p.

Baldwin, J.A., Whipple, K.X., and Tucker, G.E., 2003, Implications of the shear stress river incision model for the timescale of postorogenic decay of topography: Journal of Geophysical Research: Solid Earth, v. 108, doi:10.1029/2001JB000550.

Baynes, E.R.C., Attal, M., Niedermann, S., Kirstein, L.A., Dugmore, A.J., and Naylor, M., 2015, Erosion during extreme flood events dominates Holocene canyon evolution in northeast Iceland: Proceedings of the National Academy of Sciences, v. 112, p. 2355–2360, doi:10.1073/pnas.1415443112.

Baynes, E.R.C., van de Lageweg, W.I., McLelland, S.J., Parsons, D.R., Aberle, J., Dijkstra, J., Henry, P.-Y., Rice, S.P., Thom, M., and Moulin, F., 2018a, Beyond equilibrium: Re-evaluating physical modelling of fluvial systems to represent climate changes: Earth-Science Reviews, v. 181, p. 82–97, doi:10.1016/j.earscirev.2018.04.007.

Baynes, E.R.C., Lague, D., Attal, M., Gangloff, A., Kirstein, L.A., and Dugmore, A.J., 2018b, River self-organisation inhibits discharge control on waterfall migration: Scientific Reports, v. 8, p. 2444, doi:10.1038/s41598-018-20767-6.

Beer, A.R., and Lamb, M.P., 2021, Abrasion regimes in fluvial bedrock incision: Geology, doi:10.1130/G48466.1.

Berlin, M.M., and Anderson, R.S., 2007, Modeling of knickpoint retreat on the Roan Plateau, western Colorado: Journal of Geophysical Research: Earth Surface, v. 112, p. F03S06, doi:10.1029/2006JF000553.

Bishop, K.M., 2018, Landslide Interpretation of the Northeast Flank of Kohala Volcano, Hawaii: Environmental and Engineering Geoscience, v. 24, p. 187–205, doi:10.2113/EEG-1961.

Bishop, P., Hoey, T.B., Jansen, J.D., and Artza, I.L., 2005, Knickpoint recession rate and catchment area: the case of uplifted rivers in Eastern Scotland: Earth Surface Processes and Landforms, v. 30, p. 767–778, doi:10.1002/esp.1191.

von Blanckenburg, F., 2005, The control mechanisms of erosion and weathering at basin scale from cosmogenic nuclides in river sediment: Earth and Planetary Science Letters, v. 237, p. 462–479, doi:10.1016/j.epsl.2005.06.030.

Bookhagen, B., and Strecker, M.R., 2012, Spatiotemporal trends in erosion rates across a pronounced rainfall gradient: Examples from the southern Central Andes: Earth and Planetary Science Letters, v. 327, p. 97–110.

Bookhagen, B., Thiede, R.C., and Strecker, M.R., 2005, Late Quaternary intensified monsoon phases control landscape evolution in the northwest Himalaya: Geology, v. 33, p. 149–152.

Brocard, G.Y., Willenbring, J.K., Miller, T.E., and Scatena, F.N., 2016, Relict landscape resistance to dissection by upstream migrating knickpoints: Journal of Geophysical Research: Earth Surface, v. 121, p. 1182–1203, doi:10.1002/2015JF003678.

Burbank, D.W., Blythe, A.E., Putkonen, J., Pratt-Sitaula, B., Gabet, E., Oskin, M., Barros, A., and Ojha, T.P., 2003, Decoupling of erosion and precipitation in the Himalayas: Nature, v. 426, p. 652–655, doi:10.1038/nature02187.

Campforts, B., Vanacker, V., Herman, F., Vanmaercke, M., Schwanghart, W., Tenorio, G.E., Willems, P., and Govers, G., 2020, Parameterization of river incision models requires accounting for environmental heterogeneity: insights from the tropical Andes: Earth Surface Dynamics, v. 8, p. 447–470, doi:https://doi.org/10.5194/esurf-8-447-2020.

Carretier, S. et al., 2013, Slope and climate variability control of erosion in the Andes of central Chile: Geology, v. 41, p. 195–198, doi:10.1130/G33735.1.

Chadwick, O.A., Gavenda, R.T., Kelly, E.F., Ziegler, K., Olson, C.G., Elliott, W.C., and Hendricks, D.M., 2003, The impact of climate on the biogeochemical functioning of volcanic soils: Chemical Geology, v. 202, p. 195–223, doi:10.1016/j.chemgeo.2002.09.001.

Chatanantavet, P., and Parker, G., 2005, Modeling the bedrock river evolution of western Kaua'i, Hawai'i, by a physically-based incision model based on abrasion, *in* Tunnelling. A Decade of Progress. GeoDelft 1995-2005, p. 99–110.

Chatanantavet, P., and Parker, G., 2009, Physically based modeling of bedrock incision by abrasion, plucking, and macroabrasion: Journal of Geophysical Research: Earth Surface, v. 114, doi:10.1029/2008JF001044.

Chu, P.-S., Zhao, X., Ruan, Y., and Grubbs, M., 2009, Extreme Rainfall Events in the Hawaiian Islands: Journal of Applied Meteorology and Climatology, v. 48, p. 502–516, doi:10.1175/2008JAMC1829.1.

Clague, D.A., and Dalrymple, G.B., 1988, Age and petrology of alkalic postshield and rejuvenated-stage lava from Kauai, Hawaii: Contributions to Mineralogy and Petrology, v. 99, p. 202–218, doi:10.1007/BF00371461.

Clague, D.A., and Moore, J.G., 2002, The proximal part of the giant submarine Wailau landslide, Molokai, Hawaii: Journal of Volcanology and Geothermal Research, v. 113, p. 259–287, doi:10.1016/S0377-0273(01)00261-X.

Clague, D.A., and Sherrod, D.R., 2014, Growth and degradation of Hawaiian volcanoes, *in* Characteristics of Hawaiian volcanoes, Professional Paper, US Geological Survey, 1801, p. 97–146.

Cook, K.L., Turowski, J.M., and Hovius, N., 2013, A demonstration of the importance of bedload transport for fluvial bedrock erosion and knickpoint propagation: Earth Surface Processes and Landforms, v. 38, p. 683–695, doi:https://doi.org/10.1002/esp.3313.

Costa, J.E., 1987a, A comparison of the largest rainfall-runoff floods in the United States with those of the People's Republic of China and the world: Journal of Hydrology, v. 96, p. 101–115, doi:10.1016/0022-1694(87)90146-6.

Costa, J.E., 1987b, Hydraulics and basin morphometry of the largest flash floods in the conterminous United States: Journal of Hydrology, v. 93, p. 313–338, doi:10.1016/0022-1694(87)90102-8.

Crosby, B.T., and Whipple, K.X., 2006, Knickpoint initiation and distribution within fluvial networks: 236 waterfalls in the Waipaoa River, North Island, New Zealand: Geomorphology, v. 82, p. 16–38, doi:10.1016/j.geomorph.2005.08.023.

Crosby, B.T., Whipple, K.X., Gasparini, N.M., and Wobus, C.W., 2007, Formation of fluvial hanging valleys: Theory and simulation: Journal of Geophysical Research: Earth Surface, v. 112, doi:https://doi.org/10.1029/2006JF000566.

Dalrymple, G.B., 1971, Potassium-Argon Ages from the Pololu Volcanic Series, Kohala Volcano, Hawaii: GSA Bulletin, v. 82, p. 1997–2000, doi:10.1130/0016-7606(1971)82[1997:PAFTPV]2.0.CO;2.

De Young, N., 2000, Modeling the Geomorphic Evolution of Western Kauai, Hawaii: A study of surface processes in a basaltic terrain. [Masters]: Dalhousie University, 157 p., https://www.collectionscanada.gc.ca/obj/s4/f2/dsk1/tape4/PQDD_0018/MQ57281.pdf (accessed December 2019).

Deal, E., Braun, J., and Botter, G., 2018, Understanding the Role of Rainfall and Hydrology in Determining Fluvial Erosion Efficiency: Journal of Geophysical Research: Earth Surface, v. 123, p. 744–778, doi:10.1002/2017JF004393.

DiBiase, R.A., and Whipple, K.X., 2011, The influence of erosion thresholds and runoff variability on the relationships among topography, climate, and erosion rate: Journal of Geophysical Research: Earth Surface, v. 116, http://onlinelibrary.wiley.com/doi/10.1029/2011JF002095/full (accessed June 2016).

DiBiase, R.A., Whipple, K.X., Lamb, M.P., and Heimsath, A.M., 2015, The role of waterfalls and knickzones in controlling the style and pace of landscape adjustment in the western San Gabriel Mountains, California: GSA Bulletin, v. 127, p. 539–559, doi:10.1130/B31113.1.

Dietrich, W.E., Bellugi, D.G., Sklar, L.S., Stock, J.D., Heimsath, A.M., and Roering, J.J., 2003, Geomorphic Transport Laws for Predicting Landscape form and Dynamics, *in* Prediction in Geomorphology, American Geophysical Union (AGU), p. 103–132, doi:10.1029/135GM09.

Dixon, J.L., Chadwick, O.A., and Pavich, M.J., 2018, Climatically controlled delivery and retention of meteoric 10Be in soils: Geology, v. 46, p. 899–902, doi:10.1130/G45176.1.

Dubinski, I.M., and Wohl, E., 2013, Relationships between block quarrying, bed shear stress, and stream power: A physical model of block quarrying of a jointed bedrock channel: Geomorphology, v. 180–181, p. 66–81, doi:10.1016/j.geomorph.2012.09.007.

Ferguson, R., 2007, Flow resistance equations for gravel-and boulder-bed streams: Water resources research, v. 43, doi:10.1029/2006WR005422.

Ferguson, R.I., 2012, River channel slope, flow resistance, and gravel entrainment thresholds: Water Resources Research, v. 48, doi:10.1029/2011WR010850.

Ferrier, K.L., Huppert, K.L., and Perron, J.T., 2013a, Climatic control of bedrock river incision: Nature, v. 496, p. 206–209, doi:https://doi.org/10.1038/nature11982.

Ferrier, K.L., Perron, J.T., Mukhopadhyay, S., Rosener, M., Stock, J.D., Huppert, K.L., and Slosberg, M., 2013b, Covariation of climate and long-term erosion rates across a steep rainfall gradient on the Hawaiian island of Kaua‘i: GSA Bulletin, v. 125, p. 1146–1163, doi:10.1130/B30726.1.

Finlayson, D.P., Montgomery, D.R., and Hallet, B., 2002, Spatial coincidence of rapid inferred erosion with young metamorphic massifs in the Himalayas: Geology, v. 30, p. 219–222, doi:10.1130/0091-7613(2002)030<0219:SCORIE>2.0.CO;2.

Finnegan, N.J., Klier, R.A., Johnstone, S., Pfeiffer, A.M., and Johnson, K., 2017, Field evidence for the control of grain size and sediment supply on steady-state bedrock river channel slopes in a tectonically active setting: Earth Surface Processes and Landforms, v. 42, p. 2338–2349, doi:10.1002/esp.4187.

Finnegan, N.J., Schumer, R., and Finnegan, S., 2014, A signature of transience in bedrock river incision rates over timescales of 104-107 years: Nature, v. 505, p. 391–394.

Forte, A.M., Leonard, J.S., Rossi, M.W., Whipple, K.X., Heimsath, A.M., Sukhishvili, L., Godoladze, T., and Kadirov, F., 2022, Low variability runoff inhibits coupling of climate, tectonics, and topography in the Greater Caucasus: Earth and Planetary Science Letters, v. 584, p. 117525, doi:10.1016/j.epsl.2022.117525.

Foster, J., Bevis, M., Chen, Y.-L., Businger, S., and Zhang, Y., 2003, The Ka‘ storm (November 2000): Imaging precipitable water using GPS: Journal of Geophysical Research: Atmospheres, v. 108, doi:10.1029/2003JD003413.

Frazier, A.G., Giambelluca, T.W., Diaz, H.F., and Needham, H.L., 2016, Comparison of geostatistical approaches to spatially interpolate month-year rainfall for the Hawaiian Islands: International Journal of Climatology, v. 36, p. 1459–1470, doi:10.1002/joc.4437.

Gardner, T.W., 1983, Experimental study of knickpoint and longitudinal profile evolution in cohesive, homogeneous material: GSA Bulletin, v. 94, p. 664–672, doi:10.1130/0016-7606(1983)94<664:ESOKAL>2.0.CO;2.

Gavenda, R.T., 1994, Hawaiian quaternary paleoenvironments: A review of geological, pedological, and botanical evidence., *in* A Natural History of the Hawaiian Islands: Selected Readings II, Honolulu, University of Hawaii Press, A Natural History of the Hawaiian Islands II, p. 118–130.

Gayer, E., Michon, L., Louvat, P., and Gaillardet, J., 2019, Storm-induced precipitation variability control of long-term erosion: Earth and Planetary Science Letters, v. 517, p. 61–70, doi:10.1016/j.epsl.2019.04.003.

Giambelluca, T.W., Chen, Q., Frazier, A.G., Price, J.P., Chen, Y.-L., Chu, P.-S., Eischeid, J.K., and Delparte, D.M., 2012, Online Rainfall Atlas of Hawai‘i:

Bulletin of the American Meteorological Society, v. 94, p. 313–316, doi:10.1175/BAMS-D-11-00228.1.

Giambelluca, T.W., and Nullet, D., 1991, Influence of the trade-wind inversion on the climate of a leeward mountain slope in Hawaii: Climate Research, v. 1, p. 207–216.

Giambelluca, T.W., Shuai, X., Barnes, M.L., Alliss, R.J., Longman, R.J., Miura, T., Chen, Q., Frazier, A.G., Mudd, R.G., and Cuo, L., 2014, Evapotranspiration of Hawai ʻi: Final report submitted to the US Army Corps of Engineers—Honolulu District, and the Commission on Water Resource Management, State of Hawai ʻi,.

Goode, J.K., and Burbank, D.W., 2009, Numerical study of degradation of fluvial hanging valleys due to climate change: Journal of Geophysical Research: Earth Surface, v. 114, doi:https://doi.org/10.1029/2007JF000965.

Goodrich, D.C., Lane, L.J., Shillito, R.M., Miller, S.N., Syed, K.H., and Woolhiser, D.A., 1997, Linearity of basin response as a function of scale in a semiarid watershed: Water Resources Research, v. 33, p. 2951–2965, doi:https://doi.org/10.1029/97WR01422.

Groh, E.L., and Scheingross, J.S., 2021, Morphologic signatures of autogenic waterfalls: A case study in the San Gabriel Mountains, California: Geology, doi:10.1130/G49320.1.

Hack, J.T., 1957, Studies of longitudinal stream profiles in Virginia and Maryland: U.S. Geological Survey Professional Paper, v. 294-B.

Han, J., Gasparini, N.M., Johnson, J.P.L., and Murphy, B.P., 2014, Modeling the influence of rainfall gradients on discharge, bedrock erodibility, and river profile evolution, with application to the Big Island, Hawai'i: Journal of Geophysical Research: Earth Surface, v. 119, p. 1418–1440, doi:10.1002/2013JF002961.

Harkins, N., Kirby, E., Heimsath, A., Robinson, R., and Reiser, U., 2007, Transient fluvial incision in the headwaters of the Yellow River, northeastern Tibet, China: Journal of Geophysical Research: Earth Surface, v. 112, doi:https://doi.org/10.1029/2006JF000570.

Harris, A.J.L., Rowland, S.K., Villeneuve, N., and Thordarson, T., 2016, Pāhoehoe, ʻaʻā, and block lava: an illustrated history of the nomenclature: Bulletin of Volcanology, v. 79, p. 7, doi:10.1007/s00445-016-1075-7.

Haviv, I., Enzel, Y., Whipple, K.X., Zilberman, E., Stone, J., Matmon, A., and Fifield, L.K., 2006, Amplified erosion above waterfalls and oversteepened bedrock reaches: Journal of Geophysical Research: Earth Surface, v. 111, doi:10.1029/2006JF000461.

Hayakawa, Y., and Matsukura, Y., 2003, Recession rates of waterfalls in Boso Peninsula, Japan, and a predictive equation: Earth Surface Processes and Landforms, v. 28, p. 675–684, doi:10.1002/esp.519.

Hearty, P.J., Karner, D.B., Renne, P.R., Olson, S.L., and Fletcher, S., 2005, 40Ar/39Ar age of a young rejuvenation basalt flow: Implications for the duration of volcanism and the timing of carbonate platform development during the quaternary on Kaua'i, Hawaiian Islands: New Zealand Journal of Geology and Geophysics, v. 48, p. 199–211, doi:10.1080/00288306.2005.9515110.

Herschy, R.W., 2002, The world's maximum observed floods: Flow Measurement and Instrumentation, v. 13, p. 231–235, doi:10.1016/S0955-5986(02)00054-7.

Hinds, N.E., 1925, Amphitheater valley heads: The Journal of Geology, v. 33, p. 816–818.

Holcomb, R.T., 1987, Eruptive history and long-term behavior of Kilauea Volcano, *in* Volcanism In Hawaii, U.S.Geological Survey, v. 1, p. 261–350, https://pubs.usgs.gov/pp/1987/1350/.

Holcomb, R.T., Reiners, P.W., Nelson, B.K., and Sawyer, N.-L.E., 1997, Evidence for two shield volcanoes exposed on the island of Kauai, Hawaii: Geology, v. 25, p. 811–814, doi:10.1130/0091-7613(1997)025<0811:EFTSVE>2.3.CO;2.

Hotchkiss, S., Vitousek, P.M., Chadwick, O.A., and Price, J., 2000, Climate Cycles, Geomorphological Change, and the Interpretation of Soil and Ecosystem Development: Ecosystems, v. 3, p. 522–533, doi:10.1007/s100210000046.

Howard, A.D., 1994, A detachment-limited model of drainage basin evolution: Water Resources Research, v. 30, p. 2261–2285, doi:10.1029/94WR00757.

Howard, A.D., 1980, Thresholds in river regimes, *in* The Concept of Geomorphic Thresholds, Binghamton, N.Y., Allen and Unwin, p. 227–258.

Howard, A.D., Dietrich, W.E., and Seidl, M.A., 1994, Modeling fluvial erosion on regional to continental scales: Journal of Geophysical Research: Solid Earth, p. 13971–13986, doi:10.1029/94JB00744@10.1002/(ISSN)2169-9356.TECTOP1.

Howard, A.D., and McLane III, C.F., 1988, Erosion of cohesionless sediment by groundwater seepage: Water Resources Research, v. 24, p. 1659–1674, doi:10.1029/WR024i010p01659.

Huang, Y.-F., Gayte, M., Tsang, Y., Longman, R.J., Nugent, A.D., Kodama, K., Lucas, M.P., and Giambelluca, T.W., 2022, Hourly rainfall data from rain gauge networks and weather radar up to 2020 across the Hawaiian Islands: Scientific Data, v. 9, p. 334, doi:10.1038/s41597-022-01430-2.

Huggel, C., Clague, J.J., and Korup, O., 2012, Is climate change responsible for changing landslide activity in high mountains? Earth Surface Processes and Landforms, v. 37, p. 77–91, doi:10.1002/esp.2223.

Huppert, K.L., Royden, L.H., and Perron, J.T., 2015, Dominant influence of volcanic loading on vertical motions of the Hawaiian Islands: Earth and Planetary Science Letters, v. 418, p. 149–171, doi:10.1016/j.epsl.2015.02.027.

Izumi, N., Yokokawa, M., and Parker, G., 2017, Incisional cyclic steps of permanent form in mixed bedrock-alluvial rivers: Journal of Geophysical Research: Earth Surface, v. 122, p. 130–152, doi:https://doi.org/10.1002/2016JF003847.

Jackson, E.D., Silver, E.A., and Dalrymple, G.B., 1972, Hawaiian-Emperor Chain and Its Relation to Cenozoic Circumpacific Tectonics: GSA Bulletin, v. 83, p. 601–618, doi:10.1130/0016-7606(1972)83[601:HCAIRT]2.0.CO;2.

Jones, B.L., Chinn, S.S.W., and Brice, J.C., 1984, Olokele rock avalanche, island of Kauai, Hawaii: Geology, v. 12, p. 209–211.

Katz, M.G., and Cashman, K.V., 2003, Hawaiian lava flows in the third dimension: Identification and interpretation of pahoehoe and ′a′a distribution in the KP-1 and SOH-4 cores: Geochemistry, Geophysics, Geosystems, v. 4, doi:10.1029/2001GC000209.

Kendall, M.G., 1938, A New Measure of Rank Correlation: Biometrika, v. 30, p. 81–93, doi:10.2307/2332226.

Killick, R., Fearnhead, P., and Eckley, I.A., 2012, Optimal Detection of Changepoints With a Linear Computational Cost: Journal of the American Statistical Association, v. 107, p. 1590–1598, doi:10.1080/01621459.2012.737745.

Kirby, E., and Whipple, K.X., 2012, Expression of active tectonics in erosional landscapes: Journal of Structural Geology, v. 44, p. 54–75.

Knapp, K.R., Kruk, M.C., Levinson, D.H., Diamond, H.J., and Neumann, C.J., 2010, The International Best Track Archive for Climate Stewardship (IBTrACS): Unifying Tropical Cyclone Data: Bulletin of the American Meteorological Society, v. 91, p. 363–376, doi:10.1175/2009BAMS2755.1.

Kochel, R.C., and Piper, J.F., 1986, Morphology of large valleys on Hawaii: Evidence for groundwater sapping and comparisons with Martian valleys: Journal of Geophysical Research: Solid Earth, v. 91, p. E175–E192, doi:https://doi.org/10.1029/JB091iB13p0E175.

Lague, D., 2014, The stream power river incision model: evidence, theory and beyond: Earth Surface Processes and Landforms, v. 39, p. 38–61, doi:10.1002/esp.3462.

Lague, D., Hovius, N., and Davy, P., 2005, Discharge, discharge variability, and the bedrock channel profile: Journal of Geophysical Research: Earth Surface, v. 110, p. F04006, doi:10.1029/2004JF000259.

Lamb, M.P., and Dietrich, W.E., 2009, The persistence of waterfalls in fractured rock: GSA Bulletin, v. 121, p. 1123–1134, doi:10.1130/B26482.1.

Lamb, M.P., Finnegan, N.J., Scheingross, J.S., and Sklar, L.S., 2015, New insights into the mechanics of fluvial bedrock erosion through flume experiments and theory: Geomorphology, v. 244, p. 33–55, doi:10.1016/j.geomorph.2015.03.003.

Lamb, M.P., and Fonstad, M.A., 2010, Rapid formation of a modern bedrock canyon by a single flood event: Nature Geoscience, v. 3, p. 477–481, doi:10.1038/ngeo894.

Lamb, M.P., Howard, A.D., Dietrich, W.E., and Perron, J.T., 2007, Formation of amphitheater-headed valleys by waterfall erosion after large-scale slumping on Hawai ‘i: GSA Bulletin, v. 119, p. 805–822, doi:https://doi.org/10.1130/B25986.1.

Lapotre, M.G.A., and Lamb, M.P., 2018, Substrate controls on valley formation by groundwater on Earth and Mars: Geology, v. 46, p. 531–534, doi:10.1130/G40007.1.

Leopold, L.B., 1949, THE INTERACTION OF TRADE WIND AND SEA BREEZE, HAWAII: Journal of the Atmospheric Sciences, v. 6, p. 312–320, doi:10.1175/1520-0469(1949)006<0312:TIOTWA>2.0.CO;2.

Leopold, L.B., and Maddock Jr., T., 1953, The hydraulic geometry of stream channels and some physiographic implications: Professional Paper Report 252, 64 p., doi:10.3133/pp252.

Li, Y.-H., 1988, Denudation Rates of the Hawaiian Islands by Rivers and Groundwaters:, http://scholarspace.manoa.hawaii.edu/handle/10125/1082 (accessed April 2021).

Li, D. et al., 2022, High Mountain Asia hydropower systems threatened by climate-driven landscape instability: Nature Geoscience, v. 15, p. 520–530, doi:10.1038/s41561-022-00953-y.

Li, C., Wang, G., and Li, R., 2013, Maximum observed floods in China: Hydrological Sciences Journal, v. 58, p. 728–735, doi:10.1080/02626667.2013.772299.

Limber, P.W., and Barnard, P.L., 2018, Coastal knickpoints and the competition between fluvial and wave-driven erosion on rocky coastlines: Geomorphology, v. 306, p. 1–12, doi:10.1016/j.geomorph.2017.12.035.

Lindeløv, J.K., 2020, mcp: An R Package for Regression With Multiple Change Points:, doi:10.31219/osf.io/fzqxv.

Macdonald, G.A., Abbott, A.T., and Peterson, F.L., 1983, Volcanoes in the Sea: The Geology of Hawaii: University of Hawaii Press, 558 p.

Macdonald, G.A., Davis, D.A., and Cox, D.C., 1960, Geology and ground-water resources of the island of Kauai, Hawaii: Bulletin Other Government Series 13, http://pubs.er.usgs.gov/publication/70160871 (accessed December 2019).

Macdonald, F.A., Swanson-Hysell, N.L., Park, Y., Lisiecki, L., and Jagoutz, O., 2019, Arc-continent collisions in the tropics set Earth's climate state: Science, v. 364, p. 181–184, doi:10.1126/science.aav5300.

Mackey, B.H., Scheingross, J.S., Lamb, M.P., and Farley, K.A., 2014, Knickpoint formation, rapid propagation, and landscape response following coastal cliff retreat at the last interglacial sea-level highstand: Kaua'i, Hawai'i: GSA Bulletin, v. 126, p. 925–942, doi:10.1130/B30930.1.

Magilligan, F.J., 1992, Thresholds and the spatial variability of flood power during extreme floods: Geomorphology, v. 5, p. 373–390, doi:10.1016/0169-555X(92)90014-F.

May, C., Roering, J., Snow, K., Griswold, K., and Gresswell, R., 2017, The waterfall paradox: How knickpoints disconnect hillslope and channel processes, isolating salmonid populations in ideal habitats: Geomorphology, v. 277, p. 228–236, doi:10.1016/j.geomorph.2016.03.029.

McDougall, I., 1979, Age of shield-building volcanism of Kauai and linear migration of volcanism in the Hawaiian island chain: Earth and Planetary Science Letters, v. 46, p. 31–42, doi:10.1016/0012-821X(79)90063-3.

McDougall, I., and Swanson, D.A., 1972, Potassium-Argon Ages of Lavas from the Hawi and Pololu Volcanic Series, Kohala Volcano, Hawaii: GSA Bulletin, v. 83, p. 3731–3738, doi:10.1130/0016-7606(1972)83[3731:PAOLFT]2.0.CO;2.

McMurtry, G.M., Campbell, J.F., Fryer, G.J., and Fietzke, J., 2010, Uplift of Oahu, Hawaii, during the past 500 k.y. as recorded by elevated reef deposits: Geology, v. 38, p. 27–30, doi:10.1130/G30378.1.

Menking, J.A., Han, J., Gasparini, N.M., and Johnson, J.P.L., 2013, The effects of precipitation gradients on river profile evolution on the Big Island of Hawai'i: GSA Bulletin, v. 125, p. 594–608, doi:10.1130/B30625.1.

Mitchell, N.A., and Yanites, B.J., 2021, Bedrock River Erosion through Dipping Layered Rocks: Quantifying Erodibility through Kinematic Wave Speed: Earth Surface Dynamics Discussions, p. 1–46, doi:10.5194/esurf-2021-3.

Molnar, P., Anderson, R.S., Kier, G., and Rose, J., 2006, Relationships among probability distributions of stream discharges in floods, climate, bed load transport, and river

incision: Journal of Geophysical Research: Earth Surface, v. 111, doi:10.1029/2005JF000310.

Molnar, P., and England, P., 1990, Late Cenozoic uplift of mountain ranges and global climate change: chicken or egg? Nature, v. 346, p. 29–34, doi:10.1038/346029a0.

Montgomery, D.R., and Foufoula-Georgiou, E., 1993, Channel network source representation using digital elevation models: Water Resources Research, v. 29, p. 3925–3934, doi:https://doi.org/10.1029/93WR02463.

Montgomery, D.R., and Gran, K.B., 2001, Downstream variations in the width of bedrock channels: Water Resources Research, v. 37, p. 1841–1846, doi:https://doi.org/10.1029/2000WR900393.

Moore, J.G., and Clague, D.A., 1992, Volcano growth and evolution of the island of Hawaii: Geological Society of America Bulletin, v. 104, p. 1471–1484.

Moore, J.G., Clague, D.A., Holcomb, R.T., Lipman, P.W., Normark, W.R., and Torresan, M.E., 1989, Prodigious submarine landslides on the Hawaiian Ridge: Journal of Geophysical Research: Solid Earth, v. 94, p. 17465–17484, doi:10.1029/JB094iB12p17465.

Morisawa, M.E., 1962, Quantitative Geomorphology of Some Watersheds in the Appalachian Plateau: GSA Bulletin, v. 73, p. 1025–1046, doi:10.1130/0016-7606(1962)73[1025:QGOSWI]2.0.CO;2.

Murphy, B.P., Johnson, J.P.L., Gasparini, N.M., and Sklar, L.S., 2016, Chemical weathering as a mechanism for the climatic control of bedrock river incision: Nature, v. 532, p. 223–227, doi:10.1038/nature17449.

Nativ, R., and Turowski, J.M., 2020, Site Dependence of Fluvial Incision Rate Scaling With Timescale: Journal of Geophysical Research: Earth Surface, v. 125, p. e2020JF005808, doi:https://doi.org/10.1029/2020JF005808.

Nearing, M.A., Pruski, F.F., and O'Neal, M.R., 2004, Expected climate change impacts on soil erosion rates: A review: Journal of Soil and Water Conservation, v. 59, p. 43–50.

Neely, A.B., and DiBiase, R.A., 2020, Drainage Area, Bedrock Fracture Spacing, and Weathering Controls on Landscape-Scale Patterns in Surface Sediment Grain Size: Journal of Geophysical Research: Earth Surface, v. 125, p. e2020JF005560, doi:https://doi.org/10.1029/2020JF005560.

Oki, D.S., Rosa, S.N., and Yeung, C.W., 2010, Flood-frequency estimates for streams on Kaua'i, O'ahu, Moloka'i, Maui, and Hawai'i, State of Hawai'i: U.S. Geological Survey Scientific Investigations Report 5035, 121 p.

Okubo, C.H., 2004, Rock mass strength and slope stability of the Hilina slump, Kīlauea volcano, Hawai'i: Journal of Volcanology and Geothermal Research, v. 138, p. 43–76, doi:10.1016/j.jvolgeores.2004.06.006.

Ortega, J.A., Wohl, E., and Livers, B., 2013, Waterfalls on the eastern side of Rocky Mountain National Park, Colorado, USA: Geomorphology, v. 198, p. 37–44, doi:10.1016/j.geomorph.2013.05.010.

Ouimet, W.B., Whipple, K.X., Royden, L.H., Sun, Z., and Chen, Z., 2007, The influence of large landslides on river incision in a transient landscape: Eastern margin of the Tibetan Plateau (Sichuan, China): GSA Bulletin, v. 119, p. 1462–1476, doi:10.1130/B26136.1.

Palucis, M.C., and Lamb, M.P., 2017, What controls channel form in steep mountain streams? Geophysical Research Letters, v. 44, p. 2017GL074198, doi:10.1002/2017GL074198.

Palucis, M.C., Ulizio, T., Fuller, B., and Lamb, M.P., 2018, Intense Granular Sheetflow in Steep Streams: Geophysical Research Letters, v. 45, p. 5509–5517, doi:https://doi.org/10.1029/2018GL077526.

Parker, C., Clifford, N.J., and Thorne, C.R., 2011, Understanding the influence of slope on the threshold of coarse grain motion: Revisiting critical stream power: Geomorphology, v. 126, p. 51–65, doi:10.1016/j.geomorph.2010.10.027.

Parker, G., Wilcock, P.R., Paola, C., Dietrich, W.E., and Pitlick, J., 2007, Physical basis for quasi-universal relations describing bankfull hydraulic geometry of single-thread gravel bed rivers: Journal of Geophysical Research: Earth Surface, v. 112, doi:10.1029/2006JF000549.

Pelletier, J.D. et al., 2015, Forecasting the response of Earth's surface to future climatic and land use changes: A review of methods and research needs: Earth's Future, v. 3, p. 220–251, doi:10.1002/2014EF000290.

Perron, J.T., 2017, Climate and the Pace of Erosional Landscape Evolution: Annual Review of Earth and Planetary Sciences, v. 45, p. 561–591, doi:10.1146/annurev-earth-060614-105405.

Perron, J.T., and Royden, L., 2013, An integral approach to bedrock river profile analysis: Earth Surface Processes and Landforms, v. 38, p. 570–576, doi:10.1002/esp.3302.

Pfeiffer, A.M., Finnegan, N.J., and Willenbring, J.K., 2017, Sediment supply controls equilibrium channel geometry in gravel rivers: Proceedings of the National Academy of Sciences, v. 114, p. 3346–3351, doi:10.1073/pnas.1612907114.

Phillips, C.B., and Jerolmack, D.J., 2019, Bankfull Transport Capacity and the Threshold of Motion in Coarse-Grained Rivers: Water Resources Research, v. 55, p. 11316–11330, doi:10.1029/2019WR025455.

Phillips, C.B., and Jerolmack, D.J., 2016, Self-organization of river channels as a critical filter on climate signals: Science, v. 352, p. 694–697, doi:10.1126/science.aad3348.

Porder, S., Hilley, G.E., and Chadwick, O.A., 2007, Chemical weathering, mass loss, and dust inputs across a climate by time matrix in the Hawaiian Islands: Earth and Planetary Science Letters, v. 258, p. 414–427, doi:10.1016/j.epsl.2007.03.047.

Prancevic, J.P., and Lamb, M.P., 2015, Unraveling bed slope from relative roughness in initial sediment motion: Journal of Geophysical Research: Earth Surface, v. 120, p. 474–489, doi:10.1002/2014JF003323.

Prancevic, J.P., Lamb, M.P., and Fuller, B.M., 2014, Incipient sediment motion across the river to debris-flow transition: Geology, v. 42, p. 191–194, doi:10.1130/G34927.1.

Price, J.P., and Elliott-Fisk, D., 2004, Topographic History of the Maui Nui Complex, Hawai'i, and Its Implications for Biogeography: Pacific Science, v. 58, p. 27–45, doi:10.1353/psc.2004.0008.

Raming, L.W., and Whipple, K.X., 2022, When knickzones limit upstream transmission of base-level fall: An example from Kaua'i, Hawai'i: Geology, doi:10.1130/G50019.1.

Raymo, M.E., 1991, Geochemical evidence supporting T. C. Chamberlin's theory of glaciation: Geology, v. 19, p. 344–347, doi:10.1130/0091-7613(1991)019<0344:GESTCC>2.3.CO;2.

Raymo, M.E., and Ruddiman, W.F., 1992, Tectonic forcing of late Cenozoic climate: Nature, v. 359, p. 117–122, doi:10.1038/359117a0.

Rigon, R., Rodriguez-Iturbe, I., Maritan, A., Giacometti, A., Tarboton, D.G., and Rinaldo, A., 1996, On Hack's Law: Water Resources Research, v. 32, p. 3367–3374, doi:10.1029/96WR02397.

Roda-Boluda, D.C., D'Arcy, M., McDonald, J., and Whittaker, A.C., 2018, Lithological controls on hillslope sediment supply: insights from landslide activity and grain size distributions: Earth Surface Processes and Landforms, v. 43, p. 956–977, doi:10.1002/esp.4281.

Rodier, J.A., and Roche, M., 1984, World catalogue of maximum observed floods =: Repertoire mondial des crues maximales observees: Wallingford, Oxfordshire,

International Association of Hydrological Sciences, IAHS publication no. 143, 354 p.

Roe, G.H., Montgomery, D.R., and Hallet, B., 2003, Orographic precipitation and the relief of mountain ranges: Journal of Geophysical Research: Solid Earth, v. 108, p. 2315, doi:10.1029/2001JB001521.

Rossi, M.W., Whipple, K.X., and Vivoni, E.R., 2016, Precipitation and evapotranspiration controls on daily runoff variability in the contiguous United States and Puerto Rico: Journal of Geophysical Research: Earth Surface, v. 121, p. 128–145, doi:10.1002/2015JF003446.

Rowland, S.K., and Garbeil, H., 2000, Slopes of Oceanic Basalt Volcanoes, *in* Remote Sensing of Active Volcanism, American Geophysical Union (AGU), p. 223–247, doi:10.1029/GM116p0223.

Ryan, A.J., and Whipple, K.X., 2020, Amphitheatre-headed canyons of Southern Utah: Stratigraphic control of canyon morphology: Earth Surface Processes and Landforms, v. 45, p. 3607–3622, doi:doi.org/10.1002/esp.4987.

Sassolas-Serrayet, T., Cattin, R., and Ferry, M., 2018, The shape of watersheds: Nature Communications, v. 9, p. 3791, doi:10.1038/s41467-018-06210-4.

Satake, K., Smith, J.R., and Shinozaki, K., 2002, Three-Dimensional Reconstruction and Tsunami Model of the Nuuanu and Wailau Giant Landslides, Hawaii, *in* Hawaiian Volcanoes: Deep Underwater Perspectives, American Geophysical Union (AGU), p. 333–346, doi:10.1029/GM128p0333.

Scheingross, J.S., and Lamb, M.P., 2017, A Mechanistic Model of Waterfall Plunge Pool Erosion into Bedrock: Journal of Geophysical Research: Earth Surface, v. 122, p. 2079–2104, doi:10.1002/2017JF004195.

Scheingross, J.S., and Lamb, M.P., 2021, Mass balance controls on sediment scour and bedrock erosion in waterfall plunge pools: Geology, doi:10.1130/G48881.1.

Scherler, D., DiBiase, R.A., Fisher, G.B., and Avouac, J.-P., 2017, Testing monsoonal controls on bedrock river incision in the Himalaya and Eastern Tibet with a stochastic-threshold stream power model: Journal of Geophysical Research: Earth Surface, v. 122, p. 1389–1429, doi:10.1002/2016JF004011.

Schumm, S.A., 1979, Geomorphic Thresholds: The Concept and Its Applications: Transactions of the Institute of British Geographers, v. 4, p. 485–515, doi:10.2307/622211.

Schwanghart, W., and Scherler, D., 2017, Bumps in river profiles: uncertainty assessment and smoothing using quantile regression techniques: Earth Surface Dynamics, v. 5, p. 821–839, doi:https://doi.org/10.5194/esurf-5-821-2017.

Schwanghart, W., and Scherler, D., 2020, Divide mobility controls knickpoint migration on the Roan Plateau (Colorado, USA): Geology, doi:10.1130/G47054.1.

Schwanghart, W., and Scherler, D., 2014, Short Communication: TopoToolbox 2 – MATLAB-based software for topographic analysis and modeling in Earth surface sciences: Earth Surface Dynamics, v. 2, p. 1–7, doi:https://doi.org/10.5194/esurf-2-1-2014.

Scott, G.A.J., and Street, J.M., 1976, The role of chemical weathering in the formation of Hawaiian Amphitheatre-headed valleys.: Zeitschrift fr Geomorphologie, Annals of geomorphology.,.

Seidl, M.A., Dietrich, W.E., and Kirchner, J.W., 1994, Longitudinal profile development into bedrock: An analysis of Hawaiian channels: Journal of Geology, v. 102, p. 457, doi:10.1086/629686.

Seidl, M.A., Finkel, R.C., Caffee, M.W., Hudson, G.B., and Dietrich, W.E., 1997, Cosmogenic Isotope Analyses Applied to River Longitudinal Profile Evolution: Problems and Interpretations: Earth Surface Processes and Landforms, v. 22, p. 195–209, doi:10.1002/(SICI)1096-9837(199703)22:3<195::AID-ESP748>3.0.CO;2-0.

Shelef, E., Haviv, I., and Goren, L., 2018, A Potential Link Between Waterfall Recession Rate and Bedrock Channel Concavity: Journal of Geophysical Research: Earth Surface, v. 123, p. 905–923, doi:10.1002/2016JF004138.

Sherrod, D.R., Murai, T., and Tagami, T., 2007, New K–Ar ages for calculating end-of-shield extrusion rates at West Maui volcano, Hawaiian island chain: Bulletin of Volcanology, v. 69, p. 627–642, doi:10.1007/s00445-006-0099-9.

Sherrod, D.R., Sinton, J.M., Watkins, S.E., and Brunt, K.M., 2021, Geologic map of the State of Hawaii: U.S. Geological Survey Scientific Investigations Map USGS Numbered Series 3143, 72 p., doi:10.3133/sim3143.

Shobe, C.M., Tucker, G.E., and Rossi, M.W., 2018, Variable-Threshold Behavior in Rivers Arising From Hillslope-Derived Blocks: Journal of Geophysical Research: Earth Surface, v. 123, p. 1931–1957, doi:10.1029/2017JF004575.

Sinton, J.M., Eason, D.E., and Duncan, R.A., 2017, Volcanic evolution of Molokaʻi, Hawaiʻi: Implications for the shield to postshield transition in Hawaiian volcanoes: Journal of Volcanology and Geothermal Research, v. 340, p. 30–51, doi:10.1016/j.jvolgeores.2017.04.011.

Sklar, L.S., and Dietrich, W.E., 2004, A mechanistic model for river incision into bedrock by saltating bed load: Water Resources Research, v. 40, doi:10.1029/2003WR002496.

Sklar, L.S., and Dietrich, W.E., 2001, Sediment and rock strength controls on river incision into bedrock: Geology, v. 29, p. 1087–1090, doi:10.1130/0091-7613(2001)029<1087:SARSCO>2.0.CO;2.

Sklar, L.S., and Dietrich, W.E., 2006, The role of sediment in controlling steady-state bedrock channel slope: Implications of the saltation–abrasion incision model: Geomorphology, v. 82, p. 58–83, doi:10.1016/j.geomorph.2005.08.019.

Small, E.E., Blom, T., Hancock, G.S., Hynek, B.M., and Wobus, C.W., 2015, Variability of rock erodibility in bedrock-floored stream channels based on abrasion mill experiments: Journal of Geophysical Research: Earth Surface, v. 120, p. 1455–1469, doi:10.1002/2015JF003506.

Snyder, N.P., Whipple, K.X., Tucker, G.E., and Merritts, D.J., 2003, Importance of a stochastic distribution of floods and erosion thresholds in the bedrock river incision problem: Journal of Geophysical Research: Solid Earth, v. 108, p. 2117, doi:10.1029/2001JB001655.

Stearns, H.T., and Macdonald, G.A., 1942, General geology and ground-water resources of the island of Maui, Hawaii: Advertiser Publishing Co.

Stearns, H.T., and Macdonald, G.A., 1946, Geology and ground-water resources of the island of Hawaii: Honolulu Advertising 9, https://pubs.er.usgs.gov/publication/70160867 (accessed August 2022).

Stearns, H.T., Macdonald, G.A., and Swartz, J.H., 1940, Geology and ground-water resources of the islands of Lanai and Kahoolawe, Hawaii: Advertiser Publishing Co.

Stearns, H.T., and Vaksvik, K.N., 1935, Geology and ground-water resources of the island of O ʻahu, Hawai ʻi. Hawai ʻi Division of Hydrography: Bulletin, v. 1, p. 479.

Stock, J., and Dietrich, W.E., 2003, Valley incision by debris flows: Evidence of a topographic signature: Water Resources Research, v. 39, doi:10.1029/2001WR001057.

Stock, J.D., and Montgomery, D.R., 1999, Geologic constraints on bedrock river incision using the stream power law: Journal of Geophysical Research: Solid Earth, v. 104, p. 4983–4993, doi:10.1029/98JB02139.

Stock, J.D., Montgomery, D.R., Collins, B.D., Dietrich, W.E., and Sklar, L., 2005, Field measurements of incision rates following bedrock exposure: Implications for process controls on the long profiles of valleys cut by rivers and debris flows: GSA Bulletin, v. 117, p. 174–194, doi:10.1130/B25560.1.

Thaler, E.A., and Covington, M.D., 2016, The influence of sandstone caprock material on bedrock channel steepness within a tectonically passive setting: Buffalo National River Basin, Arkansas, USA: Journal of Geophysical Research: Earth Surface, v. 121, p. 1635–1650, doi:10.1002/2015JF003771.

Thiede, R.C., Bookhagen, B., Arrowsmith, J.R., Sobel, E.R., and Strecker, M.R., 2004, Climatic control on rapid exhumation along the Southern Himalayan Front: Earth and Planetary Science Letters, v. 222, p. 791–806, doi:10.1016/j.epsl.2004.03.015.

Tucker, G.E., 2004, Drainage basin sensitivity to tectonic and climatic forcing: implications of a stochastic model for the role of entrainment and erosion thresholds: Earth Surface Processes and Landforms, v. 29, p. 185–205, doi:10.1002/esp.1020.

Vehtari, A., Gelman, A., and Gabry, J., 2017, Practical Bayesian model evaluation using leave-one-out cross-validation and WAIC: Statistics and Computing, v. 27, p. 1413–1432, doi:10.1007/s11222-016-9696-4.

Veneziano, D., and Niemann, J.D., 2000, Self-similarity and multifractality of fluvial erosion topography: 2. Scaling properties: Water Resources Research, v. 36, p. 1937–1951, doi:https://doi.org/10.1029/2000WR900054.

Verdian, J.P., Sklar, L.S., Riebe, C.S., and Moore, J.R., 2020, Sediment size on talus slopes correlates with fracture spacing on bedrock cliffs: Implications for predicting initial sediment size distributions on hillslopes: Earth Surface Dynamics Discussions, p. 1–23, doi:https://doi.org/10.5194/esurf-2020-54.

Vitousek, P., Asner, G.P., Chadwick, O.A., and Hotchkiss, S., 2009, Landscape-level variation in forest structure and biogeochemistry across a substrate age gradient in Hawaii: Ecology, v. 90, p. 3074–3086, doi:10.1890/08-0813.1.

Vitousek, P., Dixon, J.L., and Chadwick, O.A., 2016, Parent material and pedogenic thresholds: observations and a simple model: Biogeochemistry, v. 130, p. 147–157, doi:10.1007/s10533-016-0249-x.

Voigtlander, J.V., Clark, M.K., Zekkos, D., Greenwood, W.W., Anderson, S.P., Anderson, R.S., and Godt, J.W., 2018, Strong variation in weathering of layered rock maintains hillslope-scale strength under high precipitation: Earth Surface Processes and Landforms, v. 43, p. 1183–1194, doi:doi.org/10.1002/esp.4290.

Ward, D.J., and Galewsky, J., 2014, Exploring landscape sensitivity to the Pacific Trade Wind Inversion on the subsiding island of Hawaii: Journal of Geophysical Research: Earth Surface, v. 119, p. 2014JF003155, doi:10.1002/2014JF003155.

Watts, A.B., and Brink, U.S.T., 1989, Crustal structure, flexure, and subsidence history of the Hawaiian Islands: J. Geophys. Res, p. 863–870.

Weissel, J.K., and Seidl, M.A., 1997, Influence of rock strength properties on escarpment retreat across passive continental margins: Geology, v. 25, p. 631–634, doi:10.1130/0091-7613(1997)025<0631:IORSPO>2.3.CO;2.

Wentworth, C.K., 1927, Estimates of Marine and Fluvial Erosion in Hawaii: The Journal of Geology, v. 35, p. 117–133.

Wentworth, C.K., 1928, Principles of Stream Erosion in Hawaii: The Journal of Geology, v. 36, p. 385–410.

Wentworth, C.K., and Macdonald, G.A., 1953, Structures and Forms of Basaltic Rocks in Hawaii: USGS Bulletin USGS Numbered Series 994, doi:10.3133/b994.

Whipple, K.X., DiBiase, R.A., Crosby, B., and Johnson, J.P.L., 2022, 6.40 - Bedrock Rivers, *in* Shroder, J. (Jack) F. ed., Treatise on Geomorphology (Second Edition), Oxford, Academic Press, p. 865–903, doi:10.1016/B978-0-12-818234-5.00101-2.

Whipple, K.X., Forte, A.M., DiBiase, R.A., Gasparini, N.M., and Ouimet, W.B., 2017, Timescales of landscape response to divide migration and drainage capture: Implications for the role of divide mobility in landscape evolution: Journal of Geophysical Research: Earth Surface, v. 122, p. 248–273, doi:https://doi.org/10.1002/2016JF003973.

Whipple, K.X., and Tucker, G.E., 1999, Dynamics of the stream-power river incision model: Implications for height limits of mountain ranges, landscape response timescales, and research needs: Journal of Geophysical Research: Solid Earth, v. 104, p. 17661–17674.

White, S.E., 1949, Processes of erosion on steep slopes of oahu, Hawaii: American Journal of Science, v. 247, p. 168–186, doi:10.2475/ajs.247.3.168.

Willett, S.D., 1999, Orogeny and orography: The effects of erosion on the structure of mountain belts: Journal of Geophysical Research: Solid Earth, v. 104, p. 28957–28981, doi:10.1029/1999JB900248.

Wobus, C.W., Crosby, B.T., and Whipple, K.X., 2006, Hanging valleys in fluvial systems: Controls on occurrence and implications for landscape evolution: Journal of Geophysical Research: Earth Surface, v. 111, doi:10.1029/2005JF000406.

Wohl, E., and Merritt, D.M., 2008, Reach-scale channel geometry of mountain streams: Geomorphology, v. 93, p. 168–185, doi:https://doi.org/10.1016/j.geomorph.2007.02.014.

Wolfe, E.W., and Morris, J., 1996, Geologic map of the island of Hawaii: US Geological Survey, 2524-A.

Yang, R., Willett, S.D., and Goren, L., 2015, In situ low-relief landscape formation as a result of river network disruption: Nature, v. 520, p. 526–529, doi:10.1038/nature14354.

APPENDIX A

CHAPTER 2 SUPPLEMENTARY:

ADDITIONAL DETAILS ON TOPOGRAPHIC ANALYSIS, FIELD METHODS, AND STOCHASTIC THRESHOLD MODEL

TOPOGRAPHIC ANALYSIS

Topographic analysis was conducted using TopoToolbox (Schwanghart and Scherler, 2014) and Cloud Compare (CloudCompare,2021). For topographic data we used a USGS 10m DEM, merged with a resampled 5 m lidar derived grid and point cloud obtained from Open Topography (2013), and 10 m resampled bathymetry data from The School of Ocean and Earth Science and Technology, University of Hawaii at Manoa. To identify relatively preserved and uneroded surfaces of the shield volcano we fit a convex hull to contours at 50 m intervals, with contours covering -800 m to -600 m below sea-level and from 800 m to the maximum elevation above sea-level. We used a thin plate spline to interpolate between points extracted from the convex hulls to generate an un-incised reconstruction of the initial volcano. Sea-cliff height was estimated as the difference in elevation from the reconstructed surfaces and the channel outlet for a given valley. Using the approach outlined by Schwanghart and Scherler (2020), we automatically detected knickpoints with a threshold value of 25 on a stream network defined by a minimum drainage area of $1x10^5 m^2$. We identified the location of the slope-break knickpoints by identifying a change in gradient of the stream profile in in χ-elevation space. We measured distance from the nearest outlet or tributary junction to the base of the knickzone. To identify the lower limit of the knickzone we used the ischange function implemented in MATLAB to identify where the channel gradient first reaches 40% below the knickzone. We chose this value because sediment cover is inherently unstable above 40% and prone to failure and in-channel debris flows (Prancevic et al., 2014) suggesting that bedrock should be perpetually exposed above this gradient.

Drainage area loss is observed for the southernmost valleys with an approximate loss of 3 km^2 distributed over the headwaters of at least 5 valleys, an approximate average of 0.6 km^2. Drainage area loss was mapped using Google Earth and the geological map from Macdonald et al (1960). We used the divide at Waimea canyon as the current boundary for drainage area loss and the contact between the Olokele formation and Nā Pali formation as the original divide location. This is a reasonable approach because in uneroded sections the contact between the two formation sets a local topographic high. However, for all valleys there are no wind gaps or other evidence of significant drainage area loss recorded in the DEM subsequently the above approach may over-estimate drainage area loss. Overall the effects of drainage area loss appear to be minimal, this is reinforced by the observations that (1) several valleys with apparent drainage area loss do not preserve knickzones and (2) the northern portion of our study area appears to be isolated from drainage area loss but contains some of the largest knickzones.

FIELD METHODS

To test for differences in rock mass properties, we measured joint spacing and estimated rock strength using a type-N Schmidt Hammer. For ‘a‘ā flows and dikes, joint spacing was measured on the main joint set perpendicular to the lip of the waterfall along a scan line, which typically ranged in length from 10-15m from the lip of the waterfall until we encountered sediment. In some cases, joint orientation was irregular, such that blocks where not perfectly rectangular or perpendicular to the lip of the waterfall (Fig. A1). Effort was made to measure the widest part in these cases. The same approach was

applied for pāhoehoe flows exposed along canyon walls and below waterfalls. Clinker is typically a clastic material, subsequently we measured the clast diameter as a proxy for joint spacing. For application of the Schmidt hammer, we used clean, intact, near horizontal surfaces free from small scale defects and for each surface we took an average of 25 measurements spaced several cm apart. Channel gradient was measured with a Suunto clinometer for the reaches immediately above the knickzone and later compared and verified with lidar derived topography.

MODEL OF THRESHOLD EXCEEDANCE

In order to identify q_c, we calculated τ^* across a range of unit discharge,

$$\tau^* = \frac{\rho_w g h S}{g(\rho_s - \rho_w)D}, \qquad (1)$$

where g is the acceleration due to gravity, h is flow depth , ρ_w and ρ_s are the density of water (1000kg/m^3) and sediment respectively (2800kg/m^3), S is channel gradient, and D is a representative grain size diameter. We used the variable power equation (Ferguson, 2007) to estimate flow depth,

$$h = \frac{q}{u^*} \frac{\sqrt{\left(\frac{h}{ks}\right)^{\frac{5}{3}} + \left(\frac{a_1}{a_2}\right)^2}}{a1\left(\frac{h}{ks}\right)}, \qquad (2)$$

where a_1 and a_2 are empirical coefficients equal to 6.5 and 2.5 respectively (Ferguson, 2012) and ks is a reference roughness length scale. In our model we set ks equal to D. To identify q_c we found the unit discharge where $\tau^* = \tau_c^*$, where τ_c^* is the non-dimensional critical shear stress. To estimate τ_c^* we followed Prancevic and Lamb (2015) where $\tau_c^* = 0.19{C_f}^{0.34}$ and C_f is the friction coefficient estimated from Equation (2), where u is depth averaged velocity and $q = uh$ and $C_f = \left(\frac{u^*}{u}\right)^2$.

To evaluate the role of a stochastic discharge in exceeding threshold conditions we used a local USGS stream gage record of peak discharges (n = 56) fit with a Weibull distribution (Figs. A2 & A3, Rossi et al., 2016). We used Hack's law (Hack, 1957) to generate drainage area (A) for a synthetic catchment, where $A = kX^h$, with k and h estimated from the topography with values of 0.8 and 1.8 respectively and X is distance in meters. To scale q with A we first accounted for a drainage area dependence on discharge with the following equation,

$$Q(A) = Q_{ref}\left(\frac{A}{A_{ref}}\right)^c, \qquad (3)$$

where Q_{ref} is a random discharge from the peak flood distribution, A_{ref} is the drainage area of the gage station, and c is the mean value (0.76) of the area exponent calculated for regression estimates of peak floods on the leeward side of Kauai (Oki et al., 2010). We used the empirical relationship of channel width for bedrock channels $W_b = 3.3A^{0.36}$ (Whipple et al., 2022) to estimate the width (W_b) of a channel at bankfull discharge. Width, however, should vary with flood size. To account for this we used the following equation for at-a-station width (W) (Leopold and Maddock, 1953),

$$\frac{W}{W_b} = \left(\frac{Q}{Q_b}\right)^{\omega_s}, \qquad (4)$$

where Q_b is the reference flood size for W_b. Without additional information on Q_b, we assume that Q_b should be the bankfull discharge which often is approximated by the 2-year flood and in this case is ~7 m^3/s. Notably 7 m^3/s aligns with a break in the change of gage height against a change in discharge (Fig. A6). For the exponent ω_s we follow the argument by DiBiase and Whipple (2011) that a tradeoff between width and sidewall friction result in relatively fixed value of 0.25. Combining (3) and (4) we obtain the unit discharge as,

$$q = \frac{Q_{ref}^{1-\omega_s} Q_b^{\omega_s} A^{c(1-\omega_s)} {A_{ref}}^{c(\omega_s-1)}}{W_b}, \qquad (5).$$

From (5) we then estimated the probability of boulder entrainment for a given drainage area as the number of events that exceeded q_c divided by the total number of events.

We checked the validity of (2) and (5) by comparing predicted values of h with measured values of gage height. We used data from USGS stream gages on Oahu where field measurements of stream flow are available. These streams tend to be steep (~ 10-20%) and bed material consists of boulders and gravel—similar to the streams on the west coast of Kaua'i. Our analysis suggests Equation (2) does a reasonable job of predicting flow depth for values of *ks* around 1.5 (Fig. A5). Though gage height is often measured from a given datum reference point, flow depth estimated from Equation (2) is near 1:1 with measurements of gage height given some vertical offset (Fig. A5 B).

To evaluate the applicability of equations (2) and (5) for the Nahomalu stream gage on the west coast of Kaua'i, we used the most recent stage measurements from a large flood event recorded on 3/11/2021 that covered a range of discharges from 1.4 to 39.6 m^3s^{-1}. For each discharge we calculated h using the reported channel gradient for the gage station (8%). Because gage height is typically measured from some reference point we adjusted the measured gage height by subtracting a value of 0.35 [m] from all measurements. A value of 1.5 for ks yielded a steeper slope (~1.3, Fig. A6) of predicted h vs gage height then observed for gages on Oahu. Higher values of ks (~2.5) reduce the slope of h vs gage height to near 1:1, though these channel are filled with coarse sediment (Fig. A6 C&D) a value of 2.5 is likely too high. Measurements of grain-sizes from ortho imagery suggest the largest grain sizes are around 1m in diameter. Similarly our estimates of channel width appear reasonable as Wb at the gage station is predicted to be 7.5 m, while our field measurements suggests bankfull channel width varies between 7-8 m for nearby reaches. Qb = 7 also appears to be reasonable estimate as shown by the changes in gage height versus discharge (Fig. A6 A). Consequently, because we have constraints on other important factors such as grain size, channel width, and Qb, the fact that gage height does not increase 1:1 with predicted flow depth may simply be consequence of the uncertainty in the indirect measurements used to estimate discharge for the recorded flood events.

FIGURES

Figure A1. Photos of bedrock conditions at or near the lips of waterfalls. Scale in photos is 10 cm. In virtually all case it was impossible to confirm joints were through going and in general joint width varied considerably and most blocks appeared firmly attached.

Figure A2. Photos of bed material in reaches upstream of knickzones. Photo on left has person for scale (~ 2m). Photo on right: grain size ranges from gravel to meter sized boulders.

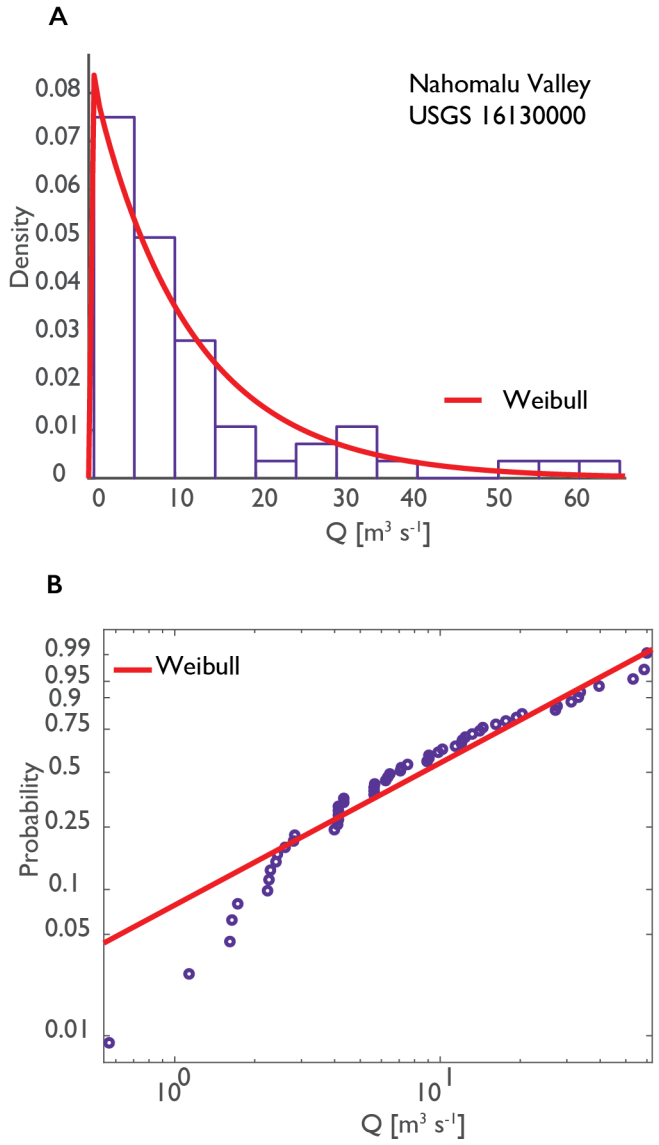

Figure A3. Evaluation of the Weibull distribution of peak discharge from USGS Gage Station 16130000 Nahomalu Valley. A) Histogram and Weibull probability distribution (red-line). (B) Probability plot of peak flood discharges illustrating goodness of fit. Red-line shows expected values from the fit Weibull distributions, the closer the data are to the red-line the better the fit. Y-axis represents the quantiles of the distribution/data converted to probability values. Though at small discharges the data deviates from the predicted probability this should have little effect on the analysis since these discharges are well below threshold conditions. We also evaluated the fit of the distribution using a Kolmogorov-Smirnov test ($p = 0.6262$) which indicates that there is no statistical evidence against the null hypothesis that the data originate from a different distribution.

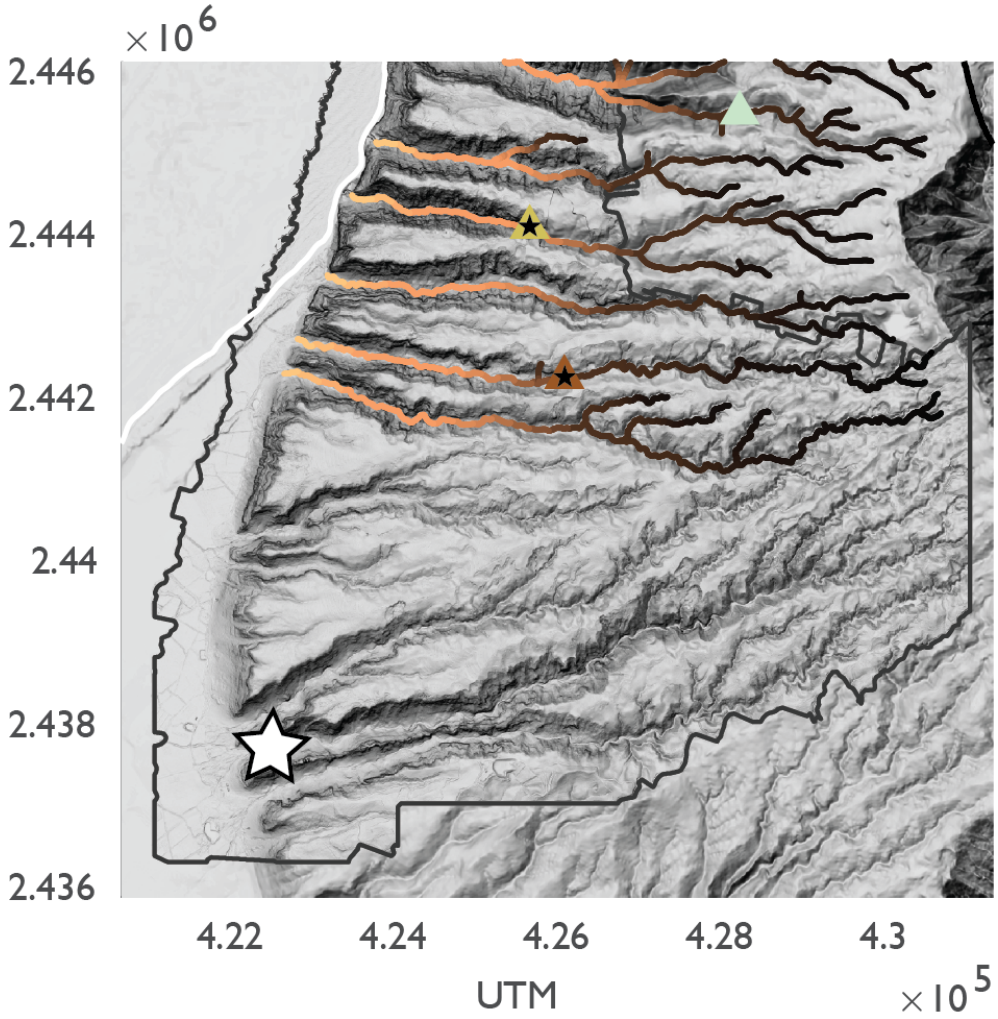

Figure A4. Location (white star) of USGS Gage Station 16130000 relative to canyons in study. Brown triangle is the knickzone from Mackey et al, 2014.

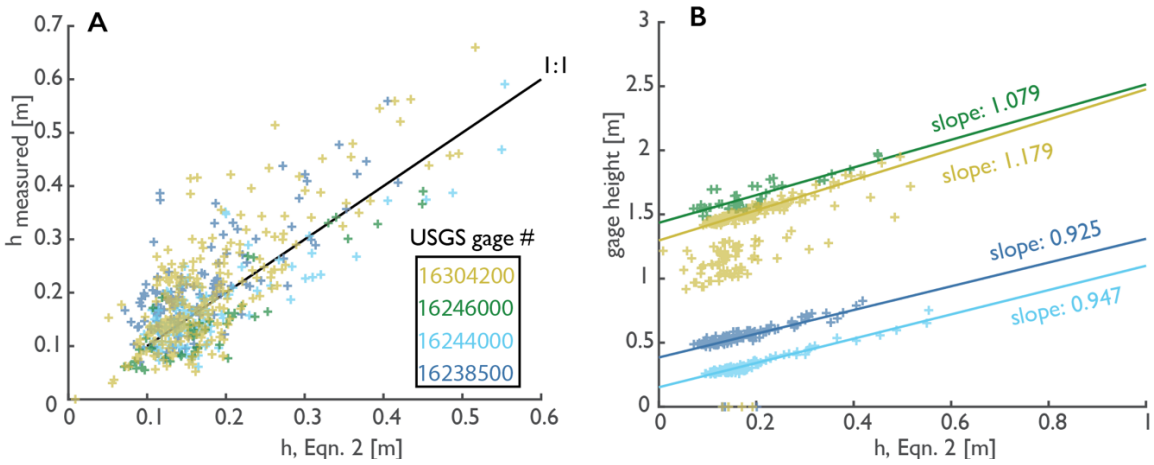

Figure A5. Evaluation of the variable power equation, Eq. (2), in predicting flow depth. A: Measured flow depth against predicted flow depth for USGS stream gages on Oahu. B: Gage height against predicted flow depth. Lines show best fit with reported slopes near 1, also note observed offset between gage height and h.

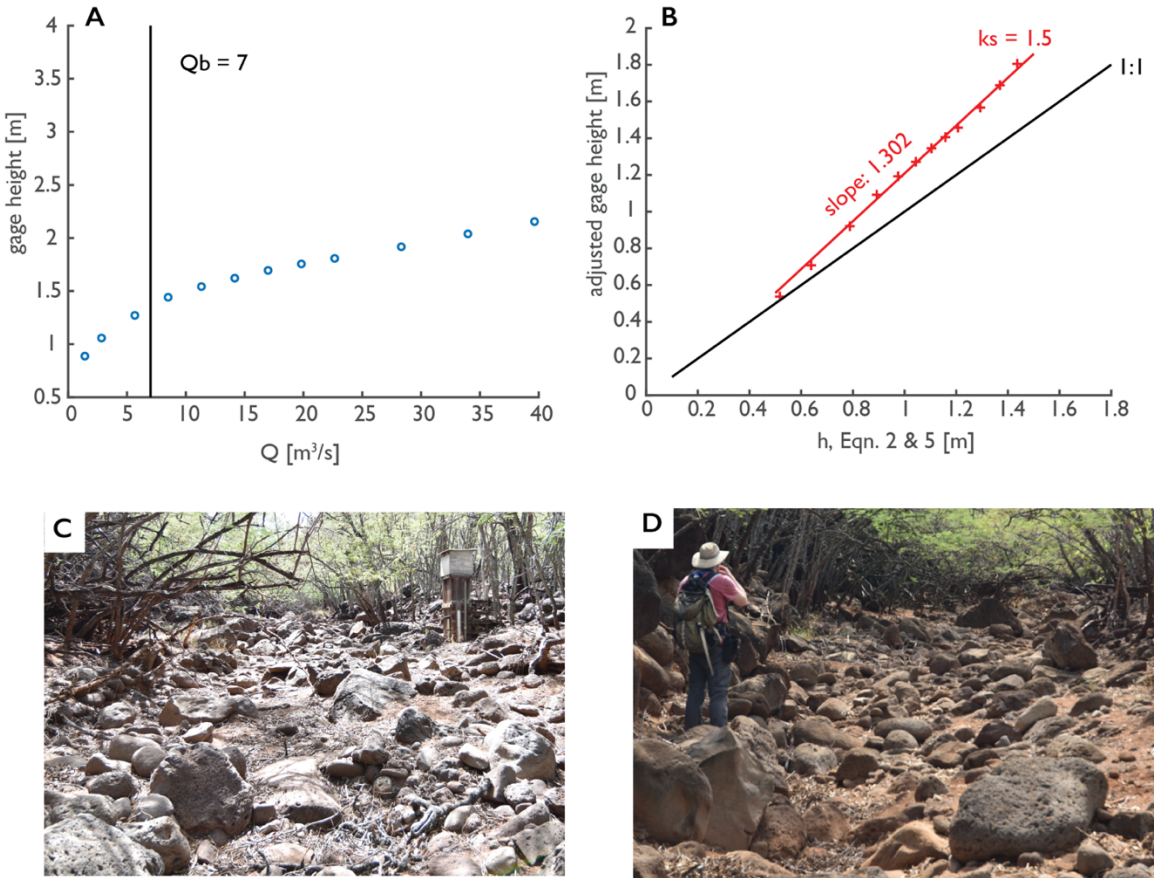

Figure A6. Evaluation of the variable power equation for Nahomalu Valley. A: Discharge (Q) vs gage height for flood event. Note change in relationship between gage height and Q at Qb = 7. B: Predicted flow depth (h) against adjusted gage height with red data and line showing predicted flow depths with ks = 1.5. C: Photo of bed conditions at gage 16130000 in Nahomalu valley shown in upper right corner. D: Photo of bed condition in channel near gage 16130000 in Nahomalu valley, person for scale is ~ 2m.

REFERENCES

CloudCompare (version 2.10.2) [GPL software]. (2021). Retrieved from http://www.cloudcompare.org/

Ferguson, R., 2007, Flow resistance equations for gravel-and boulder-bed streams: Water resources research, v. 43.

Ferguson, R.I., 2012, River channel slope, flow resistance, and gravel entrainment thresholds: Water Resources Research, v. 48, doi:10.1029/2011WR010850.

Hack, J.T., 1957, Studies of longitudinal stream profiles in Virginia and Maryland: U.S. Geological Survey Professional Paper, v. 294-B.

Leopold, L.B., and Maddock Jr., T., 1953, The hydraulic geometry of stream channels and some physiographic implications: Professional Paper Report 252, 64 p., doi:10.3133/pp252.

Oki, D.S., Rosa, S.N., and Yeung, C.W., 2010, Flood-frequency estimates for streams on Kaua'i, O'ahu, Moloka'i, Maui, and Hawai'i, State of Hawai'i: U.S. Geological Survey Scientific Investigations Report 5035, 121 p.

OpenTopography Na Pali Coast, Kauai, Hawaii. Distributed by OpenTopography. https://doi.org/10.5069/G91834D5

Prancevic, J.P., and Lamb, M.P., 2015, Unraveling bed slope from relative roughness in initial sediment motion: Journal of Geophysical Research: Earth Surface, v. 120, p. 474–489, doi:10.1002/2014JF003323.

Prancevic, J.P., Lamb, M.P., and Fuller, B.M., 2014, Incipient sediment motion across the river to debris-flow transition: Geology, v. 42, p. 191–194, doi:10.1130/G34927.1.

Rossi, M.W., Whipple, K.X., and Vivoni, E.R., 2016, Precipitation and evapotranspiration controls on daily runoff variability in the contiguous United States and Puerto Rico: Journal of Geophysical Research: Earth Surface, v. 121, p. 128–145, doi:10.1002/2015JF003446.

Schwanghart, W., and Scherler, D., 2020, Divide mobility controls knickpoint migration on the Roan Plateau (Colorado, USA): Geology, doi:10.1130/G47054.1.

Schwanghart, W., and Scherler, D., 2014, Short Communication: TopoToolbox 2 – MATLAB-based software for topographic analysis and modeling in Earth surface sciences: Earth Surface Dynamics, v. 2, p. 1–7, doi:https://doi.org/10.5194/esurf-2-1-2014.

Whipple, K.X., DiBiase, R.A., Crosby, B., and Johnson, J.P.L., 2021, Bedrock Rivers, *in* Reference Module in Earth Systems and Environmental Sciences, Elsevier, doi:10.1016/B978-0-12-818234-5.00101-2.

APPENDIX B

CHAPTER 4 SUPPLEMENTARY:

ADDITIONAL FIGURES

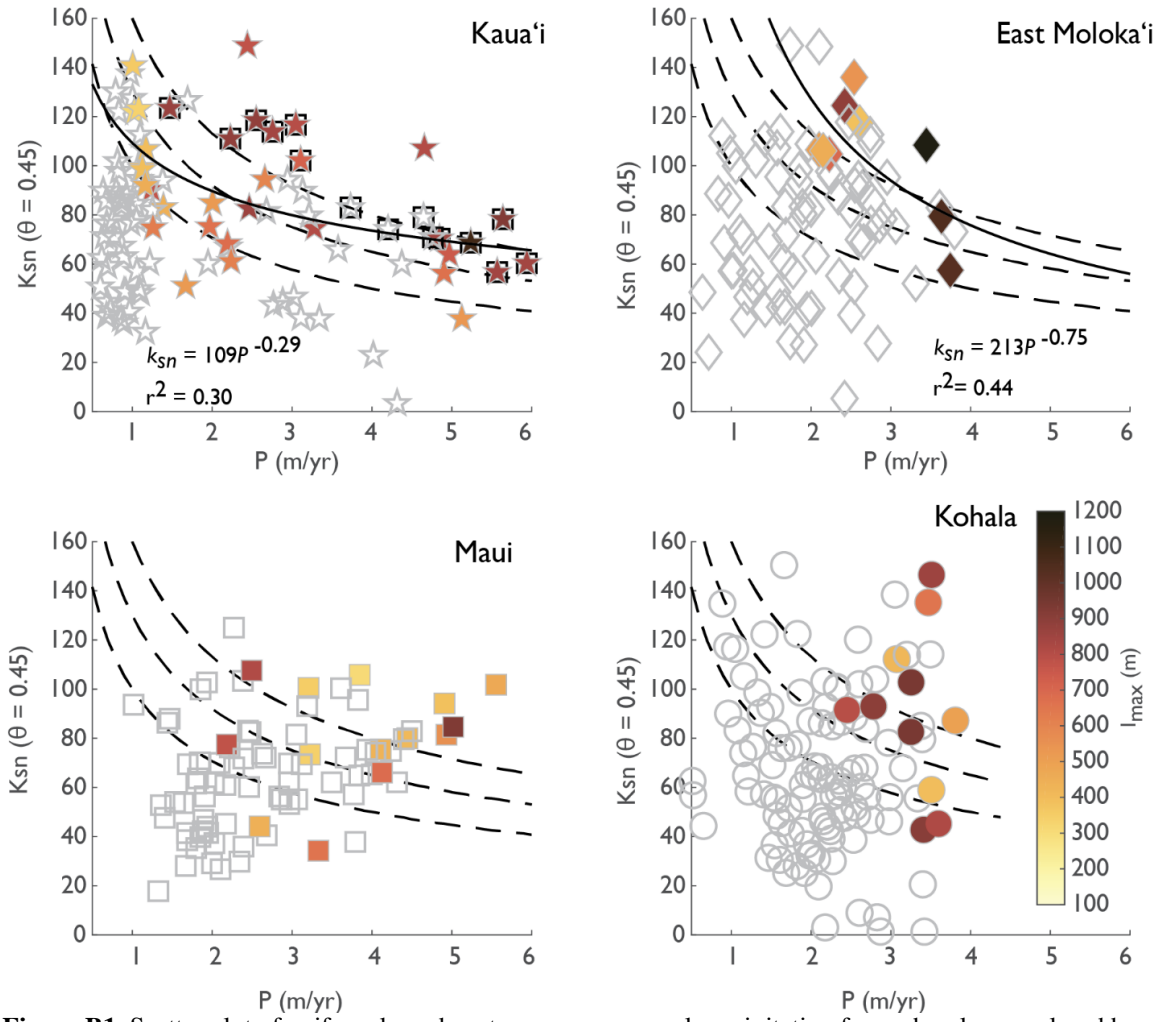

Figure B1. Scatter plot of uniform k_{sn} and upstream mean annual precipitation for each volcano colored by maximum incision depth. Dashed lines shows the theoretical predictions that $k_{sn} \propto P^{-\frac{1}{2}}$ with the upper lines showing a ~1.2 and 1.4 times increase in the threshold-setting grain size. Gray symbols indicate lightly incised canyons (I_{max} < 300 m) and or segments with more than 90% mapped alluvium (Sherrod et al. 2021). Colored symbols show deeply incised segments with less than 90% mapped alluvium. Solid grey lines show the best fit linear regression. Black squares on Kaua'i highlight segments that are associated with the Olokele member of the Nāpali formation (Figure 2). Gray solid lines show best fit for power-law relation between k_{sn} and P. For Maui and Kohala there was no detectable correlation of k_{sn} with P.

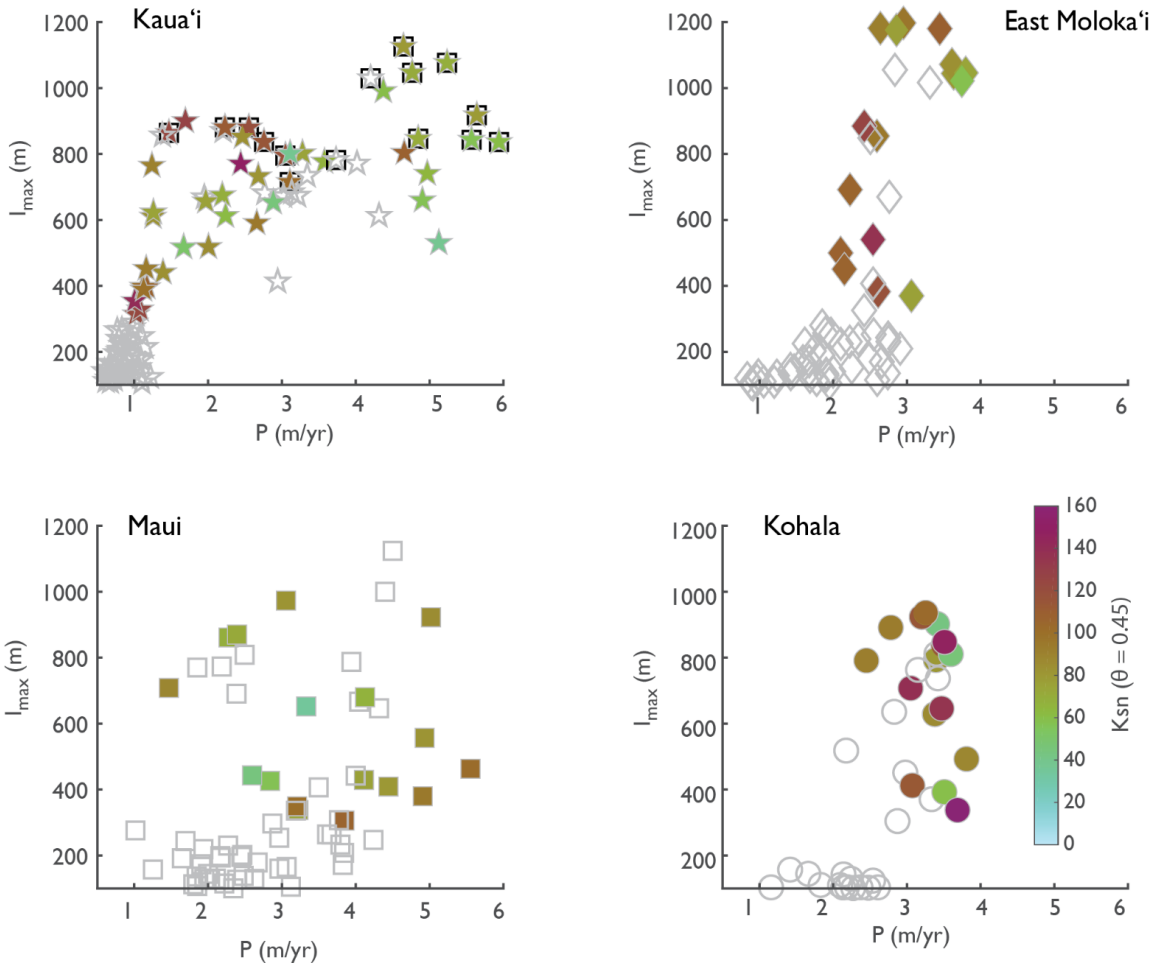

Figure B2. Scatter plot of maximum incision depth (I_{max}) against the upstream mean annual rainfall (P) for each volcano and colored by k_{sn}. Gray symbols indicate lightly incised canyons (I_{max} < 300 m) and or segments with more than 90% mapped alluvium (Sherrod et al. 2021). Colored symbols show deeply incised segments with less than 90% mapped alluvium. Black squares on Kaua'i highlight segments that are associated with the Olokele member of the Nāpali formation (Figure 2).

APPENDIX C

STATEMENT OF CO-AUTHOR PERMISSION

Chapters 2-4 were prepared independently for publication with help from Kelin X Whipple (Chapters 2-4) and Ayron Strauch (Chapters 3-4). These co-authors have acknowledged and granted permission for the publication of this material here.